

University of Louisville

ThinkIR: The University of Louisville's Institutional Repository

Electronic Theses and Dissertations

8-2023

Measurement of conduction, radiation, and convection thermal energy to assess baking performance in residential ovens.

Sean Simpson
University of Louisville

Follow this and additional works at: <https://ir.library.louisville.edu/etd>



Part of the [Food Processing Commons](#), and the [Heat Transfer, Combustion Commons](#)

Recommended Citation

Simpson, Sean, "Measurement of conduction, radiation, and convection thermal energy to assess baking performance in residential ovens." (2023). *Electronic Theses and Dissertations*. Paper 4157.
Retrieved from <https://ir.library.louisville.edu/etd/4157>

This Master's Thesis is brought to you for free and open access by ThinkIR: The University of Louisville's Institutional Repository. It has been accepted for inclusion in Electronic Theses and Dissertations by an authorized administrator of ThinkIR: The University of Louisville's Institutional Repository. This title appears here courtesy of the author, who has retained all other copyrights. For more information, please contact thinkir@louisville.edu.

MEASUREMENT OF CONDUCTION, RADIATION, AND CONVECTION
THERMAL ENERGY TO ASSESS BAKING PERFORMANCE IN RESIDENTIAL
OVENS

By

Sean Simpson
B.S, Virginia Polytechnic and State University, 2020

A Thesis
Submitted to the Faculty of the University of Louisville
J.B. Speed School of Engineering
In Partial Fulfillment of the requirements
For the degree of

Master of Science
In Mechanical Engineering

Department of Mechanical Engineering
University of Louisville
Louisville, Kentucky

August 2023

MEASUREMENT OF CONDUCTION, RADIATION, AND CONVECTION
THERMAL ENERGY TO ASSESS BAKING PERFORMANCE IN RESIDENTIAL
OVENS

By

Sean Simpson
B.S, Virginia Polytechnic and State University, 2020

A Thesis Approved On

July 13th, 2023

by the following Thesis Committee:

Dr. Ellen Brehob, Thesis Advisor

Dr. Andrea Kelecyc, Committee Member

Dr. Luis Segura, Committee Member

DEDICATION

I dedicate this thesis to my friends and family who continuously inspire me to push myself and stay curious. I rely on their encouragement and support every day.

ACKNOWLEDGEMENTS

I would like to thank my advisors, Dr. Brehob and Dr. Kelecy for their support, commitment, and advice throughout this study. Without advisors that have a genuine passion for teaching and learning, none of this would be possible. I would also like to thank the technical team at GE Appliances for their knowledge and support in this study; James Armstrong, Eric Scott Johnson, Sabrina Hannah, Amelia Hensley, and Amanda Jones. Finally, thank you to Mike Ekbundit for leading the Edison Engineering Development program at GEA and continuing to support students while providing opportunities for studies like this.

ABSTRACT

MEASUREMENT OF CONDUCTION, RADIATION, AND CONVECTION THERMAL ENERGY TO ASSESS BAKING PERFORMANCE IN RESIDENTIAL OVENS

Sean Simpson

July 13th, 2023

Residential ovens are complicated thermal environments capable of delivering convection, conduction, and radiation heat transfer to food. The amount and mode of heat transfer can change based on the design of the oven cavity, cooling systems, and oven cycle algorithms. Studies have shown that the changes in one heat transfer mode can have an impact on the quality of baked goods. The many variables involved make designing residential ovens a time consuming and costly process. The goal of this study is to adapt thermal energy sensing technology to collect energy data from a residential oven and develop correlations to quality characteristics of baked cakes. The quality characteristics measured in this study are browning, porosity, rise height, and mass loss. Testing was limited to white cakes baked in a traditional bake mode with no convection fan. The correlation models developed should reliably predict the final quality measurements of baked cakes using thermal energy data collected in an oven cycle of matching parameters.

The sensors used in this study can detect incoming thermal energy and break it up into component heat transfer modes of conduction, convection, and radiation. The sensors were placed in small cake tins to match the conditions of baking cakes. A test plan was performed to collect thermal energy data at a variety of oven temperature setpoints, rack positions, and bake times. Each test run was repeated, replacing the sensors with cakes, and the quality characteristics of the baked cakes were recorded.

The thermal energy sensors performed well, splitting energy absorbed into conduction, convection, and radiation components. The thermal data was repeatable, showing less than two percent variation after ten minutes of testing on the middle rack at any given temperature setpoint. It was confirmed from previous studies that conduction dominates a traditional bake mode, contributing about 59% of the total energy absorbed. Second is radiation and finally convection, due to the lack of an active convection fan during a traditional bake mode.

It was found that top and bottom browning L^* color values correlated linearly with radiation and conduction energy absorbed, respectively. The coefficient of determination (R^2) for these models was 0.97 for bottom browning and 0.95 for top browning. Validation data was limited, so further testing would improve the confidence of these models. The porosity and rise height metrics were not able to be correlated with the data collected. It is possible that the measurement methods of these cake quality metrics were not robust enough for reliable data, or the thermal energy data collected was not relevant to changes in

porosity or rise. Future testing could investigate alternate thermal data to determine what correlative factors can be used to predict porosity and rise. Finally, mass loss was well correlated to a polynomial regression of total energy with a 0.98 R^2 value.

TABLE OF CONTENTS

	PAGE
DEDICATION	iii
ACKNOWLEDGEMENTS.....	iv
LIST OF TABLES	xi
LIST OF FIGURES	xiv
1 Introduction.....	1
2 Literature Review	4
2.1 Heat Transfer Modes in Baking	4
2.2 Cake Performance Characteristics.....	7
2.3 Predicting Food Performance.....	11
3 Test Setup.....	15
3.1 Thermal Energy Sensors.....	15
3.2 Sensor Modifications for Cake Testing.....	18
3.3 Residential Oven Specifications	20
3.4 Cake Baking Process	22
3.5 Cake Performance Criteria	24
3.6 Experimental Test Plan	27

4	Sensor Test Results	30
4.1	Flux Measurements	30
4.2	Heat Ratios.....	36
4.3	Rack Positions.....	40
4.4	Thermal Energy Sensor Repeatability	43
5	Correlations.....	46
5.1	Browning Correlation	46
5.1.1	Bottom Browning.....	49
5.1.2	Top Browning.....	53
5.1.3	Browning Model Error	55
5.2	Porosity Correlation	57
5.3	Rise Height Correlation	61
5.4	Mass Loss Correlation.....	70
5.4.1	Mass Loss Model Error	74
6	Conclusion.....	76
6.1	Important Results	76
6.2	Future Work.....	80
	References	82
	Appendices.....	84
A	Sensor Specifications	84

B	Thermal Energy Sensor Test Plan Data	88
C	Thermal Energy Sensor Repeatability	112
D	Uncertainty Analysis	114
E	Cake Performance Repeatability	115
F	Correlations	119
	Curriculum Vitae	122

LIST OF TABLES

TABLE	PAGE
Table 3-1 Complete test plan performed once with cakes and once with thermal energy sensors for a total of 48 tests including the randomized run order.	29
Table 4-1 Heat energy absorbed by the thermal energy sensors split by heat transfer mode.	35
Table 4-2 Uncertainty analysis for total energy absorbed by thermal energy sensors divided into (a) the bottom mass and (b) the heat flux sensor.....	36
Table 4-3 Ratios of the total energy into the sensors broken down by mode of heat transfer.	39
Table 4-4 Ratios of heat transfer absorbed by mode, specifically the top, middle, and bottom rack runs at their respective maximum bake times.	40
Table 4-5 Repeatability data based on four runs (350°F, mid rack) using coefficient of variation. Colors show comparison of relative values, green is smaller and red is larger.	44
Table 5-1 Color data measured for top and bottom cake browning using DigiEye instrument.....	48
Table 5-2 Stepwise regression including interaction terms of each heat transfer mode.	52
Table 5-3 Top and bottom browning estimates and error calculations against true measured browning data.	56

Table 5-4 Porosity measurements that represent the percentage of pixels that were classified as air cells.	59
Table 5-5 Center and side rise data collected for each test run. Average values were used in correlation calculations.	63
Table 5-6 Mass loss data collected for all cakes in the test plan.	71
Table 5-7 Mass loss model error calculations for both polynomial and linear regressions based on the measured data from Table 5-6.	74
Table 6-1 Conclusion of thermal energy data and cake performance correlations that are useful for prediction.	80
Table A-1 Hukseflux FHF04 Sensor Specifications (continued next page)	84
Table A-2 Hukseflux Black and Gold Sticker Specifications	86
Table A-3 ULTEM™ 1010 Resin Thermal Properties	87
Table C-1 Repeatability data based on four runs (325°F, mid rack) using coefficient of variation. Colors show comparison of relative values, green is smaller and red is larger.	112
Table C-2 Repeatability data based on four runs (350°F, mid rack) using coefficient of variation. Colors show comparison of relative values, green is smaller and red is larger.	113
Table D-1 Uncertainty values for thermal energy sensor measurements based on worst case conditions (longest test time, etc.).	114
Table E-1 Cake browning repeatability data comparing the two cakes from each test run.	115

Table E-2 Cake porosity repeatability data comparing the two cakes from each test run. 116

Table E-3 Cake rise height repeatability data comparing the two cakes from each test run. 117

Table E-4 Cake mass loss repeatability data comparing the two cakes from each test run. 118

LIST OF FIGURES

FIGURE	PAGE
Figure 1-1 Thermal energy sensors developed by Petit-Bois (2022).....	2
Figure 2-1 Diagram of heat flux sensors used to collect thermal energy data in a residential oven Petit-Bois (2022).....	7
Figure 2-2 Graphical representation of the CIELAB color space with labeled a^* , b^* , and L^* axis, Ebenezzar et al. (2020).....	8
Figure 2-3 Cross sections of baked cake analyzed with a color imaging system (Tang & Ghosh, 2021).....	9
Figure 2-4 The color change (in the LAB color space) of bread crust during the baking process (Silva et al., 2022).....	11
Figure 3-1 Cross sectional view of thermal energy sensor developed in by Petit-Bois (2022).....	17
Figure 3-2 Energy balance of the bottom and top mass of the thermal energy sensors by Petit-Bois (2022).....	17
Figure 3-3 Cross sectional view of the thermal energy sensor assembled in a cake tin.....	20
Figure 3-4 Modified thermal energy sensors in cake tins used to measure oven environment.....	20
Figure 3-5 Diagram of heater locations in residential oven cavity.....	21
Figure 3-6 Wire mesh modifications made to the oven rack to allow repeatable placement of the cake tins across multiple tests.....	22

Figure 3-7 Modified cake tin with a needle probe to allow internal temperature measurement of the cakes while baking.....	23
Figure 3-8 Center oven air temperature of Test Run 4 (325°F, middle rack, 30 minutes) with labeled cycle stages.	24
Figure 3-9 VeriVide DigiEye System used to capture images for color analysis. The system was calibrated to D65 Standard Lighting.....	25
Figure 3-10 Example of image analysis process to determine the percentage air cell area of cake cross section.....	26
Figure 3-11 View of where the side rise measurements were taken for each cake.....	27
Figure 4-1 Heat flux measurements into the top of the thermal energy sensors from Run 4 of the test plan, oven temperature of 325°F and run for 30 minutes on the middle rack.	31
Figure 4-2 Oven temperature plot for Run 4 of the test plan, oven temperature set to 325°F and run for 30 minutes on the middle rack.	32
Figure 4-3 Conductive heat flux measured from thermal energy sensors in Run 4 of the test plan, oven temperature of 325°F and run for 30 minutes on the middle rack.....	34
Figure 4-4 Total energy absorbed by the thermal energy sensors by heat transfer mode over the course of a cycle, specifically Run 4 with oven temperature of 325°F and 30 minutes on the middle rack.	37
Figure 4-5 Average heat absorbed from all middle rack oven tests split by heat transfer mode.	38

Figure 4-6 Conduction energy absorbed during top, middle, and bottom rack tests at maximum bake times for each temperature setpoint.	41
Figure 4-7 Convection energy absorbed during top, middle, and bottom rack tests at maximum bake times for each temperature setpoint.	42
Figure 4-8 Radiation energy absorbed during top, middle, and bottom rack tests at maximum bake times for each temperature setpoint.	42
Figure 5-1 Color change of bread crust during the baking process (Silva et al., 2022).	49
Figure 5-2 Correlation between bottom browning measured in L* and total conduction energy absorbed during the test cycle.....	50
Figure 5-3 Residual plots for correlation model of bottom browning.	51
Figure 5-4 Correlation between top browning measured in L* and total radiation energy absorbed during the test cycle.....	54
Figure 5-5 Residual plots for correlation model of top browning.	55
Figure 5-6 Air cell area data plotted against total thermal energy absorbed separated by test setpoint.	60
Figure 5-7 Cake center height vs bake time separated by oven setpoint for mid rack position.	64
Figure 5-8 Cake side height vs bake time separated by oven setpoint for mid rack position.	64
Figure 5-9 Correlation between conduction thermal energy absorbed and center height of baked cakes.....	65

Figure 5-10 Graphical representation of a cake with maximum and minimum observed center rise values compared to the maximum error band of the correlation model.....	66
Figure 5-11 Cross section of a baked cake where the crust lip can be seen.	68
Figure 5-12 Side rise data vs conduction energy absorbed separated by oven setpoint.....	69
Figure 5-13 Evaporation rate as a function of fluid temperature for free water. Tests 1 – 4 tested at $\phi = 45\%$ and tests 5 – 8 with $\phi = 100\%$ (Örvös et al., 2016).	72
Figure 5-14 Weight loss as a function of total energy absorbed with a linear and polynomial regression plotted with the measured weight loss tests.....	73
Figure B-1 Test 1, Traditional Bake, 325°F Setpoint, 15 minutes, middle rack..	88
Figure B-2 Test 2, Traditional Bake, 325°F Setpoint, 20 minutes, middle rack..	89
Figure B-3 Test 3, Traditional Bake, 325°F Setpoint, 25 minutes, middle rack..	90
Figure B-4 Test 4, Traditional Bake, 325°F Setpoint, 30 minutes, middle rack..	91
Figure B-5 Test 5, Traditional Bake, 325°F Setpoint, 15 minutes, bottom rack.	92
Figure B-6 Test 6, Traditional Bake, 325°F Setpoint, 30 minutes, bottom rack.	93
Figure B-7 Test 7, Traditional Bake, 325°F Setpoint, 15 minutes, top rack.	94
Figure B-8 Test 8, Traditional Bake, 325°F Setpoint, 30 minutes, top rack.	95
Figure B-9 Test 9, Traditional Bake, 350°F Setpoint, 12 minutes, middle rack..	96
Figure B-10 Test 10, Traditional Bake, 350°F Setpoint, 17 minutes, middle rack.	97

Figure B-11 Test 11, Traditional Bake, 350°F Setpoint, 22 minutes, middle rack.	98
Figure B-12 Test 12, Traditional Bake, 350°F Setpoint, 27 minutes, middle rack.	99
Figure B-13 Test 13, Traditional Bake, 350°F Setpoint, 12 minutes, bottom rack.	100
Figure B-14 Test 14, Traditional Bake, 350°F Setpoint, 27 minutes, bottom rack.	101
Figure B-15 Test 15, Traditional Bake, 350°F Setpoint, 12 minutes, top rack.	102
Figure B-16 Test 16, Traditional Bake, 350°F Setpoint, 27 minutes, top rack.	103
Figure B-17 Test 17, Traditional Bake, 375°F Setpoint, 10 minutes, middle rack.	104
Figure B-18 Test 18, Traditional Bake, 375°F Setpoint, 14 minutes, middle rack.	105
Figure B-19 Test 19, Traditional Bake, 375°F Setpoint, 18 minutes, middle rack.	106
Figure B-20 Test 20, Traditional Bake, 375°F Setpoint, 22 minutes, middle rack.	107
Figure B-21 Test 21, Traditional Bake, 375°F Setpoint, 10 minutes, bottom rack.	108
Figure B-22 Test 22, Traditional Bake, 375°F Setpoint, 22 minutes, bottom rack.	109
Figure B-23 Test 23, Traditional Bake, 375°F Setpoint, 10 minutes, top rack.	110

Figure B-24 Test 24, Traditional Bake, 375°F Setpoint, 22 minutes, top rack.	111
Figure F-1 Residual plots for correlation between bottom browning and conduction energy absorbed.	119
Figure F-2 Residual plots for correlation between top browning and radiation energy absorbed.....	119
Figure F-3 Residual plots for attempted correlation between center rise and conduction energy.	120
Figure F-4 Residual plots for attempted correlation between side rise and conduction energy.	120
Figure F-5 Residual plots for the linear correlation between mass loss and total energy absorbed.....	121
Figure F-6 Residual plots for polynomial correlation between mass loss and total energy absorbed.....	121

1 INTRODUCTION

The typical residential oven has a complicated thermal environment which applies conductive, convective, and radiative heat transfer to cook food. Each of these heat transfer modes affects the cooking of food in different ways. Different oven cavities, convection fan systems, and even small control changes can all change the magnitude and ratios of the various forms of heat transfer applied to food. An important aspect of oven design is testing cooking performance of different oven cavities and controls to create the best possible thermal environment for many different foods. This often involves cooking many foods to get an understanding of the performance of a given oven system. For example, many batches of cakes might be cooked in an oven to develop a traditional bake cycle.

This cycle development process can get costly, but few alternate methods are available to understand how well an oven will bake food. Various sources show that quality characteristics of baked goods like cakes and breads do not depend solely on the temperature at which they are baked. Modifying the source of heat transfer applied can have an impact on the quality of the final product. This can be achieved in a residential oven by changing which heating elements are cycled on and for how long. Convection fans mounted in the oven cavity can be used to increase convective heat transfer to the food. Radiation energy from

the oven cavity can change based on the exposed surface area of the cavity itself. Oven temperature alone does not quantify these heat sources, so additional thermal energy data is required.

Previous studies have developed methods of collecting the thermal energy data required to understand the thermal environment of a residential oven. Of particular interest to the proposed study are methods of independently detecting each mode of heat transfer. In one study, Petit-Bois (2022) developed a thermal energy sensor to measure heat flux in a residential oven. A pair of these sensors can be used to measure conductive, convective, and radiative flux during the same oven cycle.

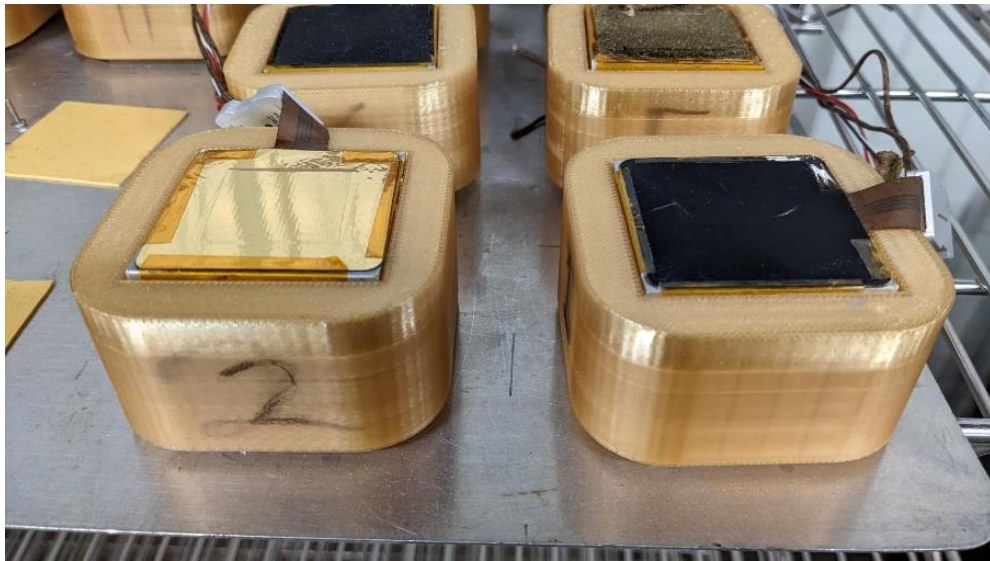


Figure 1-1 Thermal energy sensors developed by Petit-Bois (2022).

If reliable correlations between thermal data and cake quality can be found, it is possible that thermal energy sensors can replace baked goods in the

oven and oven cycle development process. The purpose of this study is to develop correlations between quality characteristics of baked cakes (browning, porosity, rise height, and mass loss) and thermal energy data. These correlations should be robust enough to predict the quality of a baked cake using thermal energy data alone.

2 LITERATURE REVIEW

A review of prior research has been broken into three main sections.

Section 2.1 will cover studies of how different modes of heat transfer affect baked products like breads and cakes. Section 2.2 identifies studies where the quality of baked goods was measured. These studies indicate what is important to measure and how those measurements are taken. Finally, Section 2.3 covers predictive models in food preparation.

2.1 Heat Transfer Modes in Baking

Past research has been done to understand heat transfer modes in ovens for the purposes of cooking food. In Standing (1974), the impact of each mode of heat transfer on biscuit baking was studied. It should be noted that this study specifically relates to band oven baking, a method traditionally used for industrial scale food preparation. To determine the constant heat transfer coefficients required for heat energy calculations, scenarios were developed to bake a biscuit using isolated modes of heat transfer. To prepare a biscuit using only conduction, a hot plate was used to apply heat only to the base of the biscuit. It was observed that it took only half as much total energy in the conduction only scenario for a biscuit to rise the same amount as a normal biscuit bake with all modes of heat transfer. The convective and radiative components were studied by baking a biscuit in an oven with the base insulated against conduction or free convection

into the bottom. A heating element and fan were positioned above the biscuit. When the element was on without the fan, pure radiation was provided to the biscuit. When the element and fan were both on, radiation and convection were both occurring. Temperature and moisture data was used to compute total heat absorbed by the biscuits. In the radiative case, it was observed that the top of the biscuits developed a normal level of crust and browning developed. When the fan was turned on, adding convective heat transfer, the resulting biscuits showed considerably less crust browning. This suggests that radiation dominates top browning in biscuit baking. Moisture data from the convective and radiative cases showed a larger moisture bakeout when the fan was applied indicating convective heat transfer dominates moisture loss.

Saxena et al. (1995) had a similar approach of baking food in conditions to isolate the modes of heat transfer. This study investigated the baking of roti in a tandoori oven, traditionally made in India and other Asian countries. Tandoor ovens are different than most gas and electric residential ovens, with the rotis placed on the inner side walls of the oven and allowed to bake until done. The applicable modes of heat transfer into the bread in this case are: conduction from the walls, free convection from surrounding air, radiation from the exposed walls, and radiation from the flames themselves. To improve the baking of tandoori roti and tandoor oven design, the individual impact of each mode of heat transfer was studied. A conduction only case was tested by placing a roti on the hot inner wall of the oven and placing an asbestos disc on the exposed surface to ensure only conduction is used to cook the product. A radiative case was studied by

hanging a roti in a folded mesh in the center of the oven, out of contact with any conductive surface. It was observed that the rotis baked without conduction did not show the characteristic crusty brown bottom that rotis are known for. The study concluded that rather than just total energy into a food product, the amount of each mode of heat transfer is critical to the baked result.

It is clear that the mode of heat transfer is critical to understanding the performance of baking food. In the study by Petit-Bois (2022) a method of measuring individual modes of heat flux in a residential oven was investigated. A food load was simulated using a sensor made of two aluminum blocks with thermocouples in the center of each block to read temperature. The aluminum masses were separated by a plastic housing and the top mass had a thin heat flux sensor stuck to the surface. There were two varieties of sensor, one with a black sticker that was designed to have a high emissivity and another with a gold sticker designed for low emissivity. The high emissivity sensor measures all heat transfer into the top surface, accounting for both convection and radiation. The low emissivity sensor will reflect radiation, only measuring convection. The difference between the sensors will account for the radiative heat transfer. The bottom of both sensors is an aluminum mass that is assumed to only absorb conductive heat transfer, which can be measured based on the change in temperature over time. Figure 2-1 below shows a cross-sectional view of a sensor assembly on a cookie sheet. These sensors were designed to be used in residential oven settings to collect data on the modes of heat transfer that food

experiences. A modified version of these sensors will be used in the proposed study to investigate heat transfer into cakes baked in cake tins.

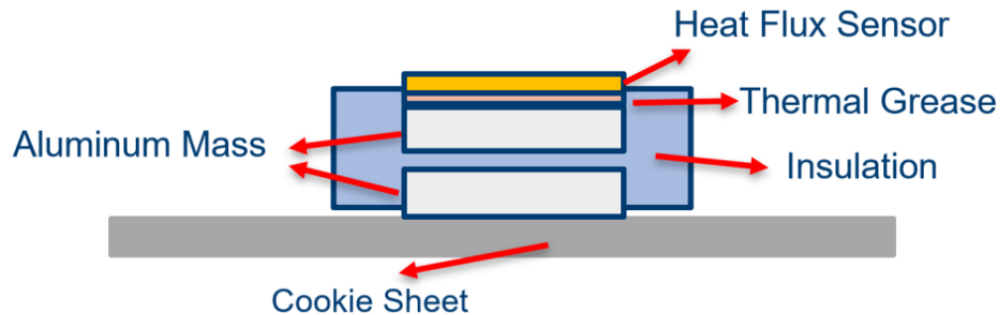


Figure 2-1 Diagram of heat flux sensors used to collect thermal energy data in a residential oven Petit-Bois (2022).

2.2 Cake Performance Characteristics

To correlate heat flux and energy data to the baking performance of cakes, quantitative metrics need to be used. The selected metrics should be able to indicate what a good cake is. Tang and Ghosh (2021) published an article investigating the use of oleogels in cake baking applications as a replacement for shortening. The oleogelation process creates a gel-like structure of oil and water without using the saturated or trans-fats that shortening does. Trials were run to compare cake products created with shortening, canola oil, unheated oleogel, and heated oleogel. The following factors of the final cake product were measured: color, specific volume, cell structure of the internal cake crumb, and cake texture. The color of the batter and final cake product were measured with a Hunterlab Miniscan XE using D65 Standard Lighting. The system measured the

aspects of the CIELAB color space, L^* (lightness of color), a^* (presence of red vs. green), and b^* (presence of yellow vs. blue). Figure 2-2 shows a graphical representation of the CIELAB color space. It is worth noting that a^* and b^* do not have finite scales like L^* and can technically be infinite. Most software programs, however, limit the readings to the range -128 to +127 to minimize data usage.

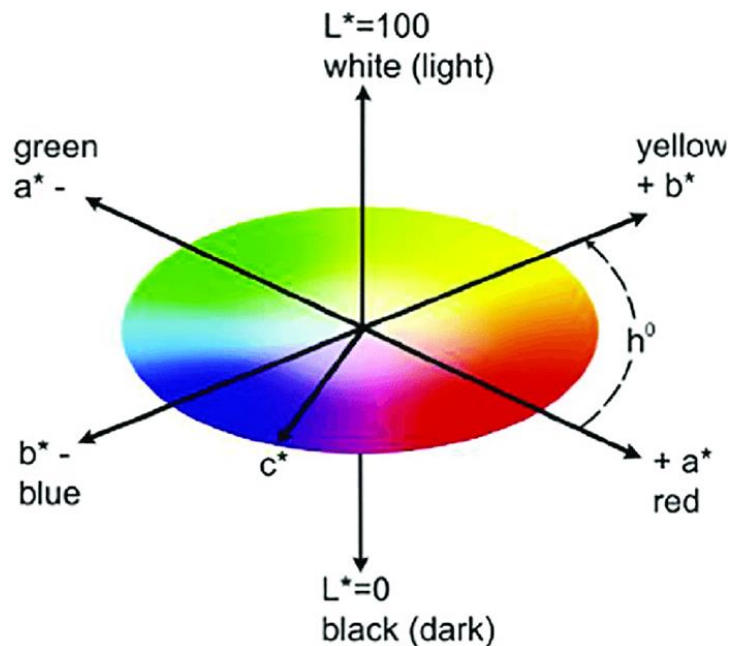


Figure 2-2 Graphical representation of the CIELAB color space with labeled a^* , b^* , and L^* axis, Ebenezzar et al. (2020).

The volume of the final cakes was determined by immersion in a rapeseed oil bath and the specific volume was calculated using that volume and mass of the cake. The cell structure of the internal cake crumb was also determined using imaging. A cross section of the cake was scanned and binarized. Software then calculated the percentage of pixels that represent open cell area in the image to indicate airiness of the cake crumb. A tight crumb with few air pockets would

result in a small air cell area percentage while a light crumb with lots of air would show a large air cell area. The porosity analysis showed that using heated oleogel caused larger air channels to form while baking. Figure 2-3 below also shows the considerable difference in crumb between shortening and canola oil as the fat in cake batter.

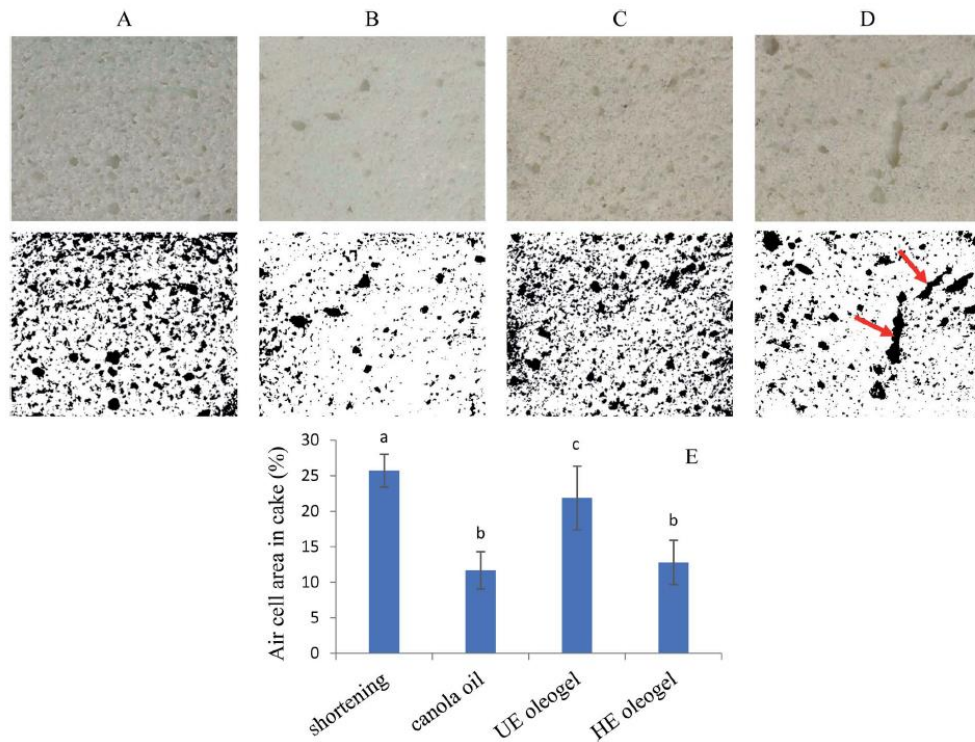


Figure 2-3 Cross sections of baked cake analyzed with a color imaging system (Tang & Ghosh, 2021).

Traditionally, the CIELAB color space is used to determine an objective difference between two colors. ΔE is a metric for absolute color change representing the distance between two points in the color space. Tuta Şimşek (2019) also used color imaging to measure performance of cake baking. This study explored a method of partial vacuum baking to improve the quality of gluten

free cakes. Several test runs were performed by varying the time, temperature, and pressure of a vacuum oven used after a varying time and temperature of conventional baking. The quality characteristics measured were firmness, observed springiness, weight loss, total color change, and specific volume. The color of the cakes was measured with a Lovibond tintometer in five locations and averaged for the cake. The reference color was a white plate and color change, ΔE , was determined for each cake. A variation analysis was performed on the listed quality characteristics and it was observed that the vacuum baking process did not have any statistical impact on the color change or specific volume of the final cakes. Additionally, in Abdanan Mehdizadeh (2022), the CIELAB color space was used for images captured during the baking of cupcakes to constantly monitor the rate of baking.

Another study, Silva et al. (2022), measured the physical properties of bread over the course of the baking period. Temperature, moisture, weight loss, volume, porosity, crumb structure, and color change were all measured as they changed with time during a bake. The goal of the study was to use an oven with controlled wall temperatures to study the effect of temperature variation on the physical properties of bread. To capture data on color during the baking process, the bread was removed from the oven at three minute intervals and imaged in a chamber equipped with D65 Standard Lighting. Those images were analyzed for color according to the CIELAB color space. L^* , a^* , and b^* measurements were then plotted against bread surface temperature to track how browning changed as crust temperature increased. Figure 2-4 shows that no color change occurs

until some threshold temperature is reached, roughly 125°C in these experiments. Once that threshold is reached, L^* drops linearly while a^* and b^* have non-linear responses, increasing to a peak before falling again. The measurement of total color change, ΔE , includes L^* , a^* , and b^* and thus displays some of the non-linearity of a^* and b^* . If a linear correlation to color change is desired, it is best that L^* is used alone.

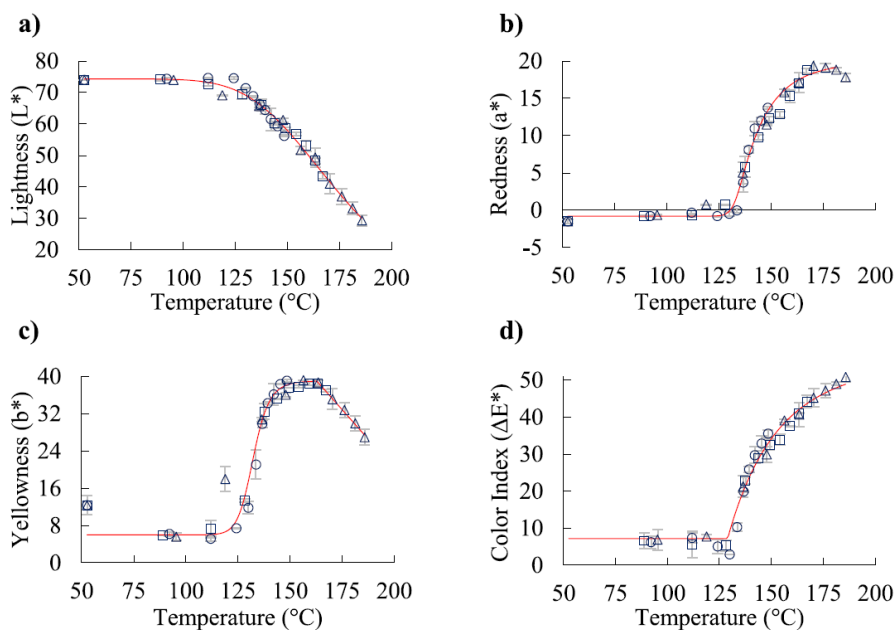


Figure 2-4 The color change (in the LAB color space) of bread crust during the baking process (Silva et al., 2022).

2.3 Predicting Food Performance

Many studies focus on the effect of various baking parameters on the quality of finished food products rather than directly predict the bake results. Sato et al. (1987) studied the baking performance of sponge cakes in a forced convection oven. The goal was to express the heating of the cake in the oven by

an apparent heat transfer coefficient. Tests were performed with varying air temperatures from 180°C to 220°C and varying air velocity between 0 m/s and 1.5 m/s. To evaluate the performance of the cakes, the weight loss, height difference, degree of browning, and firmness of the cake were measured for each run. It was determined that the air velocity and temperature had a significant impact on the weight loss, height difference, and browning of the sponge cakes while firmness was only impacted by air velocity and not temperature. Using the calculated apparent heat transfer coefficient, an equation was developed that predicts bake time from air velocity and oven temperature. The equation suggests that bake time can be reduced by increasing air velocity and/or oven temperature. Either of these changes would increase the convective heat transfer on to the food so this finding does make sense. This study did not provide any evaluation on the predictive performance of the models. They focused on the trends identified by the data and the models that confirmed those trends.

In Hermanseder et al. (2017), a farinograph was used to collect data on dough made with varying flours and correlate rheological properties to bread baking performance using a stepwise multilinear regression and an artificial neuronal network . The dough was prepared and baked in an industrial bread oven all at the same conditions. After baking, the weight, volume, volume yield, weight loss, hardness, and elasticity were measured. The dough properties were fed into a stepwise linear regression to predict the final baking characteristics. For each characteristic, any predictor with a p-value < 0.05 was determined to be

significant. Researchers found that the baking volume, volume yield, dough yield gross, dough yield net, and baking loss could be predicted using various aspects of the dough properties in a linear regression. The goodness of fit was calculated using the coefficient of determination (R^2) values for each regression. Other regressions were performed using an artificial neuronal network (ANN). Each of the eight dough parameters were set as inputs with the baking characteristics as desired outputs. The fit of the resulting models was also evaluated using R^2 and compared to the fit provided by the stepwise linear regressions. The conclusion of this paper indicates that the ANN provided the best fit correlations, however there is no theoretical basis behind the models produced by the network. The complexity of the systems involved, like gluten formation during the kneading process, make theoretical relationships with the final bake difficult to establish.

In Sadeghi et al. (2016), predictive models for temperature and moisture changes were developed for flat bread cooked by contact baking. The dough was prepared, and 1 cm thick samples were placed on a preheated aluminum slab in a residential oven for 3 minutes. Temperature sensors read the temperature of the bread at the top surface, center, and bottom surface. A model was developed based on principles of heat and mass transfer to estimate the temperature and moisture content of the bread at various locations during the baking process. Considering the thinness of the bread studied, the evaporation rate profiles are likely much different than what would be expected from a roughly 1.2 inch cake that is used in the proposed study. Notably, this study focused on modeling the moisture and temperature as a function of time for the specific system modeled.

Many studies focus on time or temperature in a specific oven configuration rather than correlate directly with total energy that might be transferable to other systems or baking configurations.

Most studies around food and baking focus on using temperature and baking time in the same oven when comparing the quality of baked goods. The effect of changing time and temperature of a traditional bake mode in the oven is studied. The proposed study will investigate the use of heat flux sensors along with thermocouples in thermal masses to collect total thermal energy data. That data will be used to correlate baking performance characteristics with thermal energy data rather than temperature or time.

3 TEST SETUP

In this study, two sets of experiments were performed. The first set used thermal energy sensors in an instrumented residential oven to collect data on the thermal energy absorbed by cakes as they baked. The second set measured the baking performance characteristics of white cakes. The two sets of experiments were performed in the same oven using identical conditions so the thermal energy measurements could be compared to cake baking characteristics of a matching run. As stated in the introduction, the goal of the study is to correlate thermal energy data to cooking performance to accurately predict cooking performance of cakes in a traditional bake mode of a residential oven.

3.1 Thermal Energy Sensors

In a previous study (Petit-Bois, 2022), thermal energy sensors were developed to characterize heat flux in a residential oven. Figure 3-1 shows a cross section of the sensor assembly. These sensors use a combination of thermopile heat flux sensors and thermocouples to collect heat flux data. Energy into the top of the sensor assembly is collected using a HukseFlux FHF04 heat flux sensor. The HukseFlux sensors are thin, flexible thermopiles that measure a temperature difference across the sensor body and output an electrical signal converted to a heat flux. They also have a Type T thermocouple positioned inside the sensor to monitor sensor temperature. These sensors have a

measurement range of $+10^4$ to -10^4 W/m² with a nominal sensitivity of 11×10^{-6} V/(W/m²). Additionally, the FHF04 sensors are designed with thermal spreaders that cover the sensor with a conductive layer. This reduces the thermal conductivity dependence of the measurement, effectively making the sensor sensitivity independent of its environment. A full specification of the sensors can be found in Table A-1 in Appendix A. Critical to this testing, HukseFlux sensors are rated for continuous use within a sensor temperature range of -95 to 250 °F. The bake cycles required to completely cook a white cake have target oven air temperatures typically between 325°F and 375°F. To use these sensors without damaging them, the sensors were fixed to aluminum masses with thermal paste to readily conduct to the aluminum. The two aluminum masses are housed in an insulative resin plastic housing constructed from ULTEM 1010 Resin. This high temperature resin is able to withstand the temperatures in the oven while leaving the aluminum masses thermally isolated. The thermal properties of ULTEM 1010 can be found in Table A-3 in the appendix. Heat that enters the heat flux sensors is conducted down into the aluminum mass, allowing the sensor to survive long enough in the oven to collect the required data.

The bottom aluminum mass contains a J-Type thermocouple fixed in the center by a set screw. This thermocouple reads the center temperature of the aluminum block. Because the bottom mass is full insulated from the top and sides by the ULTEM insulation, it is assumed that all the energy entering the bottom mass is a result of conduction from below. The conduction energy stored can be calculated using the equation:

$$q_{cond} = mc_p(T_f - T_i) \quad (1)$$

where m is the mass of the aluminum block, c_p is the specific heat of aluminum, T_f is the final temperature and T_i is the initial temperature of the aluminum block. A full energy balance of the top and bottom of the thermal energy sensors can be seen in Figure 3-2.

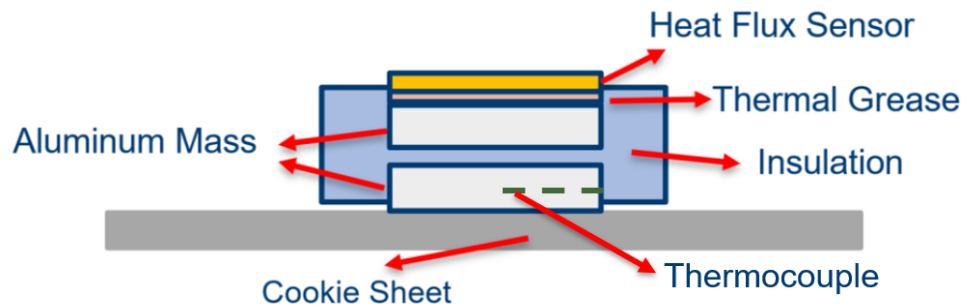


Figure 3-1 Cross sectional view of thermal energy sensor developed in by Petit-Bois (2022).

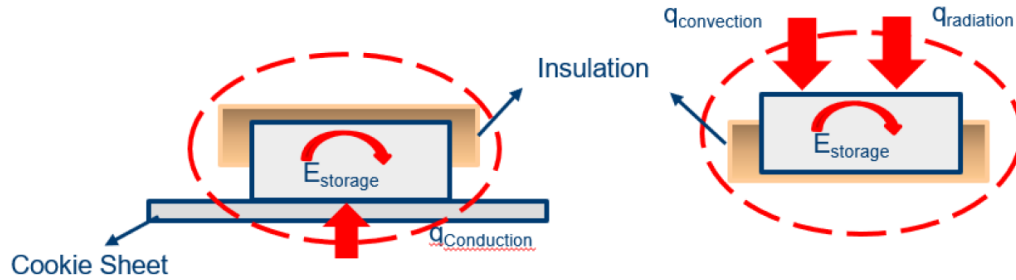


Figure 3-2 Energy balance of the bottom and top mass of the thermal energy sensors by Petit-Bois (2022).

Additionally, two different types of stickers were fixed to the heat flux sensor on the top of the sensor assembly, a black sticker with a high emissivity

and a gold sticker with a low emissivity. The sticker specification can be found in Table A-2 in the appendix. The black sticker absorbs both convection and radiation heat transfer modes from above while the gold sticker reflects radiation, only experiencing convective heat transfer. When two sensors are placed in an oven, one black and one gold, it can be assumed that both receive similar amounts of convection energy. This means the gold sensor will provide the convective component of heat transfer while the difference between the two sensor readings will be the radiative heat transfer. Finally, the bottom mass of each sensor measures conduction heat transfer into the bottom of the assembly. Using two sensor assemblies allows for the three main modes of heat transfer to be individually measured in a residential oven. Two of the sensors used in Petit-Bois (2022) were selected for use in this study, one with a black sticker and one with a gold sticker. According to the manufacturer's calibration, the sensors selected have a sensitivity of $11.52 \times 10^{-6} \text{ V}/(\text{W}/\text{m}^2) \pm 0.58 \times 10^{-6} \text{ V}/(\text{W}/\text{m}^2)$ and $11.18 \times 10^{-6} \text{ V}/(\text{W}/\text{m}^2) \pm 0.56 \times 10^{-6} \text{ V}/(\text{W}/\text{m}^2)$ for the black and gold sensors, respectively.

3.2 Sensor Modifications for Cake Testing

In the study by Petit-Bois, 12 of the thermal energy sensors were placed in an array on an aluminum cookie sheet. Some effort was made to correlate trends of heat flux with sugar cookie baking; however, no strong conclusions were made. As stated before, this study will investigate direct correlations between absorbed thermal energy and baking performance, specifically with white cakes.

Therefore, modifications to the thermal sensors were made to properly measure the effects of the oven environment experienced by the cakes as they baked.

First, instead of baking cookies on a cookie sheet, cakes are baked in tins. The sensor assemblies are roughly 3 inches wide, so a similar size cake tin would be ideal to capture all energy entering the cake. A four-inch diameter aluminum cake tin was selected which fit the sensor assembly well. One of the problems experienced in the original study was the contact resistance between the sensor assemblies and the cookie sheet they rested on. To address this issue, a gap pad of thermally conductive silicone rubber was placed between the cake tin and the bottom mass of the sensor assembly. This pad formed to both materials and eliminated issues of flatness variation and provided a direct conduction path from the cake tin into the sensor. To further improve this connection, more insulative 3D printed ULTEM 1010 plastic parts were made to both center the sensor in the tin (spacer) and provide a small amount of force to press the sensor down into the cake tin (slide on clamp), effectively squishing the silicone contact pad and allowing it to completely fill the gap between sensor and cake tin. Figure 3-3 shows a cross sectional view of the cake tin sensor assembly and Figure 3-4 shows the two fully assembled sensors used in this study.

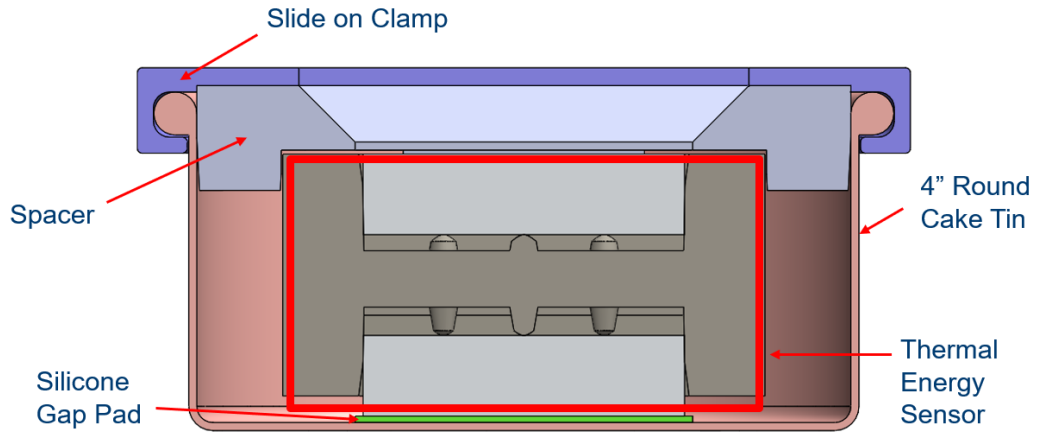


Figure 3-3 Cross sectional view of the thermal energy sensor assembled in a cake tin.



Figure 3-4 Modified thermal energy sensors in cake tins used to measure oven environment

3.3 Residential Oven Specifications

The oven used in the proposed study is a GE PTS9000 Wall Oven. There are four heating elements: a broil, broil assist, hidden bake, and convection element with power levels of 3300, 1000, 3850, and 2400 watts, respectively.

Figure 3-5 below shows where each element is placed in the oven cavity.

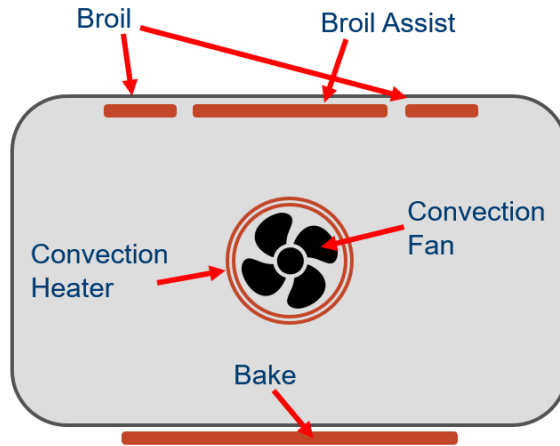


Figure 3-5 Diagram of heater locations in residential oven cavity.

The unit was also equipped with thermocouples to measure wall and air temperatures during the cycle. The proposed study focused on a traditional bake (TB) mode that cycles bake and broil elements but does not use the convection fan. This mode is radiation dominated with a small amount of free convection from the air currents within the oven cavity. Three rack positions were used for this study based on the usable positions in this oven. Measured from the bottom of the cavity, the bottom rack was 5.75 inches up, the middle rack was 8 inches up, and the top rack was 12.75 inches up. Additionally, the rack was modified with a wire mesh to ensure consistent placement of the two cake tins used as shown in Figure 3-6.



Figure 3-6 Wire mesh modifications made to the oven rack to allow repeatable placement of the cake tins across multiple tests.

3.4 Cake Baking Process

The cakes baked in this experiment were prepared in modified cake tins identical to those used for the thermal energy sensors. A small hole was cut in the side of the tin at a point roughly half the average center height of a baked cake. A piece of food grade silicone was adhered over the hole in the cake tin so a two-inch thermocouple needle probe could be inserted through the silicone into the center of the cake tin as seen in Figure 3-7.



Figure 3-7 Modified cake tin with a needle probe to allow internal temperature measurement of the cakes while baking.

Boxes of cake mix of a single lot were used in preparing the cakes for this study to maximize repeatability. The batter was prepared according to package instructions, adding oil, water, and egg whites to the dry mix. Development testing indicated that 77g of batter per four-inch cake tin would provide baked cakes with varying degrees of browning all within the life of the sensor in an oven up to 375°F. Two cakes were placed in the oven once a steady state oven temperature was achieved and baked for the time indicated for each test. Once completed, the cakes were removed from the oven so measurements could be taken. Figure 3-8 shows the center oven air temperature for an example cycle with each portion of the test cycle labeled.

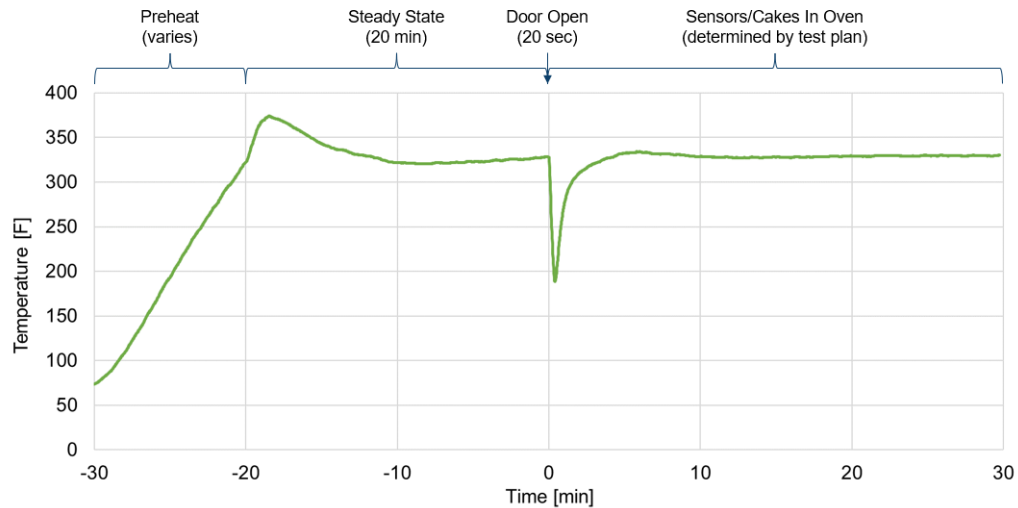


Figure 3-8 Center oven air temperature of Test Run 4 (325°F, middle rack, 30 minutes) with labeled cycle stages.

3.5 Cake Performance Criteria

To correlate thermal energy data to cake baking performance, metrics of the cake were measured. These metrics include browning, porosity, rise height, and mass loss.

Browning measurements were taken using a VeriVide DigiEye 700mm Cube color measurement system (DigiEye) seen in Figure 3-9. As with many of the studies listed in the literature review, color can be measured using the CIELAB color space. This color space consists of three main components: L^* , a^* , and b^* . L^* is a measure of the degree of lightness to darkness on a scale of 0-100 with a zero indicating completely white and 100 indicating completely black. Red and green are measured by a^* (negative values are red and positive values are green) while b^* indicates blue and yellow colors (positive for blue and

negative for yellow). Together, the L^* , a^* , and b^* values represent a point in the three dimensional “color space.” The DigiEye system was calibrated to D65 Standard Lighting and images were captured of the top and bottom of the cakes after they had cooled for 15 minutes and been removed from the cake tins. The images were then analyzed and average values of L^* , a^* , and b^* were taken for each side of the cakes.

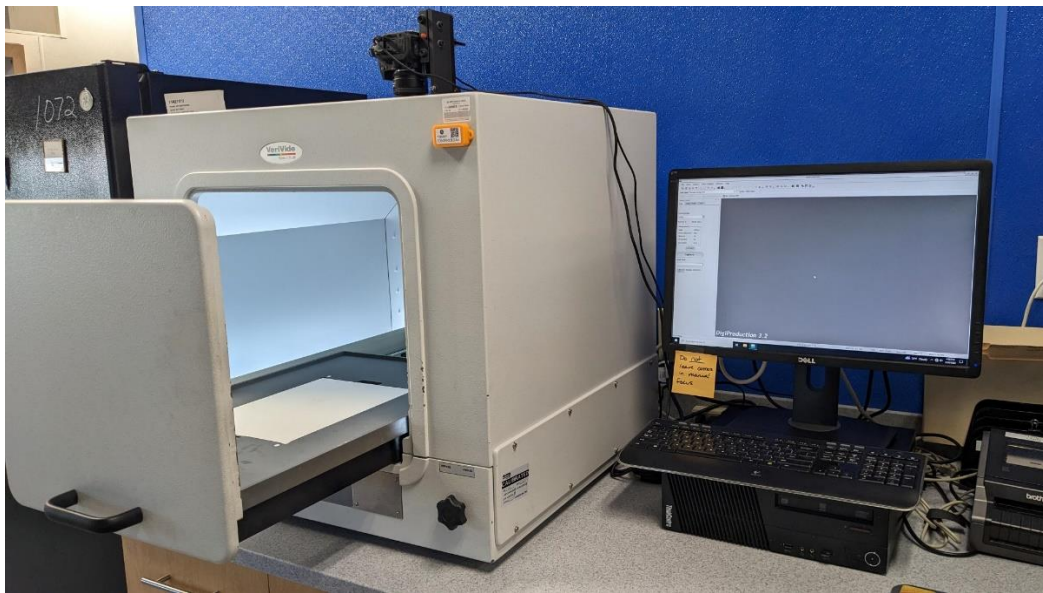


Figure 3-9 VeriVide DigiEye System used to capture images for color analysis. The system was calibrated to D65 Standard Lighting.

After color measurements were taken, each cake was cut in half based on its orientation in the oven during baking. The cakes were cut from their front most position straight back, creating a left and right side relative to the oven front. The porosity of the cakes was measured by imaging a cross section of each cake in the same DigiEye system. Each image was cropped to remove the crust and a filter applied with a threshold L^* value. Anything higher than the value selected

was considered dark enough to be an air cell and everything lighter was cake crumb. Figure 3-10 shows an example image of porosity analysis. The percentage of pixels considered to be air cells was reported as air cell percent area.

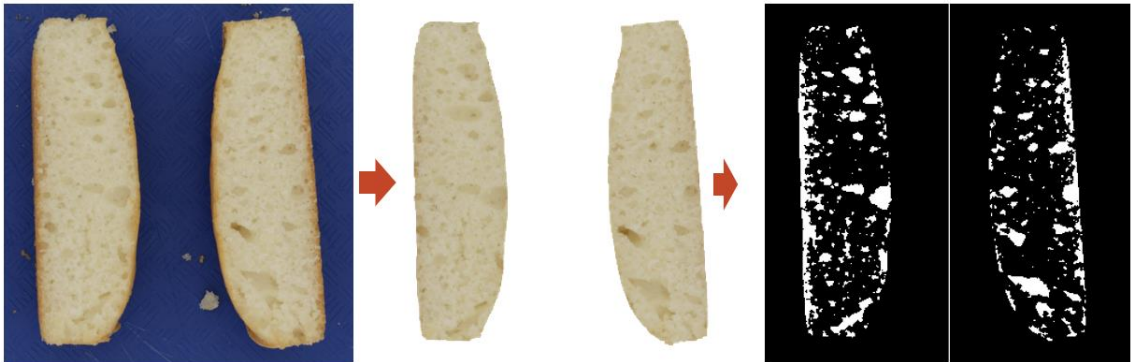


Figure 3-10 Example of image analysis process to determine the percentage air cell area of cake cross section.

Rise height was measured in two ways: side rise and center rise. The side rise was measured by placing the cross section cut from the center of the cake on a flat surface and using digital calipers to measure the distance from the table surface to the top of the cake, as seen in Figure 3-11. The measurement locations for side rise were 0.25 in from the edge of the cross section to avoid unique behavior of the cake at the side walls that can occur. The center rise was measured as the distance from the flat surface to the top of the cake directly in the center of the four-inch diameter round.

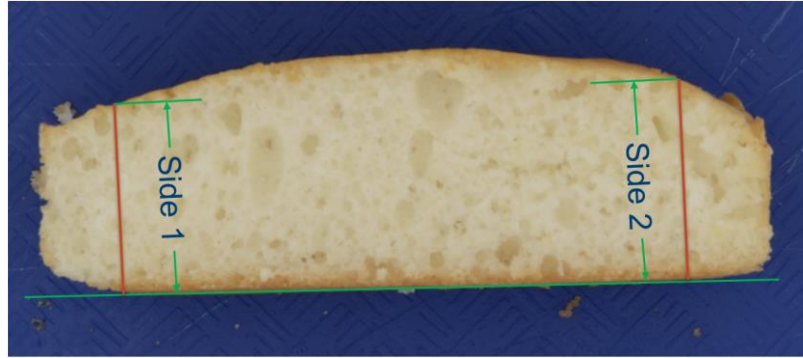


Figure 3-11 View of where the side rise measurements were taken for each cake.

Last, the mass loss was measured by subtracting the initial batter mass in the tins from the mass of the cakes immediately out of the oven. As the cakes bake, the water in the batter is converted to steam and leaves the cake. Moisture loss can be viewed as a metric of how moist the final cake product is. Excessive moisture loss indicates a dry cake which would not be a desirable outcome.

3.6 Experimental Test Plan

To generate correlations between cake performance and thermal energy data, two sets of data were required using matching oven conditions. The first set of data was collected by a pair of cake tin thermal energy sensors as described in Section 3.1 and 3.2. To begin the test procedure, the oven was preheated to the desired temperature setpoint. Once preheated, the oven was allowed to run for 20 minutes to reach a steady state temperature condition. Then the door of the oven was opened, and the thermal energy sensors were placed on the rack. The black sticker (high emissivity) sensor was placed on the left and the gold sticker (low emissivity) sensor was placed on the right. The door of the oven was

open for roughly 20 seconds each test before being closed. Once the test time had elapsed, the oven was turned off and the sensors were allowed to cool.

The second set of data used the same oven test configuration as the thermal energy sensors, but instead of placing the thermal energy sensors in the oven, cake tins with raw batter were used. Once the bake time was complete, the cakes were removed from the oven so measurements of the quality metrics listed in Section 3.5 could be measured.

To create a range of cake qualities for correlation, three center oven temperatures were chosen to bake cakes, and several bake times were selected. Testing was done for each of the three set temperatures; 325°F, 350°F, and 375°F, to identify the minimum time in the oven that would allow the internal structure of the cakes to solidify, but minimize browning. These times were found to be 15, 12, and 10 minutes, respectively. Then, the sensors were placed in the oven at each temperature setpoint and allowed to run until the heat flux sensor mounted to the top mass reached 250°F. This was used as the maximum time a cake could be baked and still have a matching sensor run without damaging the heat flux sensors. Two more bake times were selected at even increments between the maximum and minimum run times for each set temperature. The four tests show how cake baking performance varies with time in the oven, and therefore thermal energy input, changes. Additionally, each setpoint was tested at different rack positions. The maximum and minimum times were run for the highest and lowest rack positions in the oven to observe the differences in thermal energy based on location in the oven. The test plan was then

randomized in run order to spread any potential errors caused by testing on different days between all testing. A complete table of the conditions of each test performed can be found in Table 3-1.

Table 3-1 Complete test plan performed once with cakes and once with thermal energy sensors for a total of 48 tests including the randomized run order.

Run Order	Test Number	Temp Setpoint	Cook Time	Rack Position
[-]	[-]	[F]	[min]	[-]
10	1	325	15	Mid
2	2	325	20	Mid
12	3	325	25	Mid
1	4	325	30	Mid
4	5	325	15	Bot
16	6	325	30	Bot
8	7	325	15	Top
5	8	325	30	Top
23	9	350	12	Mid
7	10	350	17	Mid
13	11	350	22	Mid
17	12	350	27	Mid
24	13	350	12	Bot
15	14	350	27	Bot
11	15	350	12	Top
22	16	350	27	Top
9	17	375	10	Mid
18	18	375	14	Mid
3	19	375	18	Mid
20	20	375	22	Mid
6	21	375	10	Bot
14	22	375	22	Bot
21	23	375	10	Top
19	24	375	22	Top

4 SENSOR TEST RESULTS

In the following section the thermal energy sensor results of the test plan outlined in the Test Setup chapter will be discussed. Section 4.1 discusses the heat flux measurements into the top and bottom of each sensor measured as a function of time. Section 4.2 investigates the ratios between the different modes of heat transfer and the effect of oven temperature and rack position. In section 4.3, the effect of rack position on thermal energy data will be discussed. Finally, section 4.4 covers repeatability of the thermal energy measurements.

4.1 Flux Measurements

The thermal energy sensors produced four readings: heat flux from the HukseFlux sensors reported in mV, the temperature of the HukseFlux sensor, the temperature of the top aluminum mass, and the temperature of the bottom aluminum mass. As stated in section 3.1, the heat flux is converted from a voltage reading to heat flux using a calibration constant for each sensor. The temperature of the sensor is recorded and monitored to ensure the sensor does not exceed its maximum temperature threshold. The bottom mass temperature is used to calculate the energy stored in the aluminum mass over the course of one test, and indirectly the conduction. Figure 4-1 shows a plot of the top heat flux measurements collected for one of the test runs.

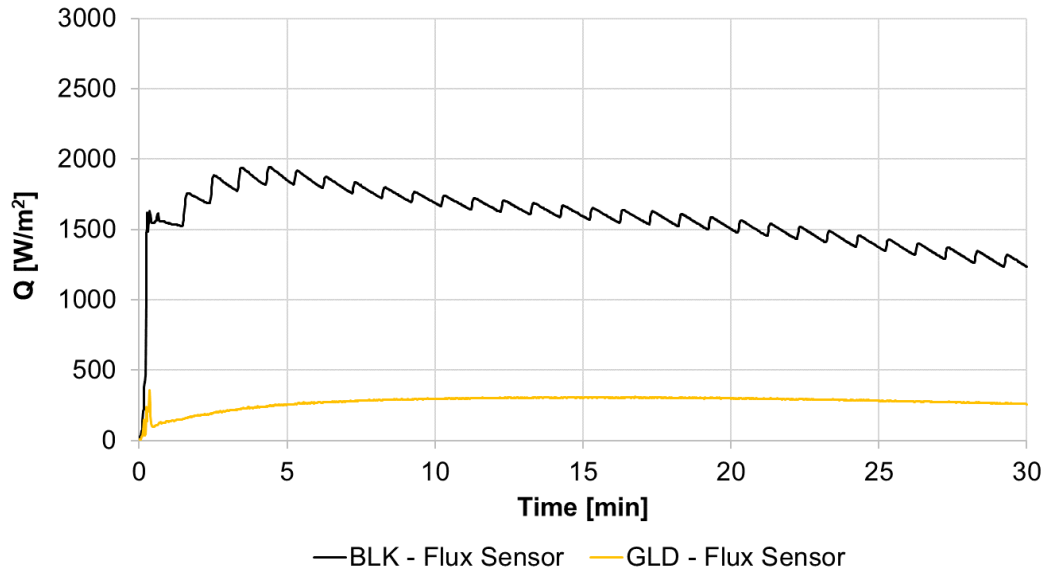


Figure 4-1 Heat flux measurements into the top of the thermal energy sensors from Run 4 of the test plan, oven temperature of 325°F and run for 30 minutes on the middle rack.

The heat flux sensors mounted to the top of the thermal energy sensor assembly begin each test reading zero flux as the sensors are resting at room temperature with no heat applied. Once placed in the oven, the heat flux measured from the black sensors jumps significantly. The gold sensor spikes slightly when first placed in the oven, but nowhere near the level of the black sensor. This suggests that throughout the test, heat flux into the top of the sensor is dominated by radiation as expected.

When it comes to the shape of the top heat flux curve in Figure 4-1, the total flux measured by the black sensor does not reach a peak until four to five minutes into the cycle. After the temperature drop caused by a door opening, the oven heaters cycle more aggressively to return to the desired temperature

setpoint quickly. This causes the flux measured to increase as heat is added to the environment. Once cycling behavior returns to normal and the heat added is simply to maintain the environment, the measured flux stabilizes.

Figure 4-2 below shows the oven temperature behavior over the course of a cycle to understand why flux changes as it does. When the oven door is opened, hot air rushes out and is replaced by cool air from the room which reduces the oven air temperature by over 100°F. It takes time for the air in the oven to come back to temperature so initial free convection will be low. The surfaces of the oven (labeled as bottom center, wall center, etc.) will also drop in temperature with the door opening, but significantly less than the air temperature. As a result, the radiation from the oven walls will be responsible for nearly all the early flux absorbed by the top of the sensors.

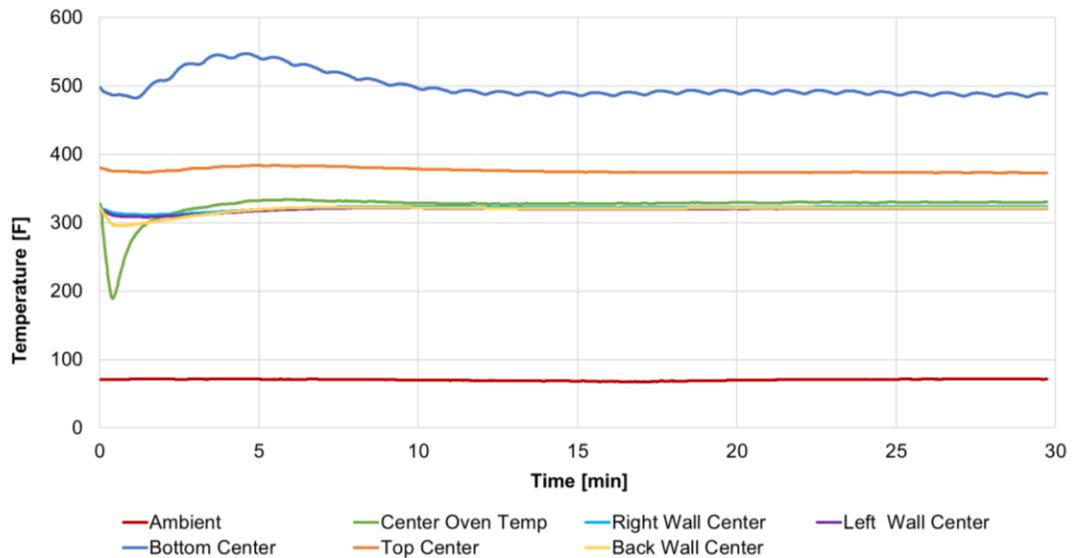


Figure 4-2 Oven temperature plot for Run 4 of the test plan, oven temperature set to 325°F and run for 30 minutes on the middle rack.

There is also an interesting sawtooth pattern visible only in the black sensor heat flux measurement (Figure 4-1). The pattern of heat flux readings matches exactly with cycling behavior of the broil element. The heating elements produce direct radiative energy to the oven when they are turned on. The gold sensor does not see this cycling because it is only capable of measuring convection energy. The air is maintained at a constant temperature and no forced convection is moving air across the sensor. Therefore, element cycling does not have a direct impact on the gold sensor whereas the black sensor (capable of measuring radiation) reflects heating element duty cycles.

Looking next at the heat flux into the bottom masses (Figure 4-3), the gold and black sensors are very similar as expected. Both sensors have a thermocouple in an aluminum mass that is used to calculate energy storage. In this case, the initial spike in flux is likely due to the rapid heat transfer from the stored energy in the oven racks to the bottom of the sensors. From there, the flux drops as the temperature of the aluminum mass increases and the difference between ambient temperature and the mass temperature decreases. Plots of the top flux, bottom flux, sensor temperature, and energy absorbed for each test can be found in Appendix C.

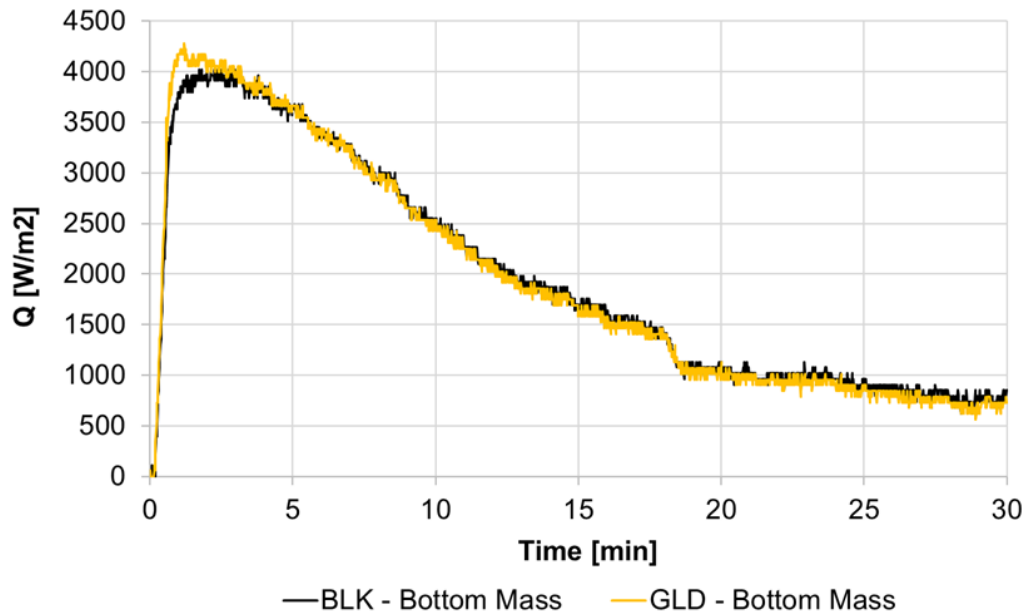


Figure 4-3 Conductive heat flux measured from thermal energy sensors in Run 4 of the test plan, oven temperature of 325°F and run for 30 minutes on the middle rack.

A quantity used in later sections is the total energy absorbed by the thermal sensor, calculated by summing the instantaneous heat flux measured each second. The energy was calculated for both the top and bottom of each thermal energy sensor to identify the three modes of heat transfer. The energy of the bottom mass of the two sensors was averaged together for a single conduction energy value for the cycle. The convection energy absorbed came directly from heat flux measured by the gold sensor and the radiation energy was calculated by subtracting the energy of the gold sensor from the black sensor to isolate the radiation component. The calculated energy absorbed from each heat transfer mode can be seen in Table 4-1. From this data, conduction is by far the most dominant mode of heat transfer followed by radiation. Very little convection

is measured, likely because no fan is running. The convection energy in these tests is from free convection and not forced convection. Most of the correlations developed in Chapter 5 use the end of cycle energy values from Table 4-1.

Table 4-1 Heat energy absorbed by the thermal energy sensors split by heat transfer mode.

Test Plan				End of Cycle Energy In			
Test #	Temp Setpoint	Cook Time	Rack Position	Conduction	Convection	Radiation	Total Energy
[-]	[F]	[min]	[-]	[J]	[J]	[J]	[J]
1	325	15	Mid	6630	599	3400	10630
2	325	20	Mid	7852	842	4511	13205
3	325	25	Mid	8521	1060	5282	14863
4	325	30	Mid	9079	1268	6086	16433
5	325	15	Bot	6769	575	3206	10550
6	325	30	Bot	9330	1236	5791	16356
7	325	15	Top	6708	686	3488	10882
8	325	30	Top	9212	1444	6355	17012
9	350	12	Mid	6370	538	3373	10281
10	350	17	Mid	7799	790	4450	13039
11	350	22	Mid	8922	1060	5619	15601
12	350	27	Mid	9776	1321	6765	17862
13	350	12	Bot	6427	503	3026	9956
14	350	27	Bot	9960	1272	6181	17412
15	350	12	Top	6481	605	3352	10438
16	350	27	Top	9878	1534	7310	18722
17	375	10	Mid	6173	473	3170	9815
18	375	14	Mid	7725	715	4356	12796
19	375	18	Mid	8932	946	5420	15299
20	375	22	Mid	9871	1199	6511	17581
21	375	10	Bot	6239	445	2923	9608
22	375	22	Bot	9909	1154	6127	17190
23	375	10	Top	6177	568	3321	10067
24	375	22	Top	9810	1346	6694	17850

The uncertainty of the end of cycle energy calculation was determined based on the measurement uncertainty of the respective sensing technology. The top heat flux sensor uncertainty was used for convection and radiation while the thermocouple and aluminum mass scale were used for conduction. The total

uncertainty by the end of cycle was roughly 390 J (8%) for the top flux sensor and 170 J (3%) for energy into the bottom of the sensors. Table 4-2 shows the uncertainty values from the measurement instruments of the top and bottom of the thermal energy sensors and the uncertainty of the final energy measurements. The percentage of uncertainty was calculated as a ratio of uncertainty to average convection plus radiation energy or conduction energy for the bottom and top uncertainty respectively.

Table 4-2 Uncertainty analysis for total energy absorbed by thermal energy sensors divided into (a) the bottom mass and (b) the heat flux sensor.

Bottom Mass Energy Storage (Conduction)		Heat flux Sensors (Convection and Radiation)	
Avg Mass	87.9 g	Hukseflux Sensor Uncertainty	5.7E-07 V/(W/m ²)
Mass Uncertainty	0.1 g	Average Power Uncertainty	0.215 W
Temperature Delta	100 K	End of Cycle Top Sensor Energy Uncertainty	387 J (8%)
Temperature Uncertainty	1.5 K		
End of Cycle Bottom Sensor Energy Uncertainty	167 J (3%)		

$$q_{cond} = mc_p(T_f - T_i)$$

$$\sum q_{top,inst}$$

4.2 Heat Ratios

With the three components of heat transfer independently measured, the ratios between conduction, convection, and radiation could be calculated with respect to time. Figure 4-4 shows an example of total energy absorbed over the course of a single cycle. While the rate of conduction energy in begins higher than convection or radiation, that rate falls off as the test continues resulting in larger ratios of convection and radiation for longer cycles.

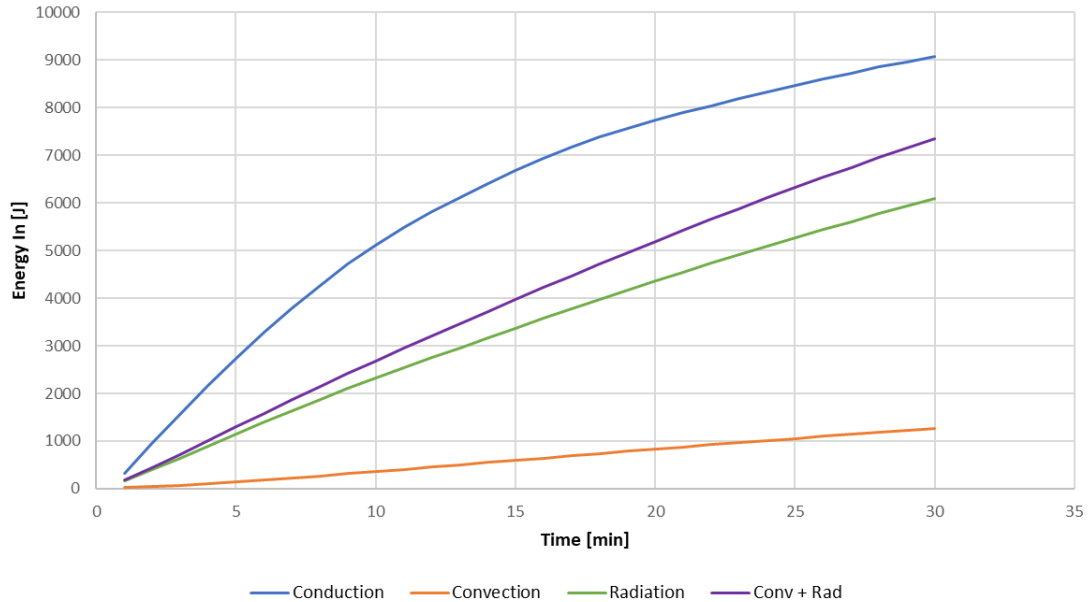


Figure 4-4 Total energy absorbed by the thermal energy sensors by heat transfer mode over the course of a cycle, specifically Run 4 with oven temperature of 325°F and 30 minutes on the middle rack.

Table 4-3 shows the total energy absorbed at the end of a test and the heat transfer ratios. A few trends are immediately obvious when looking at the heat ratio data. First, conduction is by far the most dominant mode of heat transfer in all cases with an average of 59% across all tests. Radiation is the next highest ratio with an average of 35% and finally the convection ratio averaged at 6%. The very low convection heat is expected for this bake cycle without any forced convection fan. All the convection measured by the sensor is due to free convection within the oven cavity. The conduction measured through the bottom of the thermal energy sensors is high in part because energy absorbed by the side walls of the cake tin conducts rapidly to the bottom aluminum mass used to calculate conduction energy in. Radiation, however, is only measured through

the top surface of the sensor. Figure 4-5 shows a pie chart graphic of the average heat absorbed from all middle rack oven tests split by heat transfer mode.

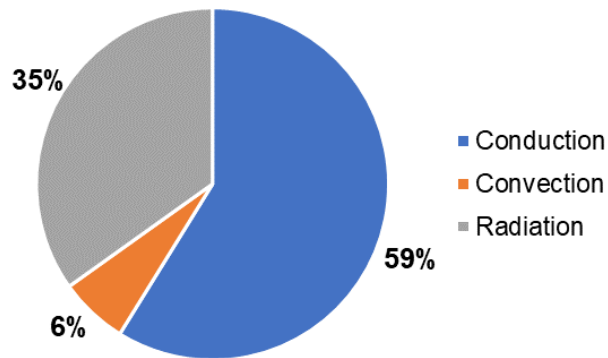


Figure 4-5 Average heat absorbed from all middle rack oven tests split by heat transfer mode.

Additionally, the heat ratios change with time in the oven. Regardless of the temperature setpoint, the longer the sensors are in the oven, the lower the conduction ratio measured. Inversely, convection and radiation ratios increase with time in the oven. This is likely because initially, the heat absorbed by the sensors is driven by the stored energy in the walls of the oven from the preheat portion of the cycle. Once in the oven for some time, all the new energy introduced comes from the heating elements like the broil element which radiates to the surface of the sensors.

Table 4-3 Ratios of the total energy into the sensors broken down by mode of heat transfer.

Test Number	Temp Setpoint	Cook Time	Rack Position	Conduction Ratio	Convection Ratio	Radiation Ratio	Total Energy
[-]	[F]	[min]	[-]	[%]	[%]	[%]	[J]
1	325	15	Mid	62.4	5.6	32.0	10630
2	325	20	Mid	59.5	6.4	34.2	13205
3	325	25	Mid	57.3	7.1	35.5	14863
4	325	30	Mid	55.3	7.7	37.0	16433
5	325	15	Bot	64.2	5.4	30.4	10550
6	325	30	Bot	57.0	7.6	35.4	16356
7	325	15	Top	61.6	6.3	32.0	10882
8	325	30	Top	54.2	8.5	37.4	17012
9	350	12	Mid	62.0	5.2	32.8	10281
10	350	17	Mid	59.8	6.1	34.1	13039
11	350	22	Mid	57.2	6.8	36.0	15601
12	350	27	Mid	54.7	7.4	37.9	17862
13	350	12	Bot	64.6	5.1	30.4	9956
14	350	27	Bot	57.2	7.3	35.5	17412
15	350	12	Top	62.1	5.8	32.1	10438
16	350	27	Top	52.8	8.2	39.0	18722
17	375	10	Mid	62.9	4.8	32.3	9815
18	375	14	Mid	60.4	5.6	34.0	12796
19	375	18	Mid	58.4	6.2	35.4	15299
20	375	22	Mid	56.1	6.8	37.0	17581
21	375	10	Bot	64.9	4.6	30.4	9608
22	375	22	Bot	57.6	6.7	35.6	17190
23	375	10	Top	61.4	5.6	33.0	10067
24	375	22	Top	55.0	7.5	37.5	17850

4.3 Rack Positions

One of the parameters varied between tests was the rack position within the oven. Data from the test plan would indicate if location in the oven alters the ratios of heat absorbed by the thermal energy sensors. By comparing tests with the same temperature and time in the oven, the impact of rack position can be seen directly. In Table 4-4, the test data is rearranged by temperature and time to view changes in rack position and the effect on heat ratios. The longest test cycles on each rack emphasize the differences.

Table 4-4 Ratios of heat transfer absorbed by mode, specifically the top, middle, and bottom rack runs at their respective maximum bake times.

Test Plan				Heat Transfer Mode Ratios		
Test #	Temp Setpoint	Cook Time	Rack Position	Conduction Ratio	Convection Ratio	Radiation Ratio
[-]	[F]	[min]	[-]	[%]	[%]	[%]
8	325	30	Top	54.15	8.49	37.36
4	325	30	Mid	55.25	7.71	37.04
6	325	30	Bot	57.04	7.55	35.41
16	350	27	Top	52.76	8.19	39.04
12	350	27	Mid	54.73	7.40	37.87
14	350	27	Bot	57.20	7.31	35.50
24	375	22	Top	54.96	7.54	37.50
20	375	22	Mid	56.14	6.82	37.03
22	375	22	Bot	57.64	6.72	35.64

The higher rack position resulted in a smaller conduction heat ratio, which matches expectations. As the sensor gets further from the bake element at the bottom of the unit, a smaller portion of the total heat absorbed comes from conduction. Inversely, the higher the sensors within the oven cavity, the higher the percentage of radiation energy absorbed. The change between the top and bottom rack is only a few hundred watts in all cases, not enough to cause

significant differences in cake performance. Figures 4-6, 4-7, and 4-8 examine the changes in each heat transfer mode between top, middle, and bottom rack for each temperature setpoint at the maximum time in the oven. These charts again confirm that as the cakes go from the top rack to bottom rack, conduction increases while convection and radiation decrease.

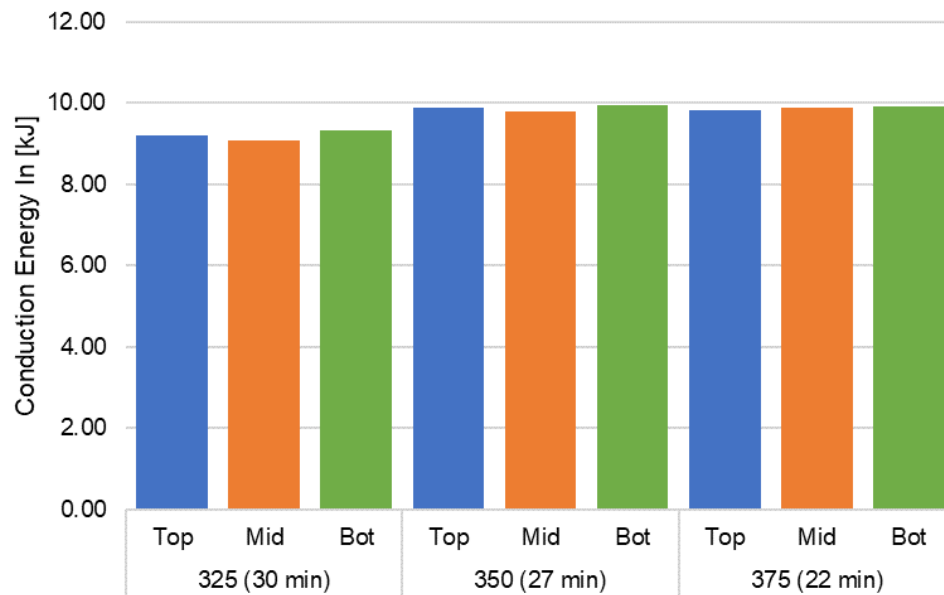


Figure 4-6 Conduction energy absorbed during top, middle, and bottom rack tests at maximum bake times for each temperature setpoint.

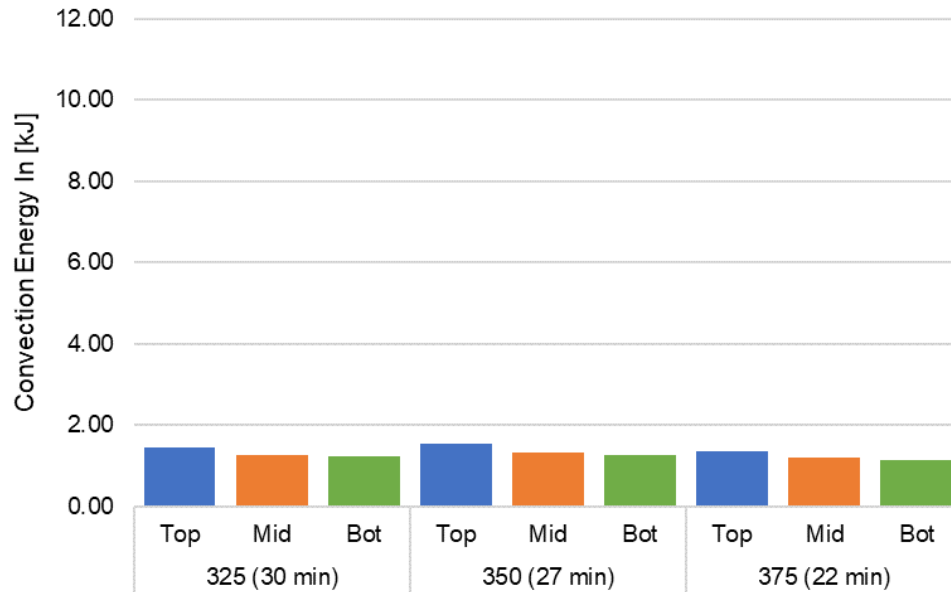


Figure 4-7 Convection energy absorbed during top, middle, and bottom rack tests at maximum bake times for each temperature setpoint.

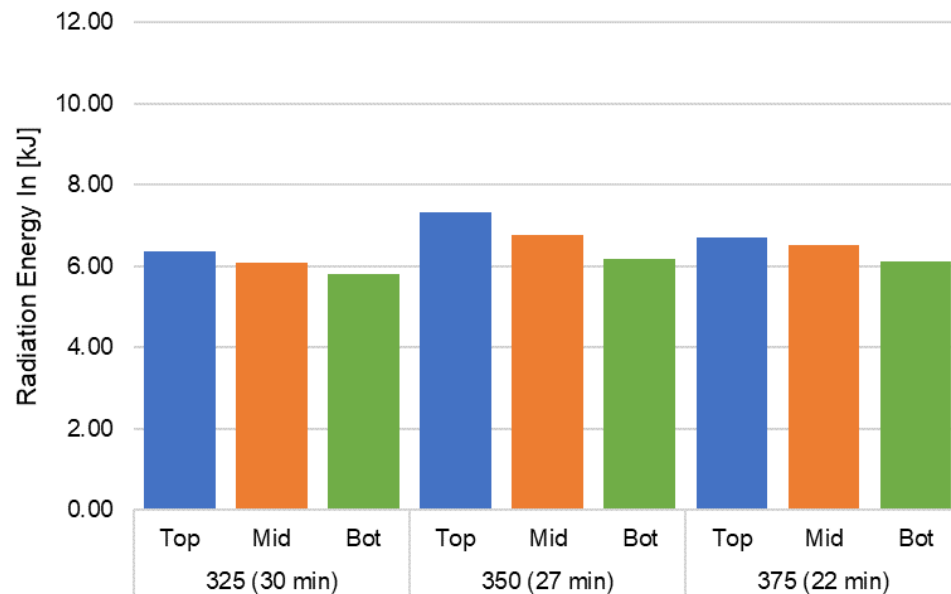


Figure 4-8 Radiation energy absorbed during top, middle, and bottom rack tests at maximum bake times for each temperature setpoint.

When studying correlations between thermal energy data and cake baking performance, some of the data from the test plan listed above will be left out. The tests on top and bottom rack positions were run for either the maximum or minimum times for the respective temperatures. If used in developing correlations, a significant amount of data would be positioned at the end points of the expected range. Using a majority of data at the extremes would reduce the impact of mid-range data on the final correlations, especially if there is a degree of non-linearity in the data. Additionally, the top and bottom rack heating could produce different results in the cake performance, making correlations difficult. In the following chapter, only mid rack data will be used to generate correlations between thermal energy and baking performance. The data on bottom and top racks can be used for future investigations.

4.4 Thermal Energy Sensor Repeatability

With the test plan above, there are no directly repeated tests. This makes it difficult to see repeatability for the sensor tests. For the sensors, both are required to calculate the energy from the test. However, it is possible to use a subset of the sensor test data to understand the test to test repeatability within a given setpoint. The mid rack cycles each have four tests repeated at identical conditions with increasing bake times. The beginning of each cycle is the same up until the point where the sensors are removed from the oven in the shortest test. The energy absorbed by the sensors can be calculated at each minute for all tests and it is expected that at any time before the sensors are removed, all four tests should read the same.

Table 4-5 shows the repeatability indicated by coefficient of variation for the four 350°F setpoint tests. Data was collected every second, and each minute a summation of the energy absorbed at that point in the cycle was calculated to produce the repeatability data. The tables showing middle rack thermal sensor repeatability for all setpoints can be found in Appendix B.

Table 4-5 Repeatability data based on four runs (350°F, mid rack) using coefficient of variation. Colors show comparison of relative values, green is smaller and red is larger.

Cycle Time	Black Sensor (Left)		Gold Sensor (Right)	
	Top Mass	Bottom Mass	Top Mass	Bottom Mass
[min]	[%]	[%]	[%]	[%]
1	4.14	4.87	2.25	6.28
2	2.52	1.29	2.06	2.17
3	2.06	1.29	1.66	0.93
4	1.74	1.88	1.44	0.69
5	1.53	1.38	1.34	0.37
6	1.47	1.46	1.31	0.74
7	1.49	1.15	1.34	0.80
8	1.56	0.83	1.38	0.59
9	1.63	0.74	1.40	0.80
10	1.69	0.70	1.43	0.63
11	1.75	0.52	1.43	0.73
12	1.79	0.59	1.42	0.84

Coefficient of variation is a metric used to determine the repeatability of measurements. It represents the ratio of standard deviation, σ , and the mean of a set of measurements, μ , as a percentage according to the equation:

$$COV = \frac{\sigma}{\mu} \quad (2)$$

For example, a coefficient of variation of 2% means the standard deviation of the measurements was 2% of the mean of that data set. In all cases, the longer the test ran, the less variation was observed between measurements. This makes sense as most of the variation between cycles will occur immediately as the sensors are placed in the oven. Slight inconsistencies in ambient temperature and sensor positioning as they are placed in the oven will alter how much heat is absorbed but those differences are minor compared to the magnitude of heat that will be absorbed by the end of the cycle. It is also worth noting that the heat absorbed by the top mass has a higher variation than the bottom mass. The top mass is more susceptible to variations in element cycling and the uncontrolled free convection in the oven cavity. The bottom mass conducts heat from the cake tin which acts as a buffer to changes in heat flux. In conclusion, the repeatability of the energy sensor data is promising, two percent or less variation in measurements between tests by the end of the cycle so the test process and equipment are acceptably repeatable.

5 CORRELATIONS

Using sensor thermal energy data and corresponding cake performance data, correlations can be developed to predict cooking performance based on energy data. In the following section, four cake quality characteristics will be investigated for correlation: top and bottom browning in Section 5.1, porosity in Section 5.2, rise height in Section 5.3, and mass loss in Section 5.4. As discussed in the previous section, all the following correlations will be made using the middle rack data of cake performance and thermal energy sensors.

5.1 Browning Correlation

One of the primary factors used to determine if a baked product is fully cooked is surface browning. Some degree of browning is desirable, but too much is not. Accurately predicting browning can improve the development of residential ovens and oven cycles. Browning in cakes is caused in part by two factors, the Millard reaction and caramelization of sugars. As described in Purlis (2010), the Millard reaction occurs when reducing sugars, amino acids, proteins, and other compounds are heated together and caramelization involves the direct heating of carbohydrates like sucrose. Both processes require heat to be absorbed so if heat flux data can be used to estimate the degree of browning, oven parameters can be tuned before any food is prepared.

Browning is typically measured by color change and the color data was collected using a DigiEye color measurement system. Once the cakes had baked and cooled for 15 minutes, they were removed from their tins and placed in the calibrated imaging chamber. Images were captured for later analysis using the DigiEye software. Simple color filters were used to isolate the cakes from the background color and the average color readings of the remaining image were calculated. As each test run involved two cakes baked simultaneously, the average of the two cakes was taken as the browning value for each test.

With regards to measuring color change within the CIELAB color space, most researchers use the statistic ΔE which represents the distance between two points in a three dimensional 'color space.' The coordinates of this color space are L^* , the measure of lightness or darkness; a^* , the measure of redness or greenness; and b^* , the measure of blueness or yellowness. To calculate the total color change, the coordinate distance is calculated using the equation:

$$\Delta E = \sqrt{(\Delta L^*)^2 + (\Delta a^*)^2 + (\Delta b^*)^2} \quad (3)$$

Table 5-1 shows browning data collected for each test. The most obvious trend that stands out is increasing test time results in more heat absorbed so the cakes get darker (L^* decreases). For any given rack and setpoint, more energy absorbed results in a darker cake. Limited repeatability data is available because two cakes were baked for each test. In the case of browning, the average repeatability was 1.3% for top browning and 3.5% for bottom browning. All cake testing repeatability data is shown in Appendix E.

Table 5-1 Color data measured for top and bottom cake browning using DigiEye instrument.

Test Plan				Top Browning				Bottom Browning			
Test #	Temp Setpoint	Cook Time	Rack Position	L*	a*	b*	ΔE	L*	a*	b*	ΔE
[-]	[F]	[min]	[-]	[-]	[-]	[-]	[-]	[-]	[-]	[-]	[-]
1	325	15	Mid	79.6	1.7	24.7	10.6	79.5	2.2	22.9	8.8
2	325	20	Mid	74.2	5.5	30.3	16.4	71.5	8.1	31.2	18.5
3	325	25	Mid	68.2	11.4	38.2	26.8	62.2	16.0	38.2	31.1
4	325	30	Mid	66.5	15.9	40.3	31.0	59.3	21.0	40.6	36.6
5	325	15	Bot	81.5	1.9	25.2	11.6	79.4	2.2	22.6	8.4
6	325	30	Bot	59.9	21.7	40.7	36.8	49.2	24.2	37.2	42.0
7	325	15	Top	80.7	2.5	26.2	12.3	80.1	3.4	25.0	11.1
8	325	30	Top	61.0	19.9	40.6	35.4	56.0	22.4	40.5	39.0
9	350	12	Mid	78.3	1.7	24.6	10.2	78.7	2.9	23.2	8.9
10	350	17	Mid	74.9	7.3	32.8	19.1	69.6	11.6	33.4	22.3
11	350	22	Mid	63.8	15.7	39.4	31.2	57.5	19.3	38.3	35.1
12	350	27	Mid	58.5	20.6	40.1	36.5	51.6	23.9	38.3	40.9
13	350	12	Bot	81.6	2.0	25.3	11.8	77.2	3.8	24.9	10.5
14	350	27	Bot	60.8	17.9	39.9	33.9	51.3	23.3	38.6	41.0
15	350	12	Top	78.4	2.2	25.4	11.0	80.9	3.6	25.7	12.0
16	350	27	Top	54.8	22.2	38.6	38.3	48.3	23.5	36.8	42.0
17	375	10	Mid	79.1	1.6	24.6	10.3	81.8	2.6	23.3	10.1
18	375	14	Mid	74.3	7.9	33.2	19.7	68.2	13.0	34.4	24.2
19	375	18	Mid	66.0	15.3	39.4	30.2	55.1	19.8	37.2	36.1
20	375	22	Mid	58.4	21.1	40.2	36.9	49.0	23.5	37.1	41.7
21	375	10	Bot	78.9	1.7	25.0	10.6	80.9	1.9	21.5	8.1
22	375	22	Bot	58.9	18.6	39.4	34.8	49.1	23.1	37.0	41.4
23	375	10	Top	77.4	2.8	27.0	12.4	78.9	4.9	28.2	14.1
24	375	22	Top	54.8	21.9	38.6	38.1	47.1	23.5	35.9	42.4

When attempting to correlate thermal energy data to color change, there are two potential metrics to use, ΔE and L^* . From Silva et al. (2022) it is shown that as the surface temperature of a baked product increases, the color measurements change due to the browning process. As seen in Figure 5-1, the rate of this change is not always linear. Initially, no color change is observed but once some threshold temperature is achieved, browning starts. L^* then decreases linearly, becoming darker, while the a^* and b^* color metrics change in very nonlinear ways. As a result, ΔE also shows a small degree of nonlinearity. In this study, L^* will be used as the cooking performance metric for browning.

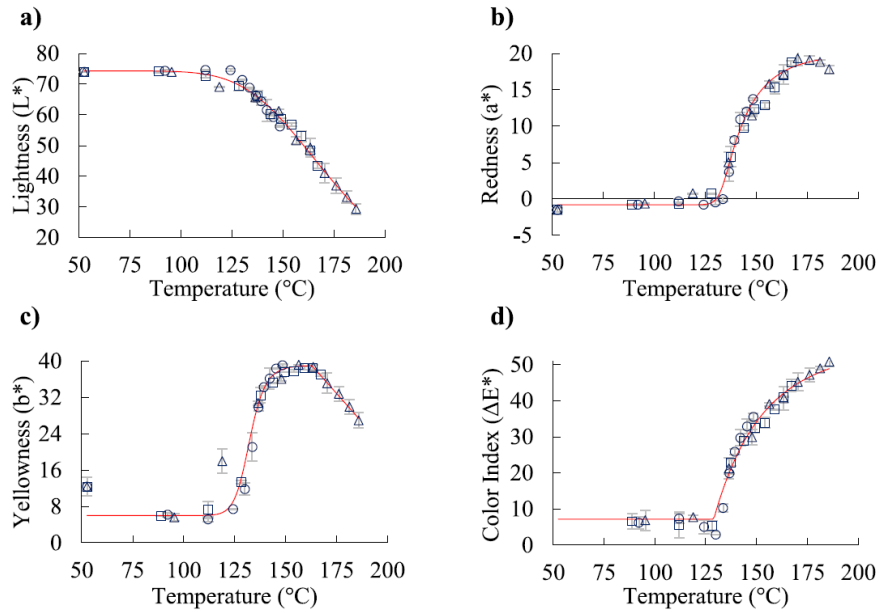


Figure 5-1 Color change of bread crust during the baking process (Silva et al., 2022).

5.1.1 Bottom Browning

To form a strong correlation between thermal energy and bottom browning of cakes, the first step is to determine which thermal energy values best correlate to browning. For a simple linear regression model, a stepwise analysis can be performed to identify which correlation factors are significant. Multiple predictor variables are used for a single response, in this case L* values from the bottom of the cakes, and each predictor has a p-value associated with it. A p-value of greater than 0.05 indicates that the predictor has no statistical significance in estimating the response variable. For this stepwise function, all three modes of heat transfer are used as initial predictors; the total energy absorbed by conduction, convection, and radiation over the test period. After the first stage of

the stepwise regression, the largest p-value is associated with radiation at 0.124. This indicates that radiation is not significant in predicting bottom browning which makes sense intuitively. Radiation measured from the top of the cakes will have little impact on the browning of the bottom. The stepwise is then continued without the radiation term, leaving only convection and conduction. Again, one of the predictors has a p-value above the threshold, this time convection with a 0.073 p-value. After convection is removed, only conduction remains with a p-value of zero. A simple linear regression using conduction energy absorbed to predict bottom L* values can be seen in Figure 5-2 below, with the associated equation and R² value. There is a grouping in the data points that is explained by the test plan. Each temperature setpoint has four evenly spaced times that vary based on the temperature setpoint. These were developed to provide the greatest range of cake browning from lightest to darkest within the life of the sensor in the oven. The groups of four points in Figure 5-2 follow the groupings of those times.

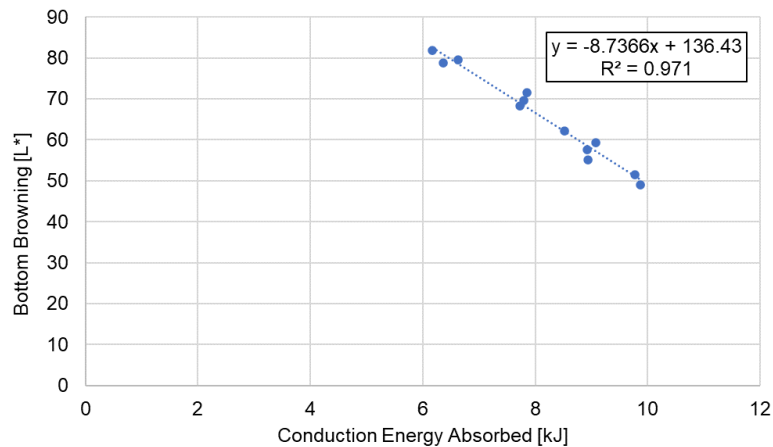


Figure 5-2 Correlation between bottom browning measured in L* and total conduction energy absorbed during the test cycle.

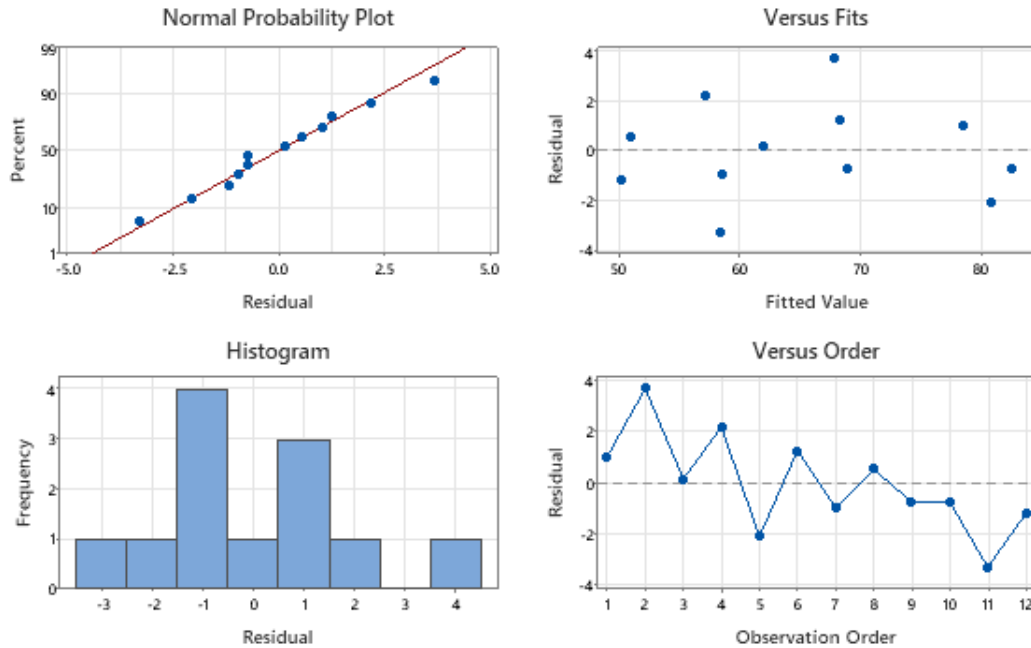


Figure 5-3 Residual plots for correlation model of bottom browning.

The R^2 value of the model is a measure of how well the regression fits the data, and a 97.1% R^2 is a very strong model. Additionally, Figure 5-3 shows plots of the residuals from this model. The Versus Fits plot shows a random distribution of residual values which indicates the linear model was a good choice. Nonlinearity would show patterns in the Versus Fits plot. Additionally, the Histogram of residuals fits a normal curve in shape and the Versus Order plot does not indicate a higher order of model would perform better. This suggests that the most dominant mode of heat transfer to bottom browning is conduction from the cake tin into the bottom of the cake.

It is also worth investigating potential interaction between heat transfer terms. This can be performed using the same stepwise regression process, but

new terms include the products of each heat transfer mode (conduction * convection, conduction * radiation, and convection * radiation). Table 5-2 below shows the process of backwards eliminating the least significant term until only significant terms are left in the model.

Table 5-2 Stepwise regression including interaction terms of each heat transfer mode.

Backward Elimination of Terms

Candidate terms: Conduction_kj, Convection_kj, Radiation_kj, Conduction_kj*Convection_kj, Conduction_kj*Radiation_kj, Convection_kj*Radiation_kj

	----Step 1----		-----Step 2-----		-----Step 3-----	
	Coef	P	Coef	P	Coef	P
Constant	86.3		82.6		116.1	
Conduction_kj	12.0	0.587	13.2	0.407	1.90	0.762
Convection_kj	25	0.923				
Radiation_kj	-21.7	0.546	-18.7	0.264	-12.2	0.371
Conduction_kj*Convection_kj	-10.4	0.773	-7.08	0.434		
Conduction_kj*Radiation_kj	-0.92	0.877	-1.483	0.138	-0.880	0.105
Convection_kj*Radiation_kj	17.6	0.289	17.4	0.243	6.39	0.055
S	1.76559		1.61341		1.57881	
R-sq	98.87%		98.87%		98.74%	
R-sq(adj)	97.52%		97.93%		98.02%	
Mallows' Cp	7.00		5.01		3.60	
AICc	101.19		79.22		67.35	
BIC	57.07		54.61		53.46	
	-----Step 4-----		-----Step 5-----			
	Coef	P	Coef	P		
Constant	118.1		101.70			
Conduction_kj						
Convection_kj						
Radiation_kj	-8.79	0.201				
Conduction_kj*Convection_kj						
Conduction_kj*Radiation_kj	-0.874	0.085	-1.448	0.000		
Convection_kj*Radiation_kj	5.60	0.001	4.97	0.002		
S	1.48730		1.56307			
R-sq	98.72%		98.41%			
R-sq(adj)	98.24%		98.06%			
Mallows' Cp	1.68		1.05			
AICc	58.72		55.04			
BIC	51.14		51.26			

α to remove = 0.1

As seen in Table 5-2, the significant terms are the two interaction terms conduction * radiation and convection * radiation. The R^2 value of this model is 98.4% which is about one percent higher than the simple linear model with conduction alone. When considering which model to use, the linear correlation is grounded in expected physics, with conduction directly impacting bottom browning. Using interaction terms improves the model slightly, however the product of two energy inputs does not have a significant physical meaning. Using the interaction terms would be purely mathematical and because the two models are nearly identical in performance, the linear correlation will be used moving forward. When designing an oven cycle, any changes that increase the ratio of bottom heat will increase the bottom browning of cakes.

5.1.2 Top Browning

Following a similar method to bottom browning, a stepwise regression was performed to correlate top browning with all three modes of heat transfer. The first correlations showed conduction to have the worst correlation with a 0.453 p-value. Once removed and rerun, both convection energy and radiation energy had a p-value of 0.037, below the 0.05 threshold of significance. However, there is another statistic called the variance inflation factor (VIF) that indicates the degree of cross correlation between variables in a linear regression. Typically, any value over 10 indicates significant cross correlation which means the two variables should not both be used in predicting the response. Using both convection and radiation, the VIF for each variable is 28. Therefore, even though the p-value of convection energy, at 0.037, is below the threshold it is removed

from the stepwise in favor of the radiation term which has a lower p-value. Repeating the regression once more with only radiation, the final model has a zero p-value and a 94.8% R^2 value indicating strong correlation between radiation energy and top browning. Figure 5-4 shows the linear correlation fitted to data and Figure 5-5 shows the statistical residuals of the model. Again, there is no suggestion of significant nonlinearity or non-normality in the model residuals, so the simple linear regression between radiation and top browning is sufficient.

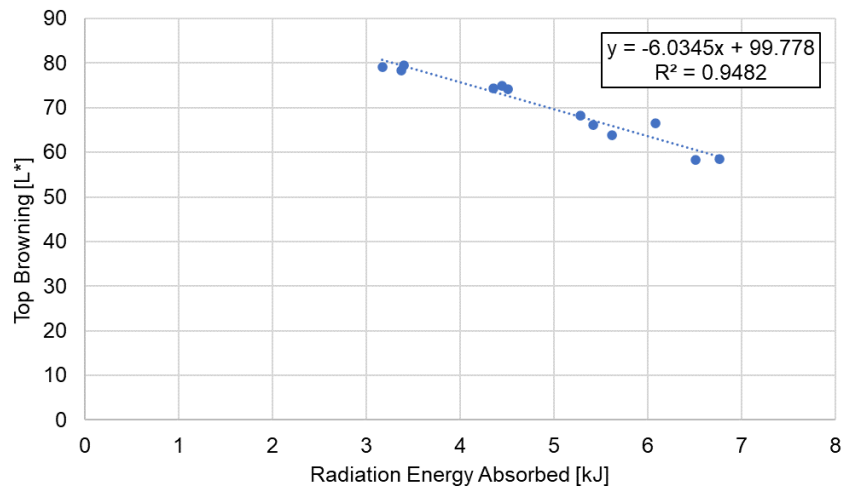


Figure 5-4 Correlation between top browning measured in L^* and total radiation energy absorbed during the test cycle.

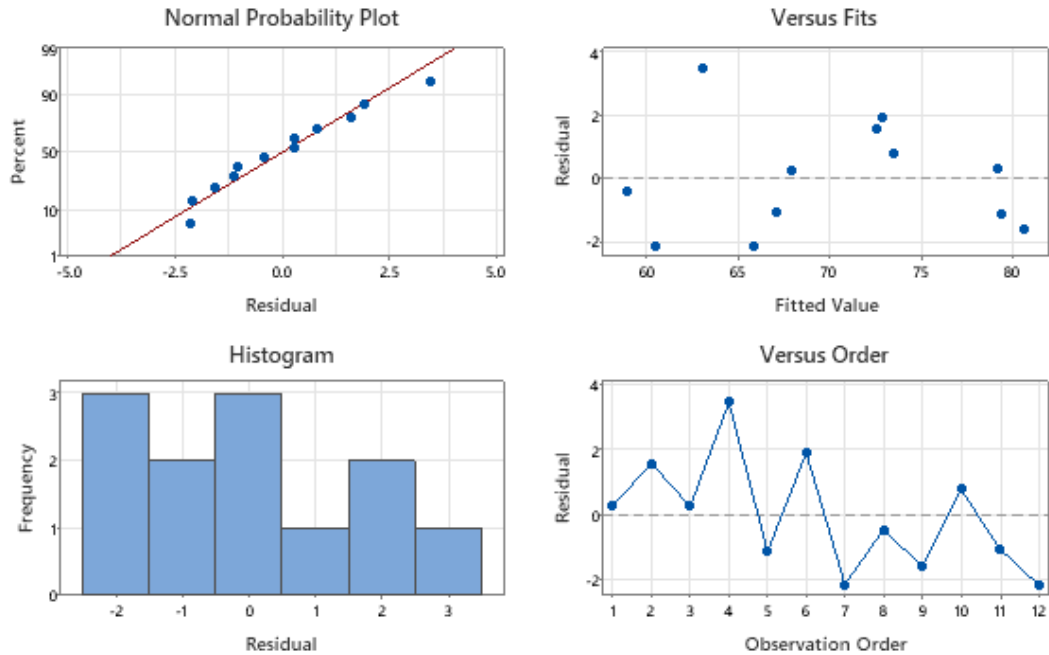


Figure 5-5 Residual plots for correlation model of top browning.

Physically, this means that radiation is the dominant mode of top browning in the case of a traditional bake cycle. This makes sense as a significant majority of the heat absorbed by the top of the cake is due to radiation. In a convection cycle, the convective component may take over but in the case of low airflow traditional bake modes, radiation is dominant.

5.1.3 Browning Model Error

The regression models that correlate heat absorbed to browning can be analyzed against the browning data from the cake tests to offer some idea of the accuracy of the model. Ideally, a second set of data would be generated to validate the model. However, given the time and material constraints on this study, the base data set is used in the error analysis. Using the regression

equations developed, the measured heat absorbed was used to calculate an estimated L* value of top and bottom browning. The estimated value was then compared to the actual measured value and the error, absolute error, and percent error were calculated. The data can be seen in Table 5-3.

Table 5-3 Top and bottom browning estimates and error calculations against true measured browning data.

Test Plan			Bottom Browning - Conduction Correlation				Top Browning - Radiation Correlation			
Test #	Temp Setpoint	Cook Time	Bottom L* Est	Error	Absolute Error	Percent Error	Top L* Est	Error	Absolute Error	Percent Error
[-]	[F]	[min]	[L*]	[L*]	[L*]	[%]	[L*]	[L*]	[L*]	[%]
1	325	15	78.5	-1.0	1.0	-1.3	79.3	-0.3	0.3	-0.4
2	325	20	67.8	-3.7	3.7	-5.2	72.6	-1.6	1.6	-2.2
3	325	25	62.0	-0.2	0.2	-0.3	67.9	-0.3	0.3	-0.4
4	325	30	57.1	-2.2	2.2	-3.7	63.1	-3.5	3.5	-5.2
9	350	12	80.8	2.1	2.1	2.6	79.4	1.1	1.1	1.4
10	350	17	68.3	-1.3	1.3	-1.8	72.9	-1.9	1.9	-2.6
11	350	22	58.5	0.9	0.9	1.6	65.9	2.1	2.1	3.3
12	350	27	51.0	-0.6	0.6	-1.1	59.0	0.4	0.4	0.7
17	375	10	82.5	0.7	0.7	0.9	80.7	1.6	1.6	2.0
18	375	14	68.9	0.7	0.7	1.1	73.5	-0.8	0.8	-1.1
19	375	18	58.4	3.3	3.3	5.9	67.1	1.0	1.0	1.6
20	375	22	50.2	1.2	1.2	2.4	60.5	2.1	2.1	3.6
			Minimum	-3.7	0.2	-5.2	Minimum	-3.5	0.3	-5.2
			Maximum	3.3	3.7	5.9	Maximum	2.1	3.5	3.6
			Average	0.0	1.5	0.1	Average	0.0	1.4	0.1

The error data confirms the good fit of this model in both top and bottom browning. In both cases, the average percentage error is 0.1% with a maximum of 5%-6% in any of the tests. The low average error indicates a good correlation, but the maximum errors give an idea of how accurate a prediction might be. Ideally, the model error would be measured using a validation data set. This data set would be collected in the same manner as the training set used to develop the model, but the validation set is used to test the model for accuracy. Unfortunately, time and cost constraints prevented the collection of a validation data set and with such a small set of remaining data, every point was needed for

the model. One method that could be implemented in the place of collecting more data is a k-fold cross validation test which splits data into multiple training and validation sets (Allen, 2012). This could be employed in the future, with or without additional data collected for validation.

An interesting follow up study would be what degree of browning difference is perceptible to the average baker. If the human eye is unable to detect a 5% difference in browning measurement for example, the model is as accurate as it would need to be. However, if a 1% difference in browning for example is very noticeable, the model would need further refining.

5.2 Porosity Correlation

The next cake performance metric analyzed was porosity. As discussed in Chapter 2, the porosity of baked goods is a determining factor in the perceived quality. Ideal structure can be interpreted differently based on the preferences of an individual, but estimating this quality can help with the development of baking cycles. For this testing and food recipe, a good structure requires a uniform and tight structure with small air cells evenly distributed and no large cavities or tunnels forming in the structure. As with the previous correlations, the goal is to provide a correlation between measured values from the thermal energy sensors and a metric representing the porosity of the fully cooked cakes.

The measurement process of porosity is described in detail in Chapter 3. The same DigiEye system from the browning measurements was used to analyze the porosity. The fully cooked cakes were cut along the center

and a cross section of each cake was imaged. A digital filter was then applied to the images to isolate the internal structure, removing the crust from the images. Another filter was applied to isolate all pixels dark enough to be considered an air cell while lighter pixels were considered crumb. Once the pixels were separated into air and crumb, the percentage of total area representing air cells was calculated. All test run data of porosity can be found in Table 5-4.

Table 5-4 Porosity measurements that represent the percentage of pixels that were classified as air cells.

Test #	Temp Setpoint	Cook Time	Porosity			Percent Difference
			Cake 1	Cake 2	Average	
[-]	[F]	[min]	[%]	[%]	[%]	[%]
1	325	15	14.3	18.2	16.2	23.5
2	325	20	17.0	18.8	17.9	10.3
3	325	25	21.8	27.0	24.4	21.4
4	325	30	25.0	20.7	22.9	18.9
5	325	15	19.1	15.9	17.5	18.6
6	325	30	21.0	21.5	21.2	2.0
7	325	15	17.1	20.1	18.6	15.9
8	325	30	21.7	20.2	21.0	7.4
9	350	12	19.5	11.9	15.7	48.6
10	350	17	16.5	23.7	20.1	36.0
11	350	22	15.4	17.2	16.3	10.7
12	350	27	14.4	22.4	18.4	43.3
13	350	12	15.9	12.6	14.3	23.2
14	350	27	22.5	13.8	18.2	47.6
15	350	12	17.3	18.9	18.1	9.1
16	350	27	26.1	25.8	26.0	1.1
17	375	10	22.5	22.1	22.3	1.6
18	375	14	22.3	24.0	23.1	7.3
19	375	18	24.2	25.0	24.6	3.5
20	375	22	12.6	18.4	15.5	37.1
21	375	10	24.4	2.2	13.3	--
22	375	22	24.4	17.4	20.9	33.8
23	375	10	15.5	18.0	16.7	15.0
24	375	22	26.0	15.2	20.6	52.3

What is immediately noticeable is the considerable variation that occurs in the test data. The percent difference between two values can be calculated by dividing the absolute difference by the average of the values. Excluding Run 21 as a measurement outlier (poor camera focus or bad calibration), between two cakes in the same run there is an average of 24% difference in the recorded

porosity. With this degree of variation, it is impossible to correlate results with heat flux data. Additionally, there are no noticeable patterns in the data that would indicate trends. Figure 5-6 shows the average porosity of each test as a function of total energy absorbed like the browning correlation.

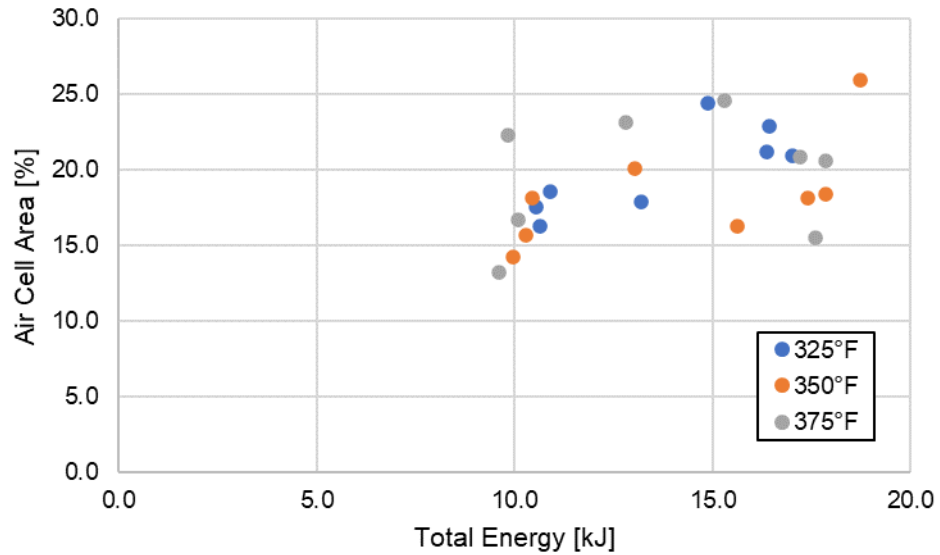


Figure 5-6 Air cell area data plotted against total thermal energy absorbed separated by test setpoint.

There are two possible reasons for the variation between cakes in a single test. First, the process of mixing the cake batter is a critical step in determining the structure of the cake. As many factors as possible were eliminated, using the same mixer, mixer attachment, mixing speed, mixing time, and so on. However, there can still be differences between the cakes caused when the cake tins are tamped against the counter to settle and even the batter. A second, and likely more important factor, is the resolution of the camera used to analyze the cake structure. For surface color measurements, the DigiEye system performs well.

The small texture of the internal structure may be of a low enough resolution that pixels on the edge of being considered air may be reading as crumb and vice versa. Each cake cross section measured roughly 400x1300 pixels. That means the area of each pixel is $\sim 0.003 \text{ in}^2$. Some of the air cells visible in the images are only a few pixels wide, so averaging of colors at the edges of these air cells may have played a part in the variation. A well-focused and high-resolution imaging system will better capture the porosity and perhaps identify correlations with the thermal energy data. It is also worth considering that the proposed test plan did not change the conditions that impact porosity enough to see noticeable differences. Oven cycles with even greater temperatures or more aggressive convection fan use might be required to measure considerable differences in porosity.

5.3 Rise Height Correlation

The amount of rise in a cake is another metric that should be understood when determining cake quality. A low rise can occur if the air in the batter was not able to expand enough before the physical structure is set. Similarly, a very high rise might have significant expansion of the air cells leading to large pockets in the cake structure. This metric could reveal trends that could not be seen in the porosity data. Two variations of rise were measured, side rise and center rise. The sides of the cakes, being closest to the baking tin, will set their structure first. The center of the cake is the last portion of the cake to come up to temperature and set its structure.

Once the fully cooked cakes cooled for 15 minutes they were removed from the tins and measured. Each cake was cut along a cross section and placed on a counter. Side rise data was recorded using a caliper to measure the distance from the counter to the top surface of left and right sides of the cross section. Both cakes from each test run were measured this way and the four side height measurements were averaged together for the side height value in Table 5-5. Similarly, a measurement at the center of each cake from the counter to the top surface was taken for center rise. The two measurements for each run were averaged to calculate the center rise data for each test. The repeatability for rise data can be found in Appendix E. Side rise has an average repeatability of 3% and center rise has an average repeatability of 2%.

Table 5-5 Center and side rise data collected for each test run. Average values were used in correlation calculations.

Test Plan				Center Rise			Side Rise		
Test Number	Temp Setpoint	Cook Time	Rack Position	Min	Max	Avg	Min	Max	Avg
[-]	[F]	[min]	[-]	[in]	[in]	[in]	[in]	[in]	[in]
1	325	15	Mid	1.33	1.36	1.34	0.99	1.07	1.02
2	325	20	Mid	1.25	1.29	1.27	0.92	1.04	0.99
3	325	25	Mid	1.26	1.27	1.26	0.90	1.01	0.97
4	325	30	Mid	1.16	1.20	1.18	0.90	0.97	0.93
5	325	15	Bot	1.26	1.28	1.27	0.97	1.05	1.01
6	325	30	Bot	1.18	1.19	1.18	0.85	0.92	0.88
7	325	15	Top	1.30	1.30	1.30	0.96	1.02	0.99
8	325	30	Top	1.21	1.22	1.22	0.91	0.96	0.94
9	350	12	Mid	1.33	1.35	1.34	0.95	1.07	1.02
10	350	17	Mid	1.21	1.21	1.21	0.89	0.93	0.91
11	350	22	Mid	1.22	1.27	1.25	0.91	1.00	0.95
12	350	27	Mid	1.20	1.22	1.21	0.89	0.93	0.91
13	350	12	Bot	1.34	1.35	1.34	0.99	1.06	1.02
14	350	27	Bot	1.17	1.18	1.18	0.84	0.98	0.92
15	350	12	Top	1.25	1.29	1.27	0.93	0.98	0.96
16	350	27	Top	1.19	1.23	1.21	0.85	0.96	0.89
17	375	10	Mid	1.29	1.32	1.31	0.92	0.99	0.95
18	375	14	Mid	1.26	1.27	1.27	0.89	0.93	0.91
19	375	18	Mid	1.22	1.24	1.23	0.83	0.94	0.89
20	375	22	Mid	1.20	1.26	1.23	0.81	0.93	0.86
21	375	10	Bot	1.28	1.30	1.29	0.93	1.01	0.97
22	375	22	Bot	1.21	1.23	1.22	0.81	0.91	0.88
23	375	10	Top	1.34	1.36	1.35	0.96	1.01	0.97
24	375	22	Top	1.19	1.23	1.21	0.81	0.94	0.88

The main trend visible in both center rise and side rise data is a decrease in cake height as bake time increases. The more time spent in the oven, the more heat is absorbed which in turn drives moisture out of the cakes. As with drying any food, as moisture leaves the total volume decreases. This trend can be seen in Figures 5-7 and 5-8. It is worth noting that the 17-minute bake time at 350°F is noticeably lower in center and side rise. This could be an anomaly from cake preparation or an impact of a less controlled ingredient like the eggs that impacted the rise of that particular batch of cakes.

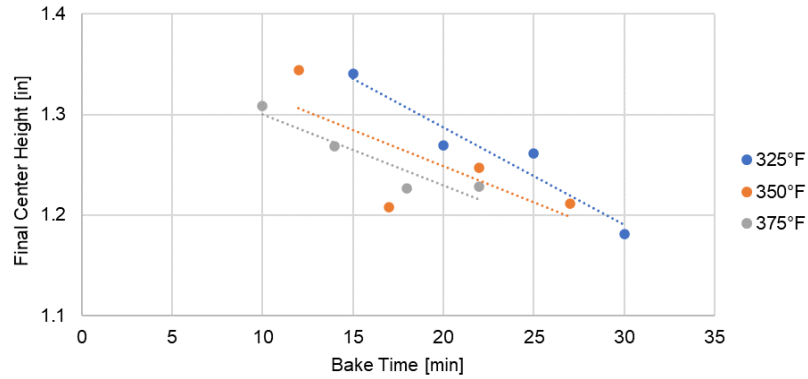


Figure 5-7 Cake center height vs bake time separated by oven setpoint for mid rack position.

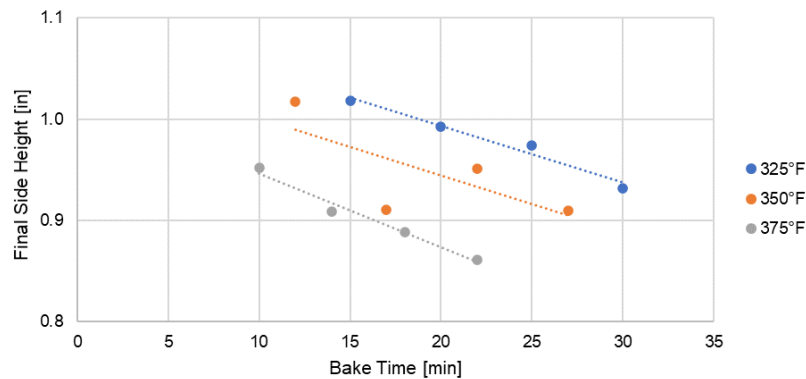


Figure 5-8 Cake side height vs bake time separated by oven setpoint for mid rack position.

As with browning, a single correlation can be made using the thermal energy data collected. Figures 5-7 and 5-8 show three roughly parallel trend lines, each representing a different oven temperature setpoint. This indicates that correlations to bake time would require a different model for every temperature. Using energy combines the temperature and time elements and collapses these trends into a single correlation. A stepwise regression was performed to determine which mode of heat transfer would best correlate to the center rise and

side rise. Starting with center rise, the stepwise regression first showed that radiation had the least correlation with a p-value of 0.79 so it was removed. Next, convection energy had a p-value of 0.70 and was removed leaving only conduction. The conduction linear correlation is shown in Figure 5-9. Rise is limited by the solidification of the cake structure as it cooks. Once set, there is no more rise that can occur, only shrinking from the further dehydration of the solid cake. Conduction energy makes sense for this correlation as the determining factor because the first locations for the structure to set are the portions touching the walls of the cake tin. Those locations are dominated by conduction energy so naturally, it will have a large impact on the rise that is measured.

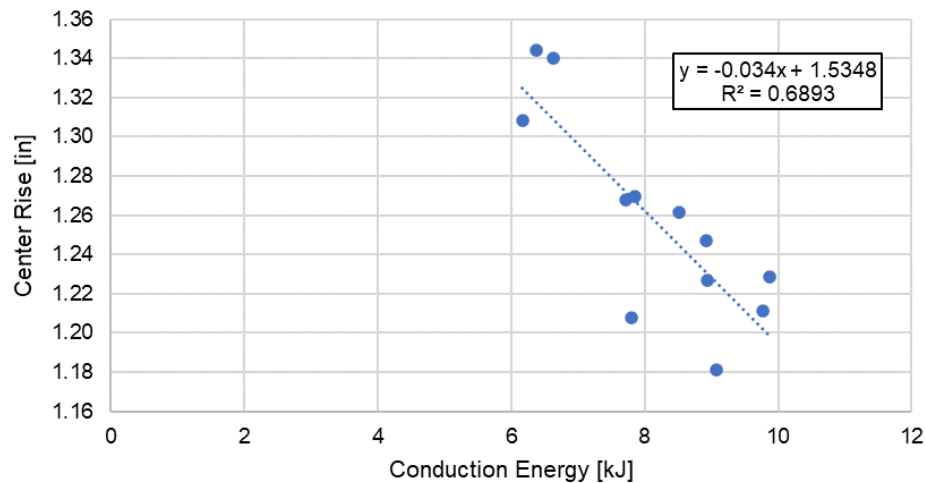


Figure 5-9 Correlation between conduction thermal energy absorbed and center height of baked cakes.

While there does not appear to be any significant non-linearity between conduction energy and center rise, the linear correlation is not very precise. The residual plots for this correlation can be found in Appendix F. The coefficient of

determination (R^2) of the model is 0.69, which is not nearly as strong as the browning correlations. There is no objective threshold for a 'good' R^2 , it is very dependent on the industry and intended use of the model. In this case, attempting to predict values using a model with this R^2 would be difficult. The maximum error from the above model is 0.06 inches. However, the smallest center rise measured was 1.16 inches while the largest was 1.35 inches. These tests should be the most extreme conditions for a cake, both too much and too little energy so there should be no tests with cakes much shorter or taller than what was measured. This means the absolute error of the measurement, 0.06 inches, is 30% of the potential measurement range. With that level of error, the rise height cannot reliably be predicted. Figure 5-10 shows a graphical representation of the maximum error within the bounds of maximum and minimum rise.

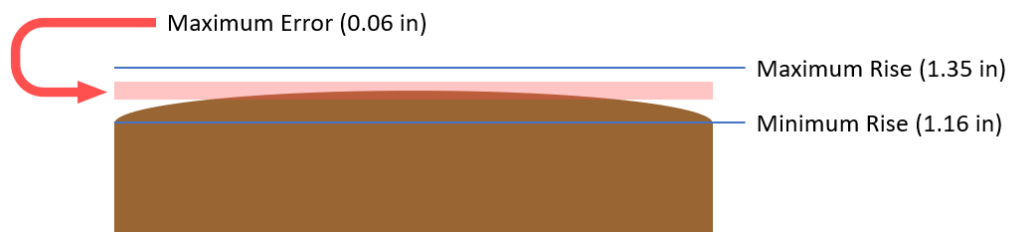


Figure 5-10 Graphical representation of a cake with maximum and minimum observed center rise values compared to the maximum error band of the correlation model.

There are a few potential reasons for the large percentage of absolute error. First, the method of measuring is responsible for some of this variation. The cakes are cut along the center and placed on a table where a caliper is used

to measure the height from the table. Because the cakes are soft and deformable, the procedure of touching the caliper against the cakes for measurement could have some inaccuracy. The caliper can be positioned slightly too low and compress the cake, appearing to be in contact but measuring a smaller value. This can be seen in Figure 5-9 which shows the measured rise data plotted with the developed correlation where two cakes measured significantly below the model prediction. Also, as discussed in the previous section the preparation of the batter can introduce variation in the amount of air incorporated into the batter. In the extreme case, a dense airless batter will not rise much regardless of the heat applied.

Looking next at the side rise, a similar process was followed. The cooked cakes were cut down the middle and the height measured. Rather than measure the height at the edge of the cross section, the height measurement was taken 0.25in from the edge of the cake to avoid the phenomenon where a lip of crust is formed higher than the rest of the cake at the edge where the batter touched the tin. This is illustrated in Figure 5-11 where the crust can be seen in a cross section.

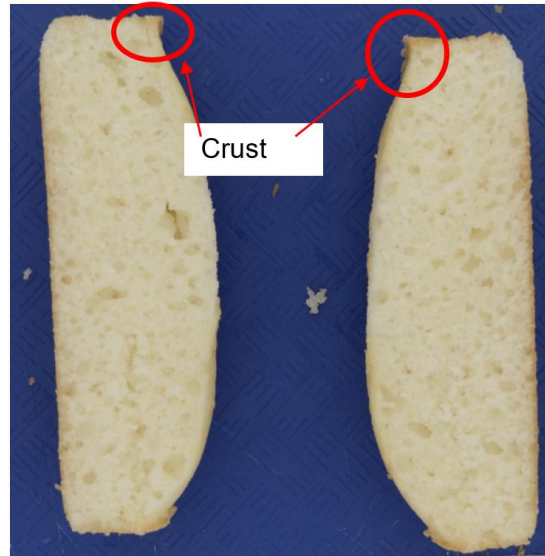


Figure 5-11 Cross section of a baked cake where the crust lip can be seen.

Like the center rise, side rise results from Table 5-5 are plotted against conduction energy absorbed in Figure 5-12. The rise decreased the longer the cakes were in the oven in most cases, however no direct correlation can be made using thermal energy data for all three setpoints. Looking at the data in Figure 5-12, a linear regression falls directly between two lines in the data itself. The 350°F setpoint straddles the regression while the 325°F and 375°F setpoints fall above and below the line, respectively.

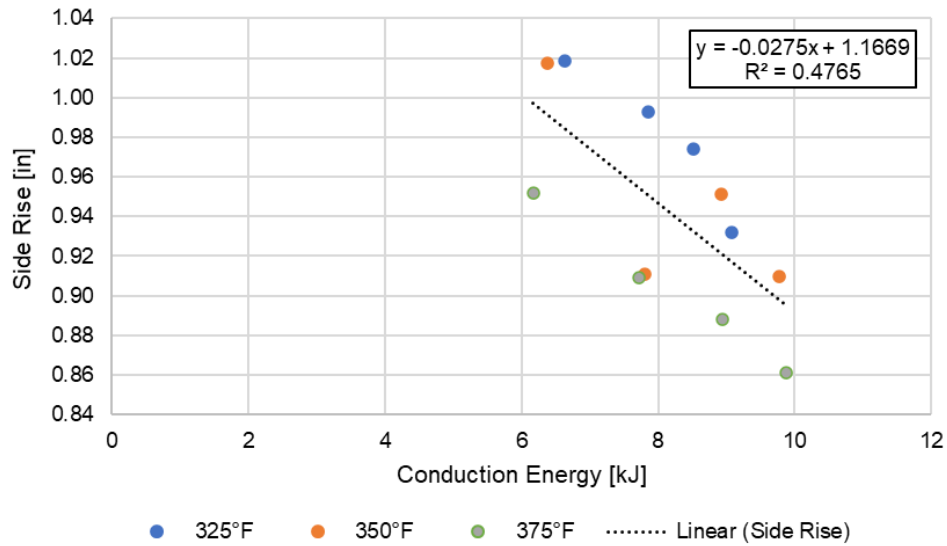


Figure 5-12 Side rise data vs conduction energy absorbed separated by oven setpoint.

As with the center rise, some variation likely comes from the measurement technique using calipers to assess height at the specified locations. Another consideration is the thermal energy metric selected for this correlation. Conduction energy absorbed over the course of the cycle will continue increasing as long as the cakes remain in the oven. However, the structure at the sides of the cake, touching the tin, are the first parts of the cake to complete the chemical process of baking. Once the sides of the cake are set, they can only shrink as moisture continues to be drawn from the cake. Because the cakes were not measured directly after the sides were set, it is unclear how much energy was required. The remaining portion of the cycle can introduce errors in how much shrinking occurred while the rest of the cake finished cooking. These factors make it difficult to produce definitive correlations related to rise height in these

conditions. Alternative test conditions like shorter bake times with smaller time increments between test lengths might better investigate this.

5.4 Mass Loss Correlation

The final cake quality metric investigated in this study is mass loss of the baked cakes. As mentioned when discussing browning, when the heat is absorbed by the cakes the liquid moisture in the cakes evaporates into the surrounding environment. Overcooked, dry cakes are undesirable, so predicting moisture loss using thermal energy data can be used to develop cycles that do not excessively dry cakes before the rest of the desirable cooking metrics are achieved.

To measure this quantity, the mass of the batter placed in the cake tins was recorded. After the test was completed, the cakes were immediately removed from the oven and measured again. The difference in mass is the amount of water that was lost during the baking process. There are extremely minor amounts of flavor and aroma molecules that leave the cake with the evaporating water, but by mass those quantities are negligible. As the cakes cool, they will continue to lose mass from steam. However, this mass loss is difficult to quantify as the surrounding environment is no longer specifically controlled and measured as in the oven cavity. This is why using the immediate mass after leaving the oven is best, to correlate directly with the thermal energy measured during the test cycle.

As with the metrics before, each of the two cakes run during a test has a mass loss figure that is averaged to provide a single mass loss value. Table 5-6 shows the data collected from the test plan, but as before only the middle rack data is used in correlations. As with the previous metrics, repeatability between the two cakes of each test is available. The mass loss repeatability is 5% and full repeatability data can be found in Appendix E

Table 5-6 Mass loss data collected for all cakes in the test plan.

Test Plan			Cake 1 (Left)			Cake 2 (Right)			Avg Weight Loss
Test #	Temp Setpoint	Cook Time	Raw Weight	Cooked Weight	Weight Loss	Raw Weight	Cooked Weight	Weight Loss	Weight Loss
[-]	[F]	[min]	[g]	[g]	[g]	[g]	[g]	[g]	[g]
1	325	15	78.4	74.9	3.5	78.6	74.8	3.8	3.6
2	325	20	78.5	72.9	5.6	78.6	72.4	6.2	5.9
3	325	25	78.6	70.9	7.7	78.6	70.6	8.0	7.8
4	325	30	78.6	68.9	9.7	78.6	68.4	10.2	9.9
5	325	15	78.4	75.1	3.3	78.6	74.8	3.8	3.5
6	325	30	78.6	67.2	11.4	78.4	66.0	12.4	11.9
7	325	15	78.6	74.8	3.8	78.4	74.3	4.1	4.0
8	325	30	78.7	67.9	10.8	78.5	67.4	11.1	11.0
9	350	12	78.6	75.5	3.1	78.5	75.0	3.5	3.3
10	350	17	78.5	72.9	5.6	78.5	72.8	5.7	5.6
11	350	22	78.6	70.8	7.8	78.4	70.2	8.2	8.0
12	350	27	78.4	67.7	10.7	78.5	67.7	10.8	10.8
13	350	12	78.6	75.3	3.3	78.6	75.5	3.1	3.2
14	350	27	78.6	68.3	10.3	78.4	67.7	10.7	10.5
15	350	12	78.4	74.9	3.5	78.4	74.8	3.6	3.6
16	350	27	78.6	67.4	11.2	78.4	66.7	11.7	11.5
17	375	10	78.6	75.8	2.8	78.4	75.4	3.0	2.9
18	375	14	78.6	73.3	5.3	78.4	73.0	5.4	5.3
19	375	18	78.6	71.2	7.4	78.5	70.4	8.1	7.8
20	375	22	78.6	69.2	9.4	78.4	68.3	10.1	9.7
21	375	10	78.6	75.5	3.1	78.6	75.3	3.3	3.2
22	375	22	78.6	69.1	9.5	78.6	69.0	9.6	9.5
23	375	10	78.6	75.3	3.3	78.4	74.8	3.6	3.5
24	375	22	78.6	68.3	10.3	78.4	67.9	10.5	10.4

The expected trends in mass loss are seen in the test results. The longer a cake stays in the oven, the more moisture is lost. However, understanding the interaction between mass loss and absorbed energy is required before

attempting correlations. In the study Örvös et al. (2016), evaporation rates were measured from free bodies of water with different ambient relative humidities. In the case of free water, the evaporation rate increases non-linearly with increasing temperature as seen in Figure 5-13. The plot shows that there is a polynomial relationship between evaporation rate and the temperature of the fluid.

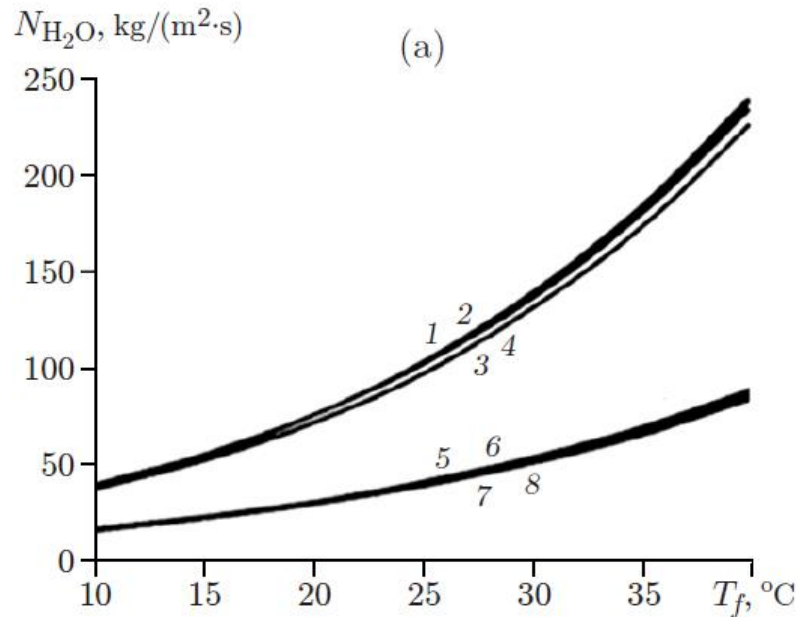


Figure 5-13 Evaporation rate as a function of fluid temperature for free water. Tests 1 – 4 tested at $\phi = 45\%$ and tests 5 – 8 with $\phi = 100\%$ (Örvös et al., 2016).

When baking cakes, the mechanisms of water evaporation from the surface of the cake are different than that of free water. The cake structure changes chemically as water is removed and water must migrate from the interior of the cake to the surface to evaporate. However, this suggests that the relationship between energy input and mass loss may not be linear. To that effect, the data from Table 5-6 was plotted against total energy absorbed as seen

in Figure 5-14. Total energy was selected because water will be driven out based on the total amount of heat absorbed by the cake, regardless of the mode of heat transfer. As the overall temperature of the cake increases, more water will leave the cake increasing the mass loss.

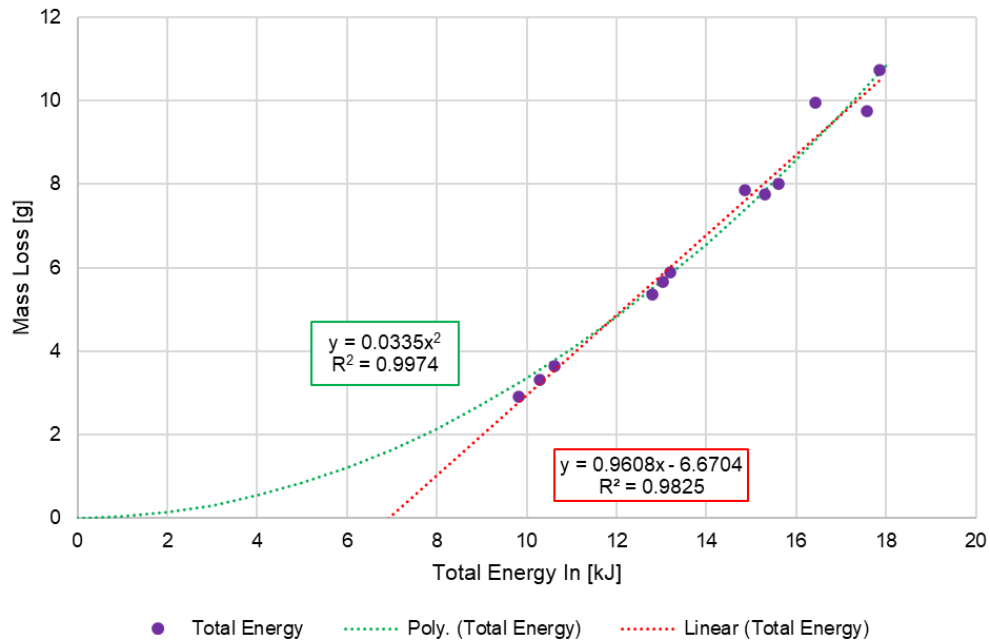


Figure 5-14 Weight loss as a function of total energy absorbed with a linear and polynomial regression plotted with the measured weight loss tests.

Two regressions are plotted in Figure 5-14, a linear and polynomial regression. The polynomial regression follows the evaporation rate functions seen above while the linear regression visually fits the data well. Both regressions show very high R^2 values, so either model should predict mass loss well. The span of data collected does not provide information on the lower end of either regression because the lowest energy data points are the first points where the cake is fully cooked, and the structure is set. Any earlier points would

be undercooked to the point of containing raw batter, so any model developed does not need to predict values in this range. The errors of each model will better inform which regression is better suited for predictive analysis.

5.4.1 Mass Loss Model Error

The two correlations developed for mass loss are a polynomial regression and linear regression between mass loss and total energy absorbed by the sensors. Each correlation was used to predict the measured values and compared back to get an idea of model errors. These values can be found in Table 5-7.

Table 5-7 Mass loss model error calculations for both polynomial and linear regressions based on the measured data from Table 5-6.

Test Number	Total Energy	Measured Mass Loss	Polynomial Regression				Linear Regression				
			Mass Loss Estimate	Error	Abs Error	Percent Error	Mass Loss Estimate	Error	Abs Error	Percent Error	
[-]	[kJ]	[g]	[g]	[g]	[g]	[%]	[g]	[g]	[g]	[%]	
1	10.6	3.6	3.8	0.1	0.1	3.8	3.5	-0.1	0.1	-2.9	
2	13.2	5.9	5.8	-0.1	0.1	-0.9	6.0	0.1	0.1	2.0	
3	14.9	7.8	7.4	-0.4	0.4	-5.6	7.6	-0.2	0.2	-3.1	
4	16.4	9.9	9.1	-0.9	0.9	-9.0	9.1	-0.8	0.8	-8.4	
9	10.3	3.3	3.5	0.2	0.2	7.4	3.2	-0.1	0.1	-2.8	
10	13.0	5.6	5.7	0.1	0.1	0.9	5.9	0.2	0.2	3.7	
11	15.6	8.0	8.2	0.2	0.2	2.0	8.3	0.3	0.3	4.0	
12	17.9	10.8	10.7	0.0	0.0	-0.5	10.5	-0.3	0.3	-2.4	
17	9.8	2.9	3.2	0.3	0.3	11.4	2.8	-0.1	0.1	-4.8	
18	12.8	5.3	5.5	0.1	0.1	2.6	5.6	0.3	0.3	5.1	
19	15.3	7.8	7.9	0.1	0.1	1.3	8.0	0.3	0.3	3.6	
20	17.6	9.7	10.4	0.6	0.6	6.3	10.2	0.5	0.5	4.8	
				Minimum	-0.9	0.0	-9.0	Minimum	-0.8	0.1	-8.4
				Maximum	0.6	0.9	11.4	Maximum	0.5	0.8	5.1
				Average	0.0	0.3	1.7	Average	0.0	0.3	-0.1

Looking at the error of both models, the linear model offers a slightly better fit and smaller errors. The linear model has an average error of 0.1% with a maximum absolute error of 8.36%. In comparison, the polynomial regression has larger error percentages overall with an average error of 1.67% and maximum

error of 11.43 %. The residual plots for both regressions can be seen in Appendix D. All estimates are within one gram of the measured value which is very precise for this testing. This model will be useful in providing a quantitative metric to grade the moisture of similar cakes. Additional study could determine what a desirable level of mass loss is or a threshold of mass loss above which the cake is considered dry.

6 CONCLUSION

This study required the use of thermal energy sensors to act as a simulated food load and collect energy data from a residential oven. The sensors selected were designed initially by Petit-Bois (2022), but some adaptations had to be made. The sensors were roughly cube shapes at three inches per side and intended to simulate sugar cookies. That study showed problems using the sensors as sugar cookies, partly due to their larger mass and volume than a cookie. In this study, the same sensors were used as a simulation for small white cakes baked in tins only four inches in diameter. The entire thermal energy sensor then fit inside the same cake tins used in baking cakes and filled a similar volume as the cakes themselves. For consistent results, sensors were fixed inside the cake tins using high temperature 3D printed ULTEM resin parts that centered the sensors and held full contact between the tin and sensor body.

6.1 Important Results

The goal of this study was to develop correlations between the quality characteristics of baked cakes and thermal energy data collected from a residential oven. Ideally, these models would be robust enough to assist in oven and oven cycle development by reducing the need for food testing until later in the process. The thermal energy data was collected in the form of total energy absorbed over a predetermined cycle time. This energy was broken down into

the three heat transfer modes: conduction, convection, and radiation. That data was then used in correlations to predict the four characteristics measured by this study that reflected the quality of the baked cakes: surface browning, porosity, rise height, and mass loss. The baking performance data used to develop these correlations comes from a total of twelve test runs. Four runs at three oven temperatures; 325°F, 350°F, and 375°F. Each cake run had two cakes baked side by side while each sensor run had an absorptive sensor (convection and radiation) and reflective sensor (convection only) similarly side by side. The sensors showed good repeatability by comparing the beginning portions of tests run on the middle rack at the same oven temperature setpoint. This showed less than two percent variation between sensor results for all setpoints by the end of a test.

The browning of each cake was separated into top and bottom browning and a stepwise regression identified the most impactful heat transfer mode for the respective surface browning. It was found that top browning was best predicted by radiation energy and bottom browning best predicted by conduction energy. Both metrics correlated very well with linear relationships to energy absorbed. In practice, a test run using the thermal energy sensors in a new cycle could predict the degree of browning observed given the conduction or radiation energy absorbed.

The porosity metric was more difficult to correlate. A large degree of variation was observed between two cakes in the same oven cycle. It is possible that the measurement system for this metric is not robust enough to capture

porosity. The small pockets of air cell area in the crumb of the cake require high resolution images to accurately determine the percentage area of air cells and crumb. Low resolution images would average some of those air cells between multiple pixels, bringing some air cells down to a crumb L^* threshold and some crumb up to air cell. A similar color imaging system that can take closer pictures at a higher focus might better calculate the true porosity of the cakes.

Additionally, thermal energy metrics used for correlation represent the thermal state at the end of the cycle or a summation of energy or flux over the course of the cycle. The setting, or transition, of a cake structure from a liquid batter to solid crumb occurs most rapidly at the beginning of the cycle. By the end, the cake has long set and additional data will cloud the behavior from the early portion of the cycle. An alternate test plan could better understand how heat flux impacts porosity and how to predict it.

The rise height metrics were also split into two subcategories, center rise and side rise. The correlation for side rise was very poor, likely for similar reasons as the porosity. The first part of the cake to set will be the sides adjacent to the cake tin. These locations come up to temperature first and transition from batter to solid cake. Once that transition occurs, very little change in the side height will occur even if data continues to be collected. Center rise is a better metric because the center of the cake is the last portion to complete the baking process. However, some of the longer times at each setpoint in the test plan leave the cakes in the oven far past even when the center of the cake finished rising. The more notable effect in this data shows how food left in the oven past

done will lose moisture and shrink. The linear correlation between center rise and conduction has a negative slope, with a low degree of predictive accuracy.

Mass loss was the final correlation metric studied. The mass loss from a cake can be entirely attributed to the mass of water evaporating from the batter and cake as it cooks. As such, end of cycle energy is a strong predictive factor. The best correlation was found using the total energy absorbed over the cycle. Regardless of the source, heat entering the cake increased the overall temperature and drove moisture out of the cake. Two potential correlations were developed, both of which provided strong results within the bounds of the data. A linear or quadratic relationship could be observed, but determining which model is truly better suited would require testing outside the range that results in desirable cakes.

Overall, heat flux measurement technology is certainly able to assist in the development of ovens and oven cycles. The quality of baked goods can be estimated using thermal data. Table 6-1 shows a summary of useful correlations developed in this study for that purpose. If a digital multi-physics simulation was developed that could yield similar results as the thermal energy sensors in this study, oven cycles could be tested in that simulation and used to directly predict baking performance. Further research can be done to improve these models and identify other useful metrics to determine food performance.

Table 6-1 Conclusion of thermal energy data and cake performance correlations that are useful for prediction.

Useful for Prediction	Baking Performance Metric	Correlation	Equation	R ²
yes	Top Browning	Radiation	$y = -6.03x + 99.78$	0.95
yes	Bottom Browning	Conduction	$y = -8.74x + 136.43$	0.97
no	Porosity	--	--	--
no	Center Rise	Conduction	$y = -0.034x + 1.53$	0.69
no	Side Rise	Conduction	$y = -0.026x + 1.17$	0.48
yes	Mass Loss	Total Energy	$y = 0.96x - 6.67$	0.98

6.2 Future Work

This study developed feasibility in correlating thermal energy data with certain cooking performance metrics of cakes. For the metrics that did correlate well (browning and mass loss), the study did not have the time or resources to complete a validation data set. A repeat of the test plan from this study would provide data to validate the proposed models and offer further insight on the predictive accuracy.

The performance metrics that did not have strong correlations (porosity and rise height) can be investigated using improved techniques. In both cases, a new test plan with more data points earlier in the cycle would better capture the impact of thermal energy. These metrics are likely influenced by the initial flux into the food so focusing on the beginning of the cycle could provide a stronger model. Using constant time increments between the different temperature setpoints could reveal the impact of early heat flux on the baked cakes. Additionally, the measurement technique for porosity can be improved with a

higher resolution imaging system. Better image quality can improve the distinction between air cell area and crumb area of a cake cross section.

Further validation can be performed on the correlations that were developed for browning and mass loss. Ideally, this method of correlating energy with baking performance metrics means other ovens can be tested the same way and the model will behave identically. This study only tested a single cycle on a single oven, so repeating a portion of the test plan (sensor data and baked cakes) would show if new ovens or cycles follow the correlations developed. A traditional bake cycle in a new oven model will likely behave similarly, but new cycles like convection bake might not fit these correlations. The convection term in this study refers to free convection as no fan was used during the bake cycle. Forced convection is quite different, especially when it comes to moisture removal which is a significant part of the baking process.

This study is an introduction to the process of predictive cooking in residential ovens, with plenty of opportunity to develop knowledge in the future.

REFERENCES

- Abdanan Mehdizadeh, S. (2022). Machine vision based intelligent oven for baking inspection of cupcake: Design and implementation. *Mechatronics*, 82. <https://doi.org/10.1016/j.mechatronics.2022.102746>
- Allen, D. (2012). The Relationship Between Variable Selection and Data Augmentation and a Method for Prediction. *Technometrics*, 16, 125-127. <https://doi.org/10.1080/00401706.1974.10489157>
- Ebeneezar, S., Prabu, D. L., Selvam, C., Cs, T., Madhu, K., Sayooj, P., & Pananghat, V. (2020). Evaluation of dietary oleoresins on the enhancement of skin coloration and growth in the marine ornamental clown fish, *Amphiprion ocellaris*. *Aquaculture*, 529, 735728. <https://doi.org/10.1016/j.aquaculture.2020.735728>
- Hermannseder, B., Ahmad, M. H., Kügler, P., & Hitzmann, B. (2017). Prediction of baking results from farinograph measurements by using stepwise linear regression and artificial neuronal networks. *Journal of Cereal Science*, 76, 64-68. <https://doi.org/https://doi.org/10.1016/j.jcs.2017.05.014>
- Örvös, M., Szabó, V., & Poós, T. (2016). Rate of evaporation from the free surface of a heated liquid. *Journal of Applied Mechanics and Technical Physics*, 57, 1108-1117. <https://doi.org/10.1134/S0021894416060195>
- Petit-Bois, K. (2022). *Development and applications of a sensor for measurement of different modes of heat transfer on foods in a residential oven*. (Publication Number 3965) University of Louisville]. <https://doi.org/10.18297/etd/3965>
- Purlis, E. (2010). Browning development in bakery products – A review [Article]. *Journal of Food Engineering*, 99(3), 239-249. <https://doi.org/10.1016/j.jfoodeng.2010.03.008>
- Sadeghi, F., Ali, R., Mohammad, S., & Nasser, H. (2016). Numerical Modeling of Heat and Mass Transfer during Contact Baking of Flat Bread [Journal Article]. *Journal of Food Process Engineering*, 39(4), 345-356. <https://doi.org/10.1111/jfpe.12227>
- Sato, H., Matsumura, T., & Shibukawa, S. (1987). Apparent heat transfer in a forced convection oven and properties of baked food [Journal Article]. *Journal of food science*, 52(1), 185. <https://search.ebscohost.com/login.aspx?direct=true&db=agr&AN=IND87087319&site=ehost-live>
- Saxena, D. C., Haridas Rao, P., & Raghava Rao, K. S. M. S. (1995). Analysis of modes of heat transfer in tandoor oven. *Journal of Food Engineering*, 26(2), 209-209. [https://doi.org/10.1016/0260-8774\(94\)00057-G](https://doi.org/10.1016/0260-8774(94)00057-G)

- Silva, T. H. L., Monteiro, R. L., Salvador, A. A., Laurindo, J. B., & Carciofi, B. A. M. (2022). Kinetics of bread physical properties in baking depending on actual finely controlled temperature [Article]. *Food Control*, 137, N.PAG-N.PAG. <https://doi.org/10.1016/j.foodcont.2022.108898>
- Standing, C. N. (1974). Individual heat transfer modes in band oven biscuit baking [Article]. *Journal of Food Science (Wiley-Blackwell)*, 39(2), 267. <https://doi.org/10.1111/j.1365-2621.1974.tb02872.x>
- Tang, Y. R., & Ghosh, S. (2021). Canola protein thermal denaturation improved emulsion-templated oleogelation and its cake-baking application. *RSC Advances*, 11(41), 25141-25157. <https://doi.org/10.1039/d1ra02250d>
- Tuta Şimşek, S. (2019). Vacuum-combined baking to enhance quality properties of gluten-free cake: Multi-response optimization study. *LWT*, 116. <https://doi.org/10.1016/j.lwt.2019.108557>

APPENDICES

A Sensor Specifications

Table A-1 Hukseflux FHF04 Sensor Specifications (continued next page)

FHF04 SPECIFICATIONS

Sensor type	foil heat flux sensor
Sensor type according to ASTM	heat flow sensor or heat flux transducer
Measurand	heat flux
Measurand in SI units	heat flux density in W/m^2
Measurement range	$(-10 \text{ to } +10) \times 10^3 \text{ W/m}^2$ at heat sink temperature $20 \text{ }^\circ\text{C}$ see appendix for detailed calculations
Sensitivity range	$9 - 13 \times 10^{-6} \text{ V/(W/m}^2\text{)}$
Sensitivity (nominal)	$11 \times 10^{-6} \text{ V/(W/m}^2\text{)}$
Directional sensitivity	heat flux from the back side to the front side (side with the dot) generates a positive voltage output signal
Increased sensitivity	multiple sensors may be put electrically in series. The resulting sensitivity is the sum of the sensitivities of the individual sensors
Expected voltage output	$(-100 \text{ to } +100) \times 10^{-3} \text{ V}$ turning the sensor over from one side to the other will lead to a reversal of the sensor voltage output
Measurement function / required programming	$\Phi = U/S$
Required readout	1 differential voltage channel or 1 single ended voltage channel, input resistance $> 10^6 \text{ } \Omega$
Optional readout	1 temperature channel
Rated load on wires	$\leq 1.6 \text{ kg}$
Rated bending radius	$\geq 7.5 \times 10^{-3} \text{ m}$
Rated temperature range, continuous use	$-70 \text{ to } +120 \text{ }^\circ\text{C}$
Rated temperature range, short intervals	$-160 \text{ to } +150 \text{ }^\circ\text{C}$ (contact Hukseflux when measuring at $-160 \text{ }^\circ\text{C}$)
Temperature dependence	$< 0.2 \text{ } \%/^\circ\text{C}$
Non-linearity	$< 5 \text{ } \%$ ($0 \text{ to } 10 \times 10^3 \text{ W/m}^2$)
Solar absorption coefficient	0.75 (indication only)
Thermal conductivity dependence	negligible, $< 3 \text{ } \%/(\text{W/m}\cdot\text{k})$ from 270 to $0.3 \text{ W/m}\cdot\text{K}$
Sensor length and width	$(50 \times 50) \times 10^{-3} \text{ m}$
Sensing area	$9 \times 10^{-4} \text{ m}^2$
Sensing area length and width	$(30 \times 30) \times 10^{-3} \text{ m}$
Passive guard area	$16 \times 10^{-4} \text{ m}^2$
Guard width to thickness ratio	40
Sensor thickness	$0.4 \times 10^{-3} \text{ m}$
Sensor thermal resistance	$11 \times 10^{-4} \text{ K/(W/m}^2\text{)}$
Sensor thermal conductivity	$0.36 \text{ W/(m}\cdot\text{K)}$
Response time (95 %)	3 s
Sensor resistance range	160 to $240 \text{ } \Omega$
Required sensor power	zero (passive sensor)

Temperature sensor	type T thermocouple
Temperature sensor accuracy	$\pm 2\%$ (of temperature in °C), see appendix
Standard wire length	2 m
Wiring	3 x copper and 1 x constantan wire, AWG 24, stranded
Wire diameter	1×10^{-3} m
Marking	dot on foil indicating front side of the heat flux sensor; 1 x label on metal connection block, showing serial number and sensitivity
IP protection class	IP67
Rated operating relative humidity range	0 to 100 %
Use under water	FHF04 is not suitable for continuous use under water
Gross weight including 2 m wires	approx. 0.5 kg
Net weight including 2 m wires	approx. 0.5 kg

INSTALLATION AND USE

Typical conditions of use	in experiments, in measurements in laboratory and industrial environments. Exposed to heat fluxes for periods of several minutes to several years. Connected to user-supplied data acquisition equipment. Regular inspection of the sensor. Continuous monitoring of sensor temperature. No special requirements for immunity, emission, chemical resistance.
Recommended number of sensors	2 per measurement location
Installation	see Chapter 5 on installation for recommendations
Bending	see Section 5.2 on installation on curved surfaces
Wire extension	see appendix on wire extension, or order sensors with longer wire
Sensor foil installation	see appendix on installation of FHF04 without wiring, without metal connection block

CALIBRATION

Calibration traceability	to SI units
Product certificate	included (showing calibration result and traceability)
Calibration method	method HFPC, according to ASTM C1130 - 17
Calibration hierarchy	from SI through international standards and through an internal mathematical procedure
Calibration uncertainty	$< \pm 5\%$ ($k = 2$)
Recommended recalibration interval	2 years
Calibration reference conditions	20 °C, heat flux of 600 W/m ² , mounted on aluminium heat sink, thermal conductivity of the surrounding environment 0.0 W/(m·K)
Validity of calibration	based on experience the instrument sensitivity will not change during storage. During use the instrument "non-stability" specification is applicable. When used under conditions that differ from the calibration reference conditions, the FHF04 sensitivity to heat flux may be different than stated on its certificate. See the chapter on instrument principle for suggested solutions
Field calibration	is possible by comparison to a calibration reference sensor. Usually mounted side by side, alternative on top of the field sensor. Preferably reference and field sensor of the same model and brand. Typical duration of test > 24 h

MEASUREMENT ACCURACY

Uncertainty of the measurement	statements about the overall measurement uncertainty can only be made on an individual basis.
--------------------------------	---

Table A-2 Hukseflux Black and Gold Sticker Specifications

BLK SPECIFICATIONS

Product type	sticker
Measurand	convective + radiative heat flux
Measurand in SI units	heat flux density in W/m ²
Measurement range	(-2 to 2) x 10 ³ W/m ² (HFP01) (-10 to 10) x 10 ³ W/m ² (FHF05 series)
Measurement function / required programming	$\Phi_{\text{convective+radiative}} = U/S$
Rated temperature range - continuous use	-40 to +150 °C
Rated temperature range - short intervals	-40 to +260 °C
Spectral range (UV-VIS-NIR-FIR)	250 to > 10000 x 10 ⁻⁹ m
Absorption over range	> 95 % see appendix for more information
Carrier material	Polyimide (Kapton®)
Coating material	fully inorganic metal-based
Adhesive	3M™ VHB™ F9460PC acrylic transfer tape
Sticker thickness	0.14 x 10 ⁻³ m
Sticker thermal resistance	10 x 10 ⁻⁴ K/(W/m ²)
Sticker thermal conductivity	1.38 x 10 ⁻¹ W/(m·K)

GLD SPECIFICATIONS

Product type	sticker
Measurand	convective heat flux
Measurand in SI units	heat flux density in W/m ²
Measurement range	(-2 to 2) x 10 ³ W/m ² (HFP01) (-10 to 10) x 10 ³ W/m ² (FHF05 series)
Measurement function / required programming	$\Phi_{\text{convective}} = U/S$
Rated temperature range - continuous use	-185 to +150 °C
Rated temperature range - short intervals	-185 to +260 °C
Spectral range (NIR-FIR)	700 to > 10000 x 10 ⁻⁹ m
Reflection over range	> 95 % see appendix for more information
Spectral range (VIS)	400 to 700 x 10 ⁻⁹ m
Reflection over range	> 80 % see appendix for more information
Solar absorption	< 20 %
Carrier material	Polyimide (Kapton®)
Coating material	gold
Adhesive	ARcare® 8026 silicone transfer tape
Sticker thickness	0.05 x 10 ⁻³ m
Sticker thermal resistance	3.5 x 10 ⁻⁴ K/(W/m ²)
Sticker thermal conductivity	1.45 x 10 ⁻¹ W/(m·K)

Table A-3 ULTEM™ 1010 Resin Thermal Properties

Property	Test Method	Typical Values	
		XY	XZ/ZX
HDT @ 66 psi	ASTM D648 Method B	214.1 °C (417.3 °F)	
HDT @ 264 psi	ASTM D648 Method B	212.2 °C (413.9 °F)	
Tg	ASTM D7426 Inflection Point	209.37 °C (408.87 °F)	
Mean CTE	ASTM E831 (-50 °C to 80 °C)	36.08 µm/[m*°C] (20.04 µin/[in*°F])	-
	ASTM E831 (80 °C to 205 °C)	29.81 µm/[m*°C] (16.56 µin/[in*°F])	-
	ASTM E831 (-50 °C to 110 °C)	-	32.50 µm/[m*°C] (18.06 µin/[in*°F])
	ASTM E831 (110 °C to 165 °C)	-	16.19 µm/[m*°C] (8.995 µin/[in*°F])
	ASTM E831 (165 °C to 200 °C)	-	4.291 µm/[m*°C] (2.384 µin/[in*°F])
Volume Resistivity	ASTM D257	>7.00*10 ¹⁴ Ω*cm	
Dielectric Constant	ASTM D150 1 kHz test condition	2.841	2.888
	ASTM D150 2 MHz test condition	3.089	3.156
Dissipation Factor	ASTM D150 1 kHz test condition	-0.002	-0.002
	ASTM D150 2 MHz test condition	0.000	0.000
Thermal Conductivity	ASTM E1952 @0C	0.2430 W/m*K 0.1404 BTU/(hr*ft*F)	
Thermal Conductivity	ASTM E1952 @30C	0.2420 W/m*K 0.1399 BTU/(hr*ft*F)	
Thermal Conductivity	ASTM E1952 @60C	0.2426 W/m*K 0.1399 BTU/(hr*ft*F)	
Thermal Conductivity	ASTM E1952 @90C	0.2417 W/m*K 0.1402 BTU/(hr*ft*F)	
Thermal Diffusivity	ASTM E1952 @0C	0.158 mm ² /s 2.45*10 ⁻⁴ in ² /s	
		0.141 mm ² /s 2.19*10 ⁻⁴ in ² /s	
Thermal Diffusivity	ASTM E1952 @30C	0.130 mm ² /s 2.02*10 ⁻⁴ in ² /s	
		0.121 mm ² /s 1.88*10 ⁻⁴ in ² /s	
Specific Gravity	ASTM D257 @23 °C	1.29	
UL Flammability	ANSI/UL 746B	V0- Blue Card #E345258	

B Thermal Energy Sensor Test Plan Data

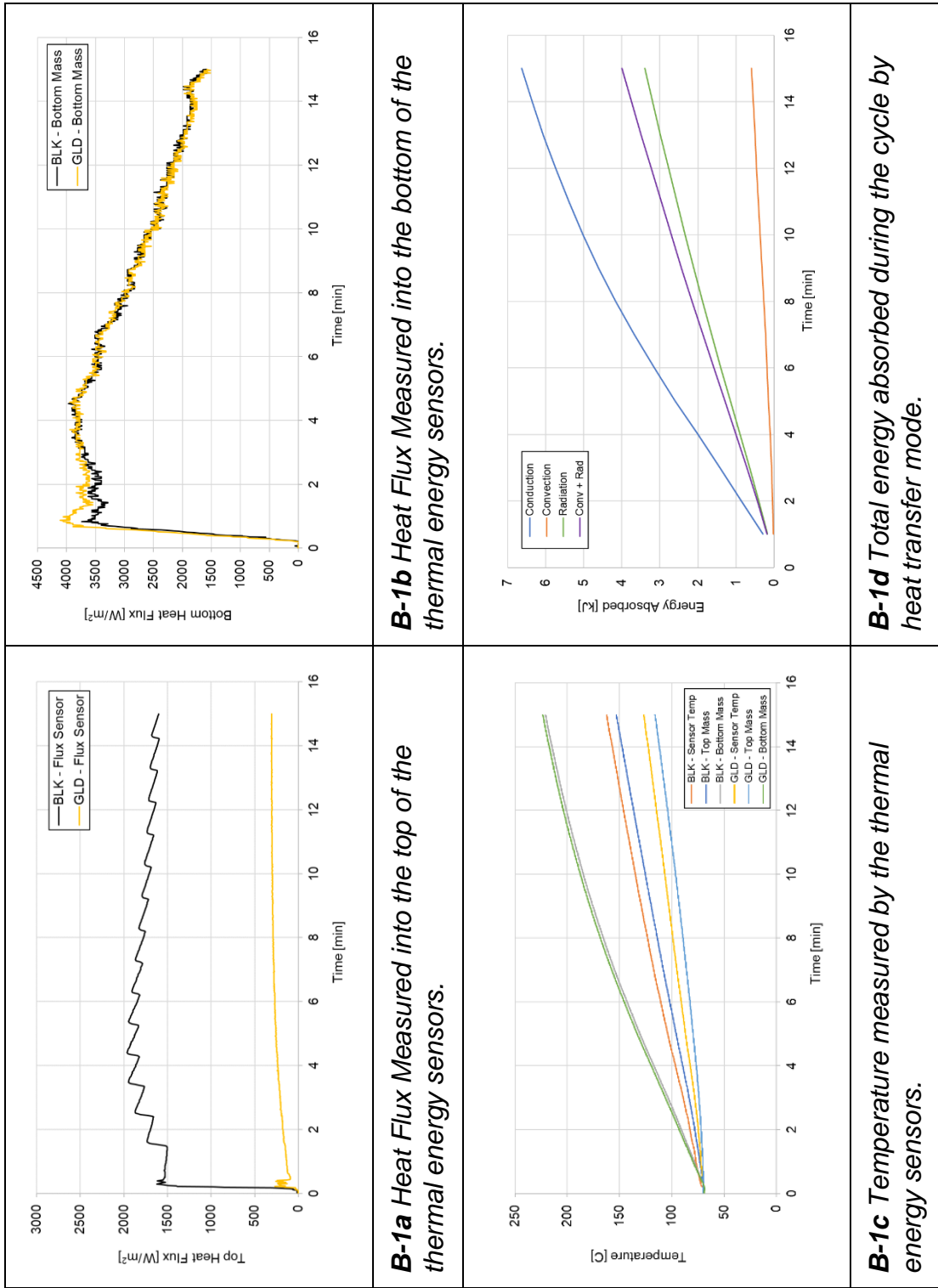


Figure B-1 Test 1, Traditional Bake, 325°F Setpoint, 15 minutes, middle rack.

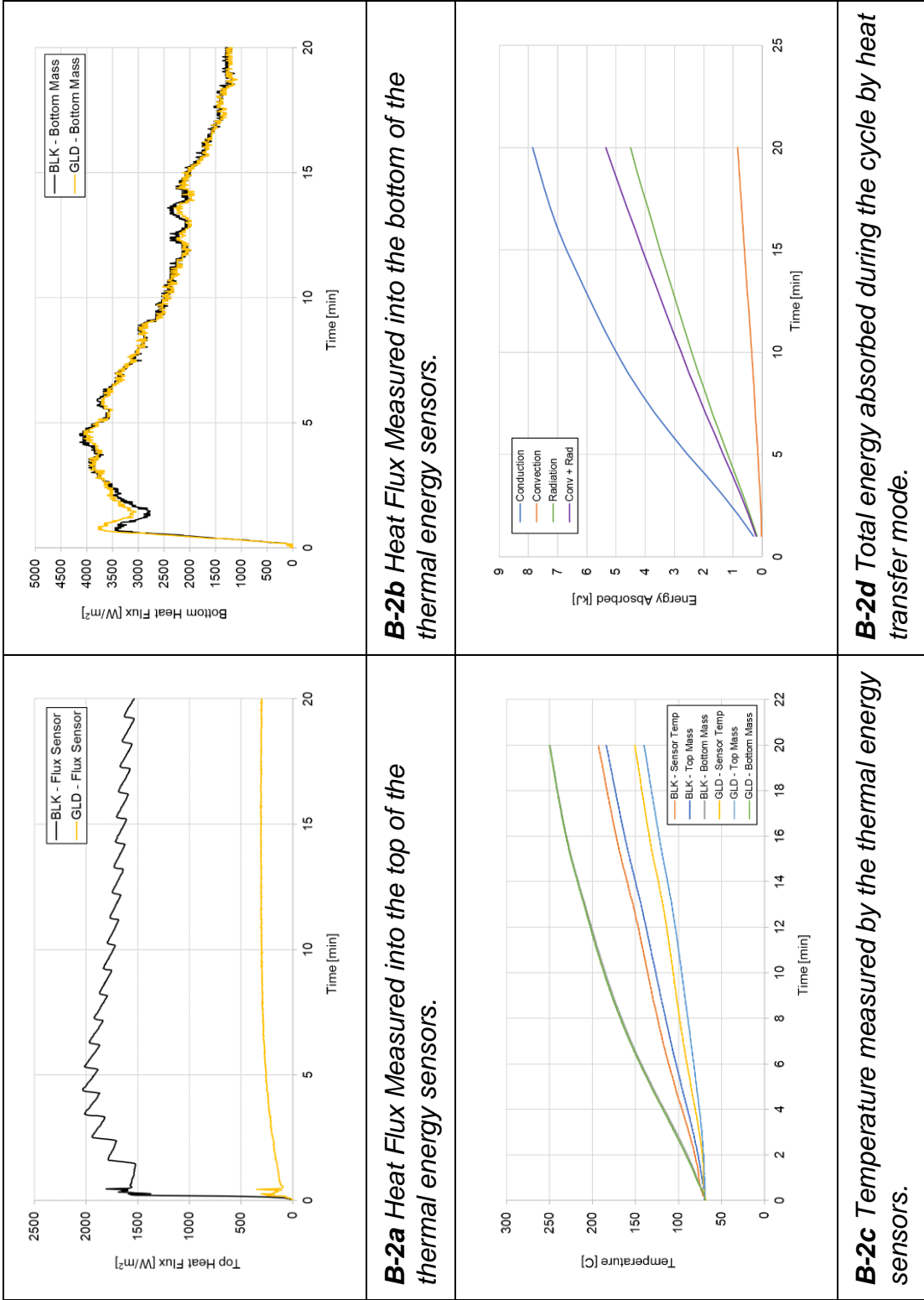


Figure B-2 Test 2, Traditional Bake, 325°F Setpoint, 20 minutes, middle rack.

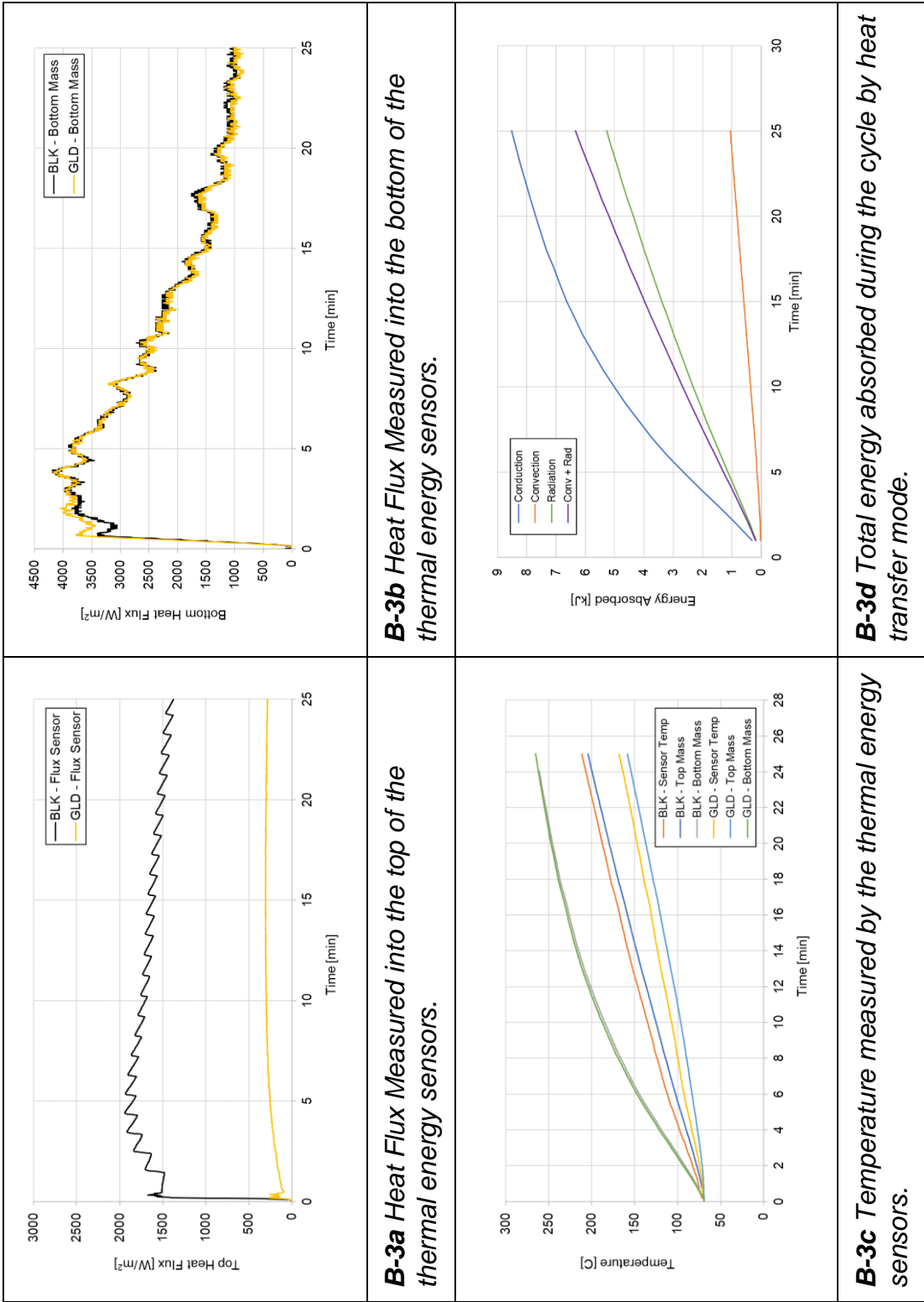


Figure B-3 Test 3, Traditional Bake, 325°F Setpoint, 25 minutes, middle rack.

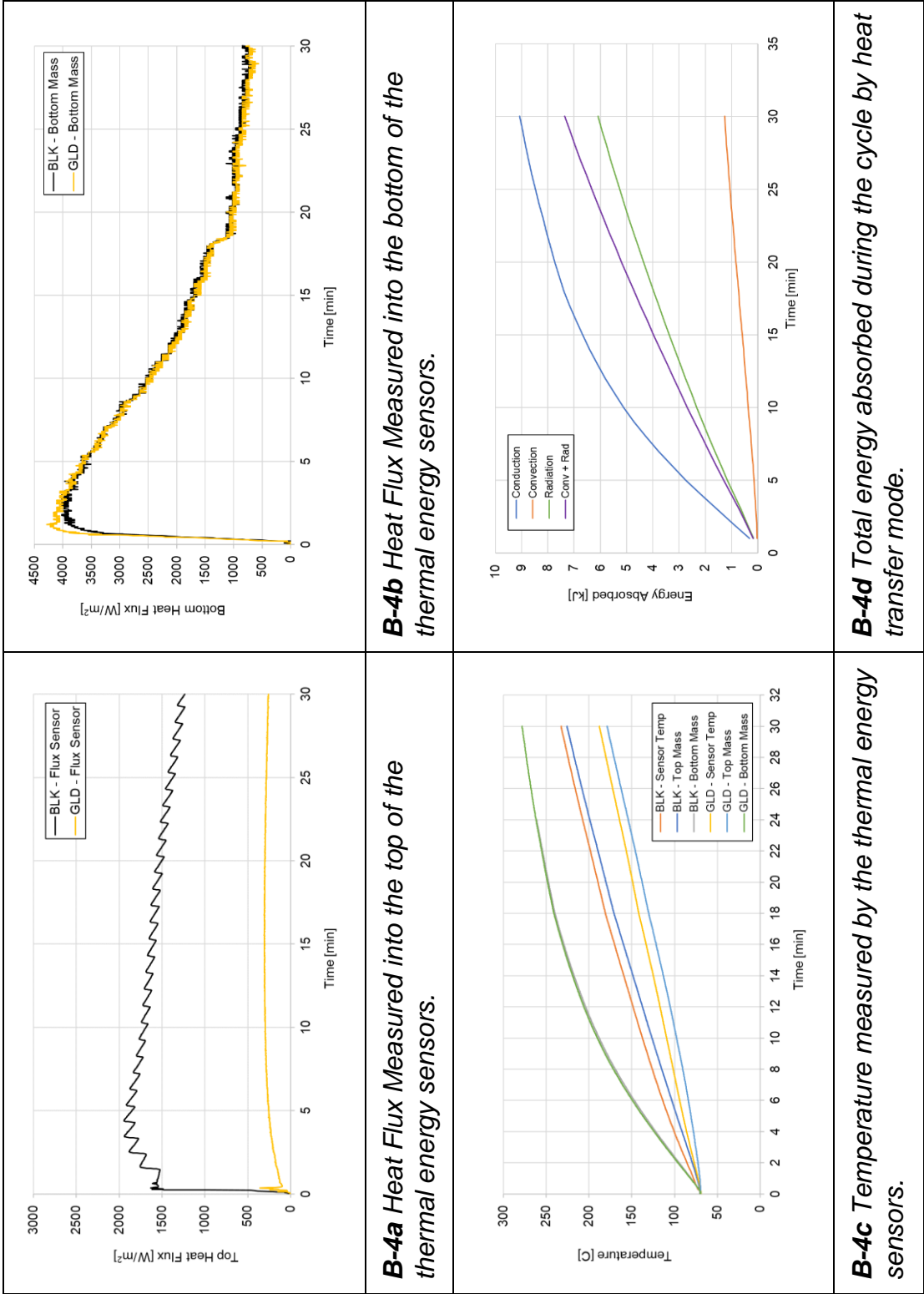


Figure B-4 Test 4, Traditional Bake, 325°F Setpoint, 30 minutes, middle rack.

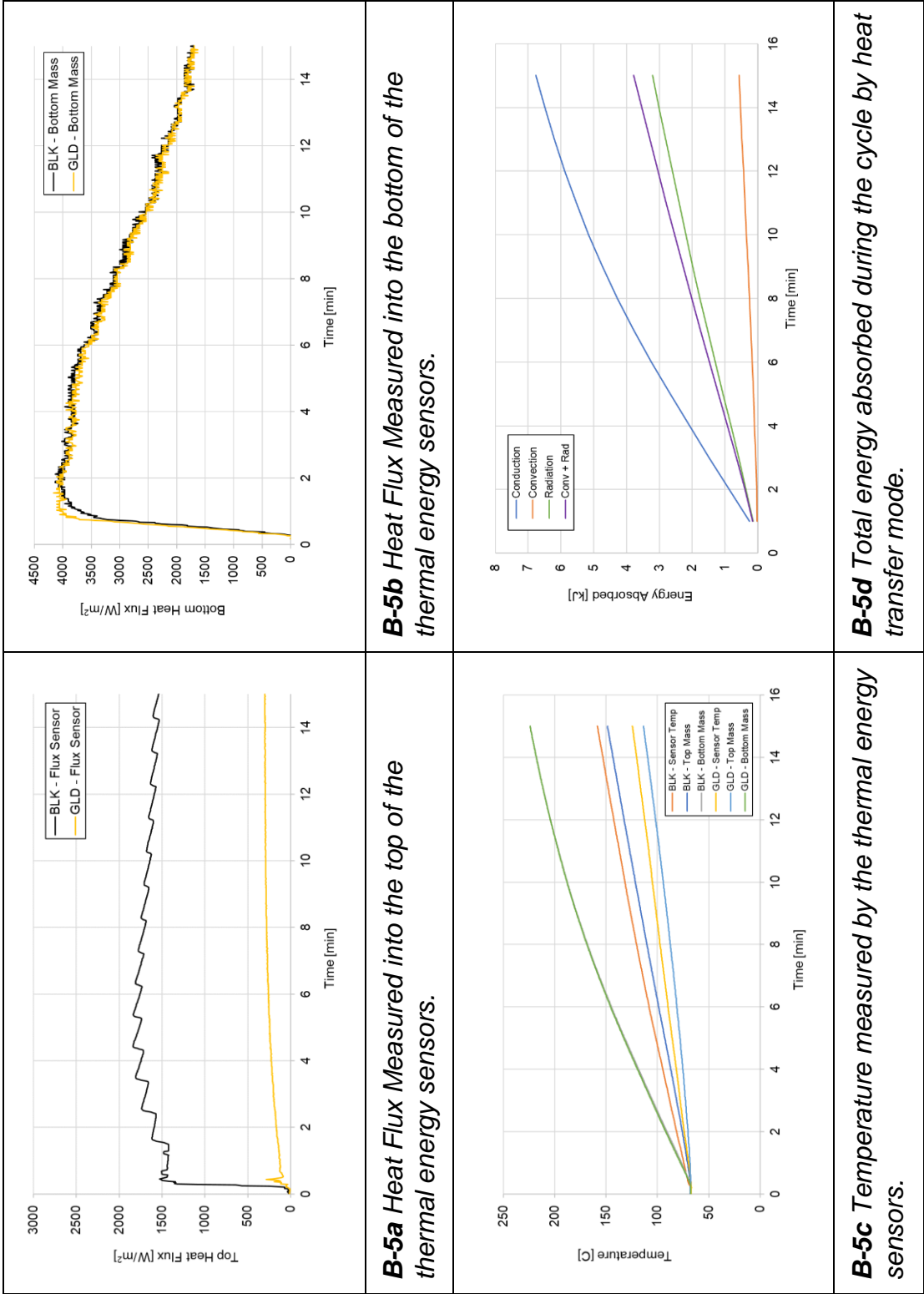


Figure B-5 Test 5, Traditional Bake, 325°F Setpoint, 15 minutes, bottom rack.

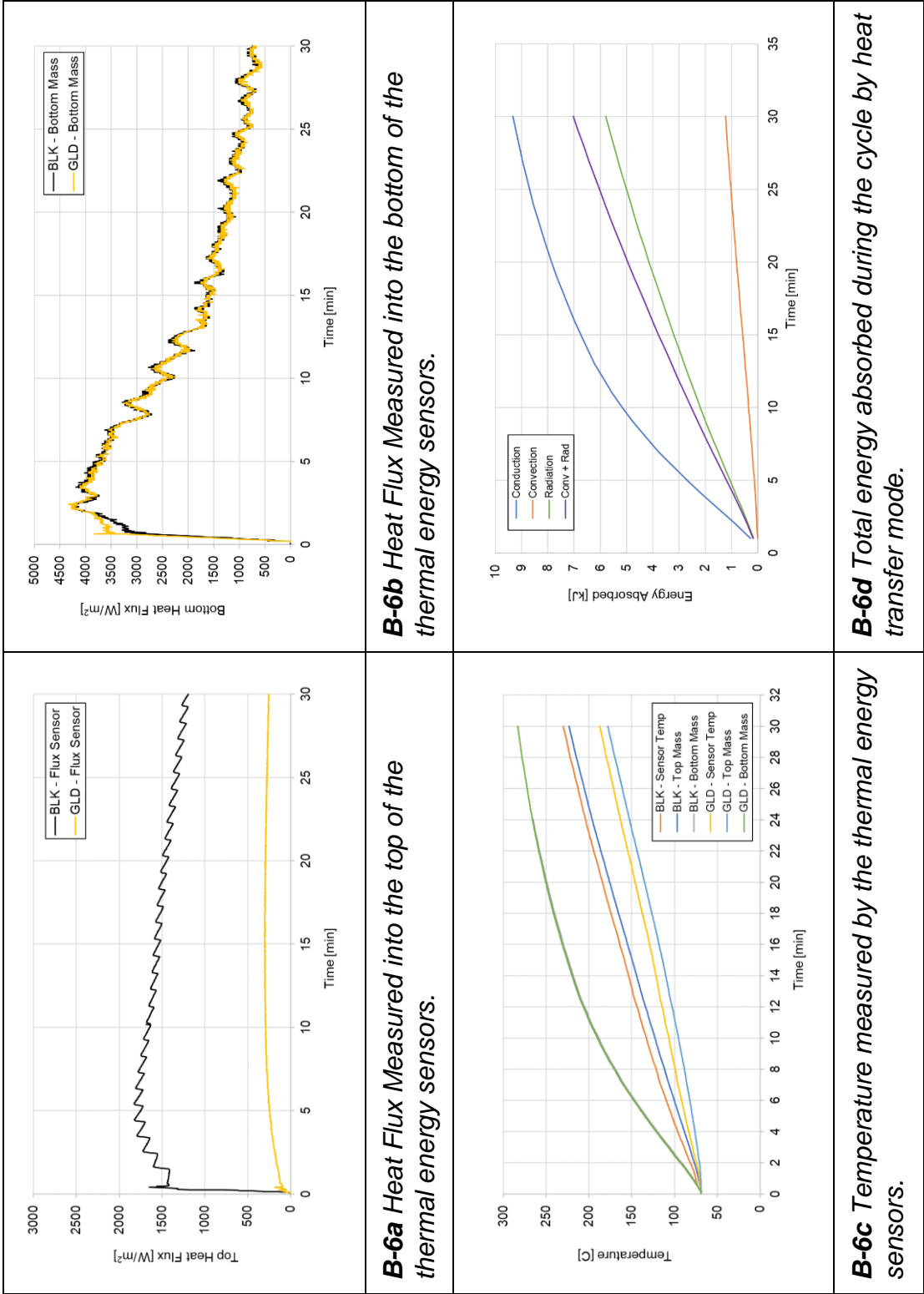


Figure B-6 Test 6, Traditional Bake, 325°F Setpoint, 30 minutes, bottom rack.

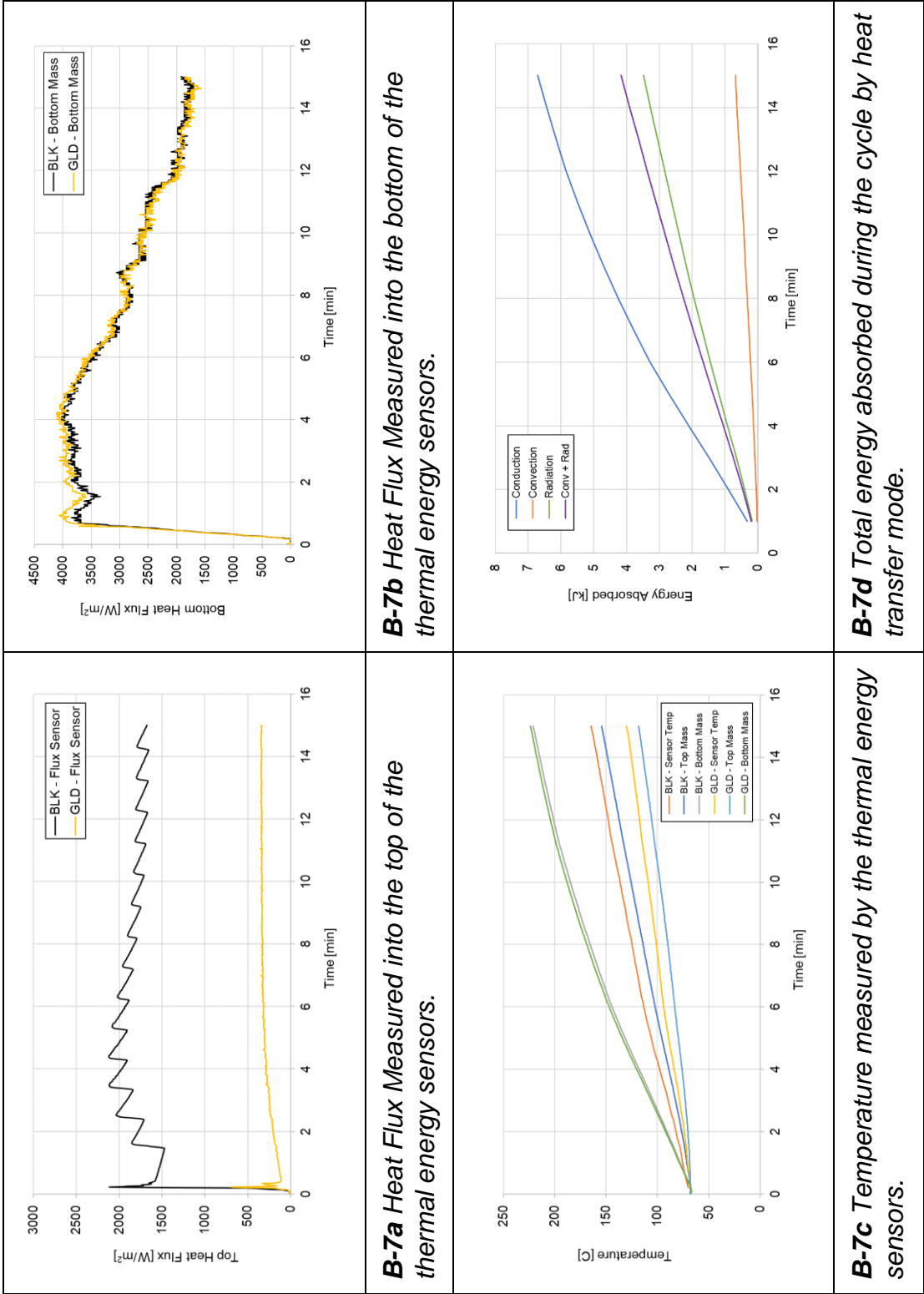


Figure B-7 Test 7, Traditional Bake, 325°F Setpoint, 15 minutes, top rack.

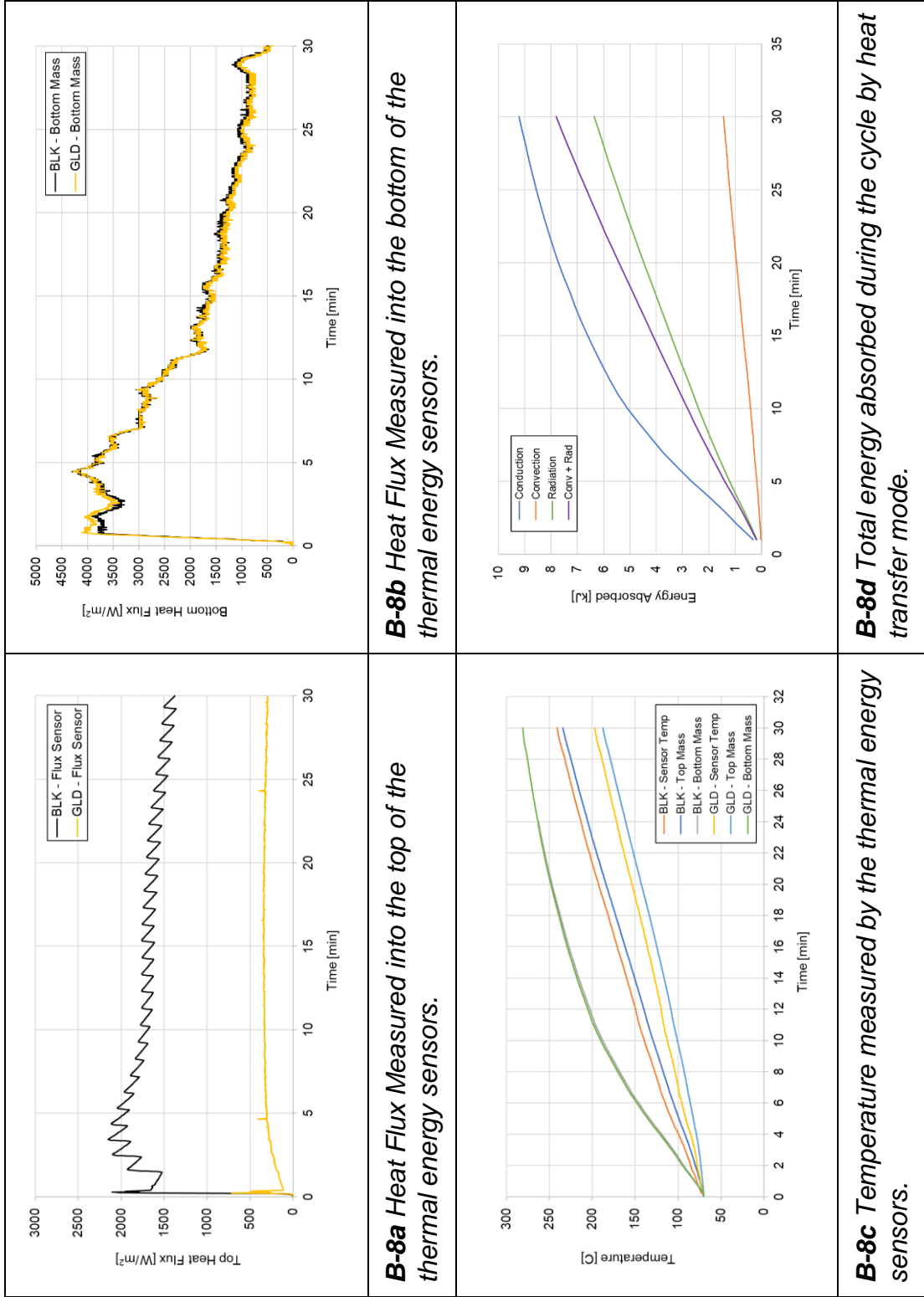


Figure B-8 Test 8, Traditional Bake, 325°F Setpoint, 30 minutes, top rack.

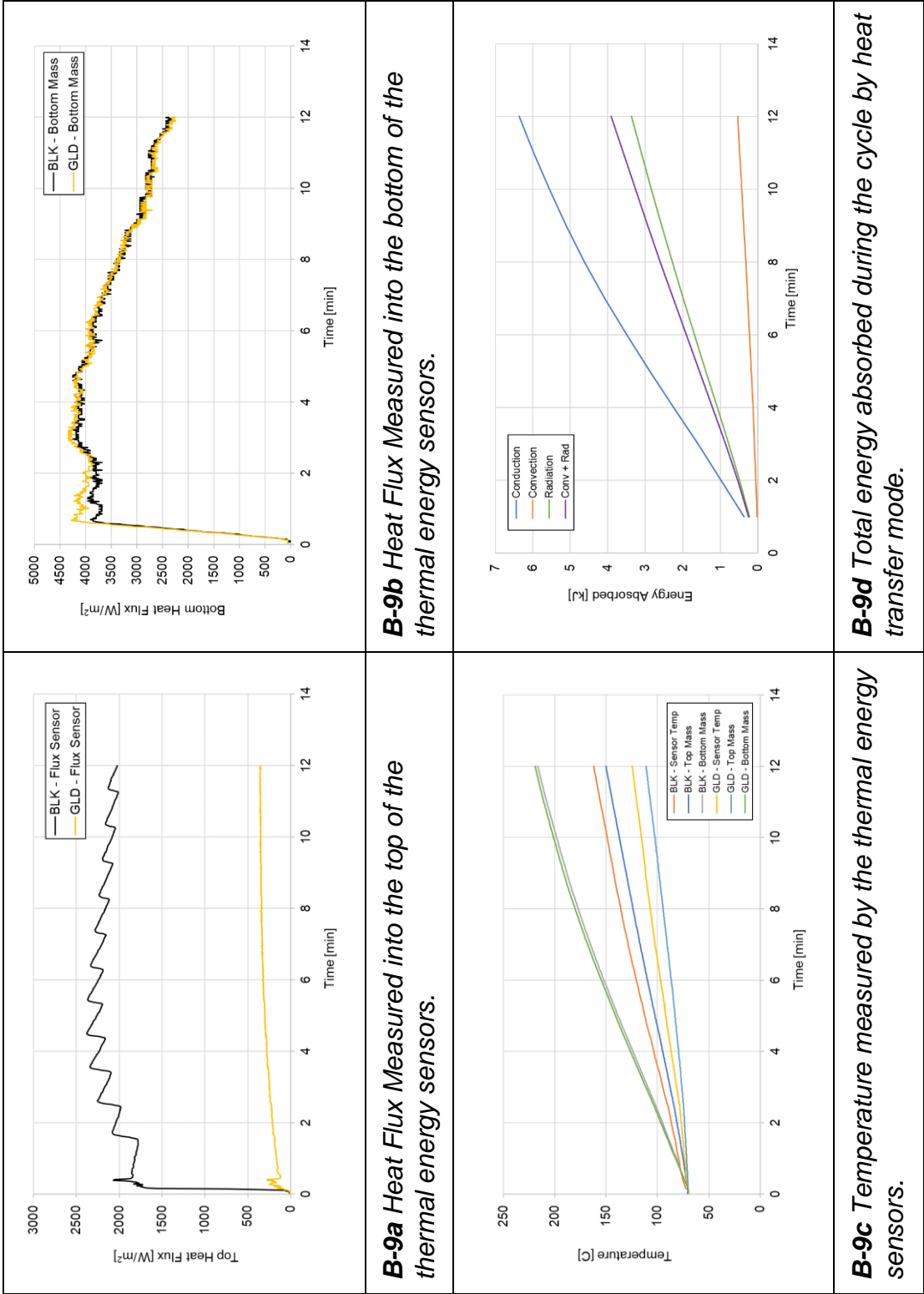


Figure B-9 Test 9, Traditional Bake, 350°F Setpoint, 12 minutes, middle rack.

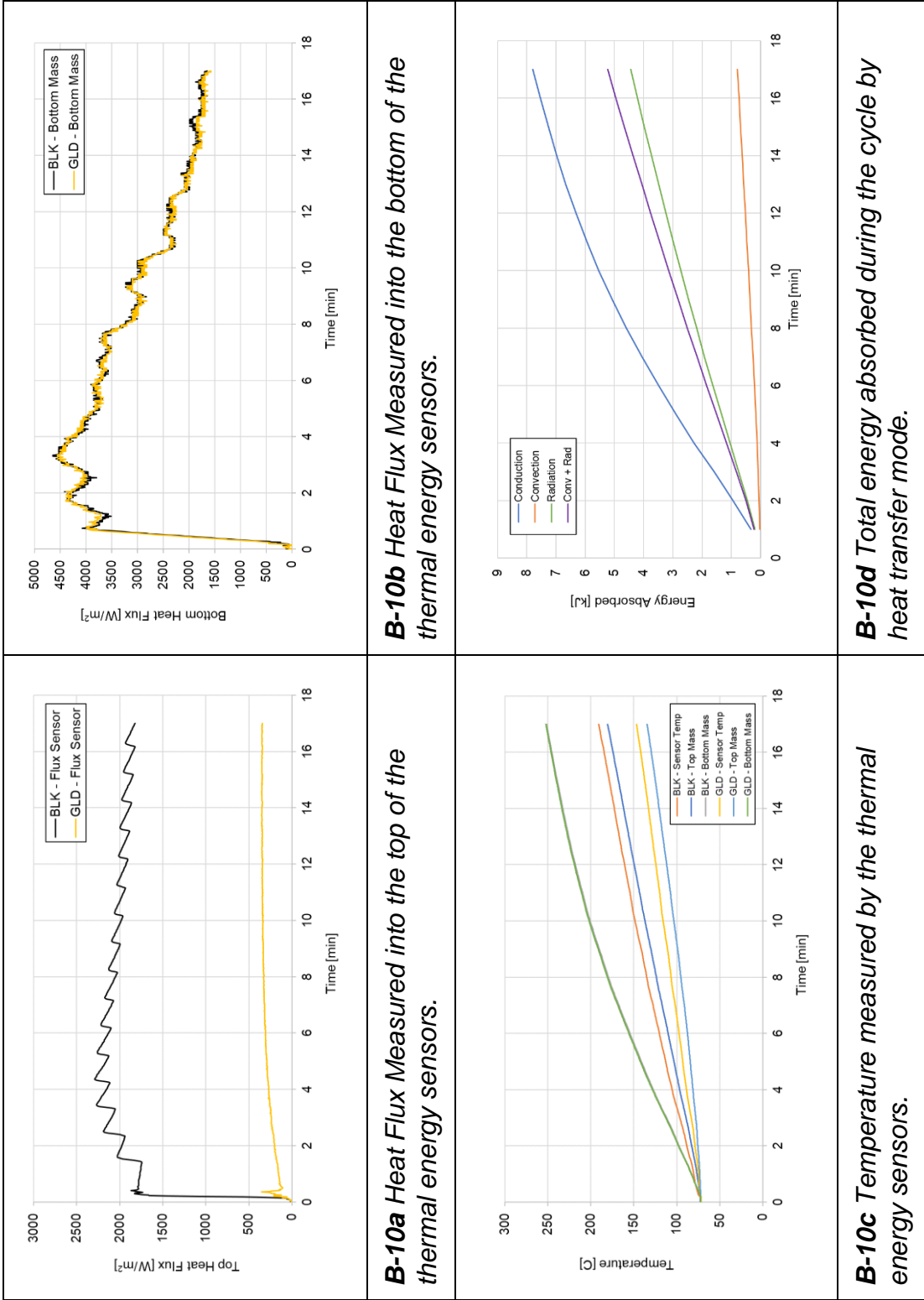


Figure B-10 Test 10, Traditional Bake, 350°F Setpoint, 17 minutes, middle rack.

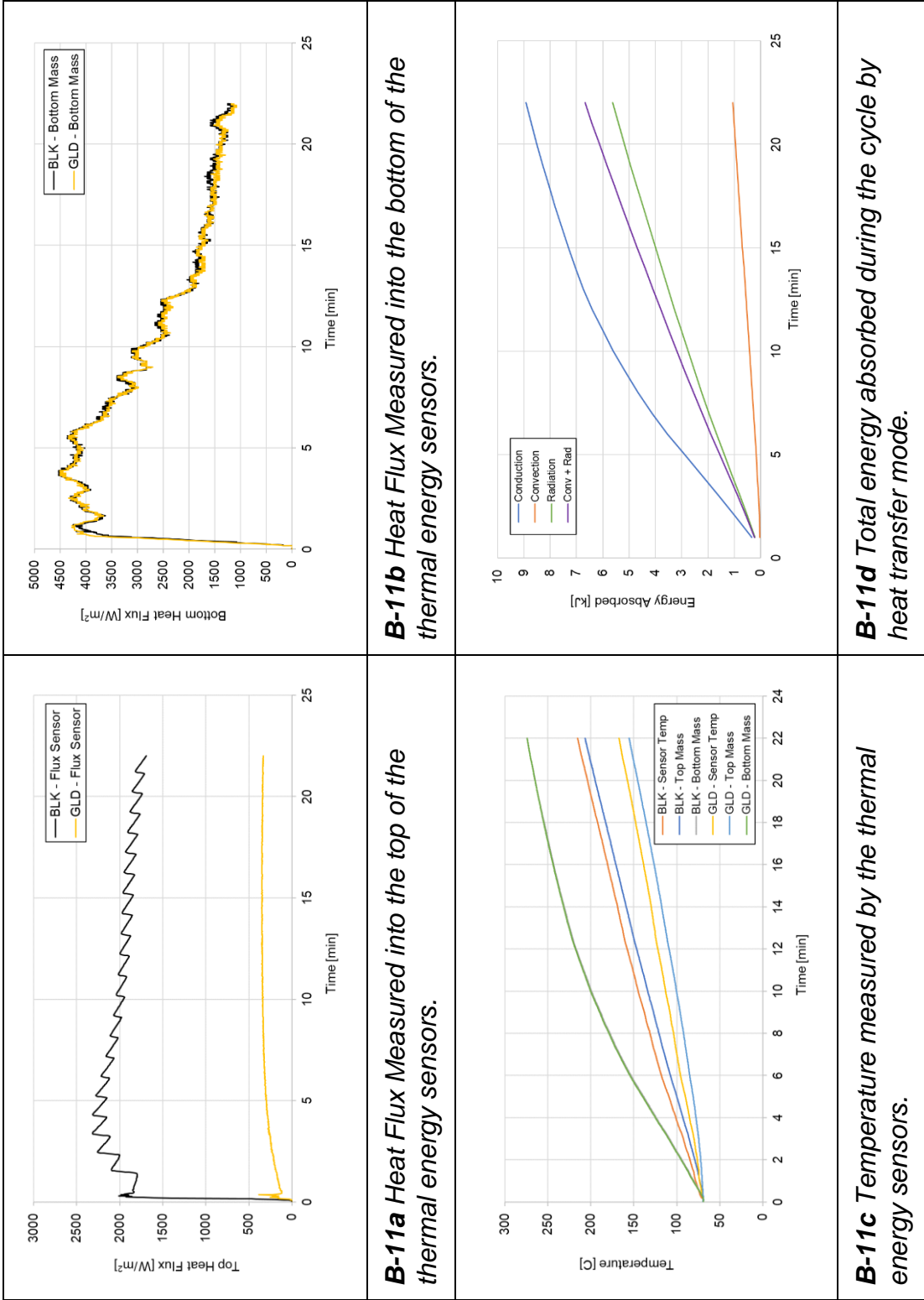


Figure B-11 Test 11, Traditional Bake, 350°F Setpoint, 22 minutes, middle rack.

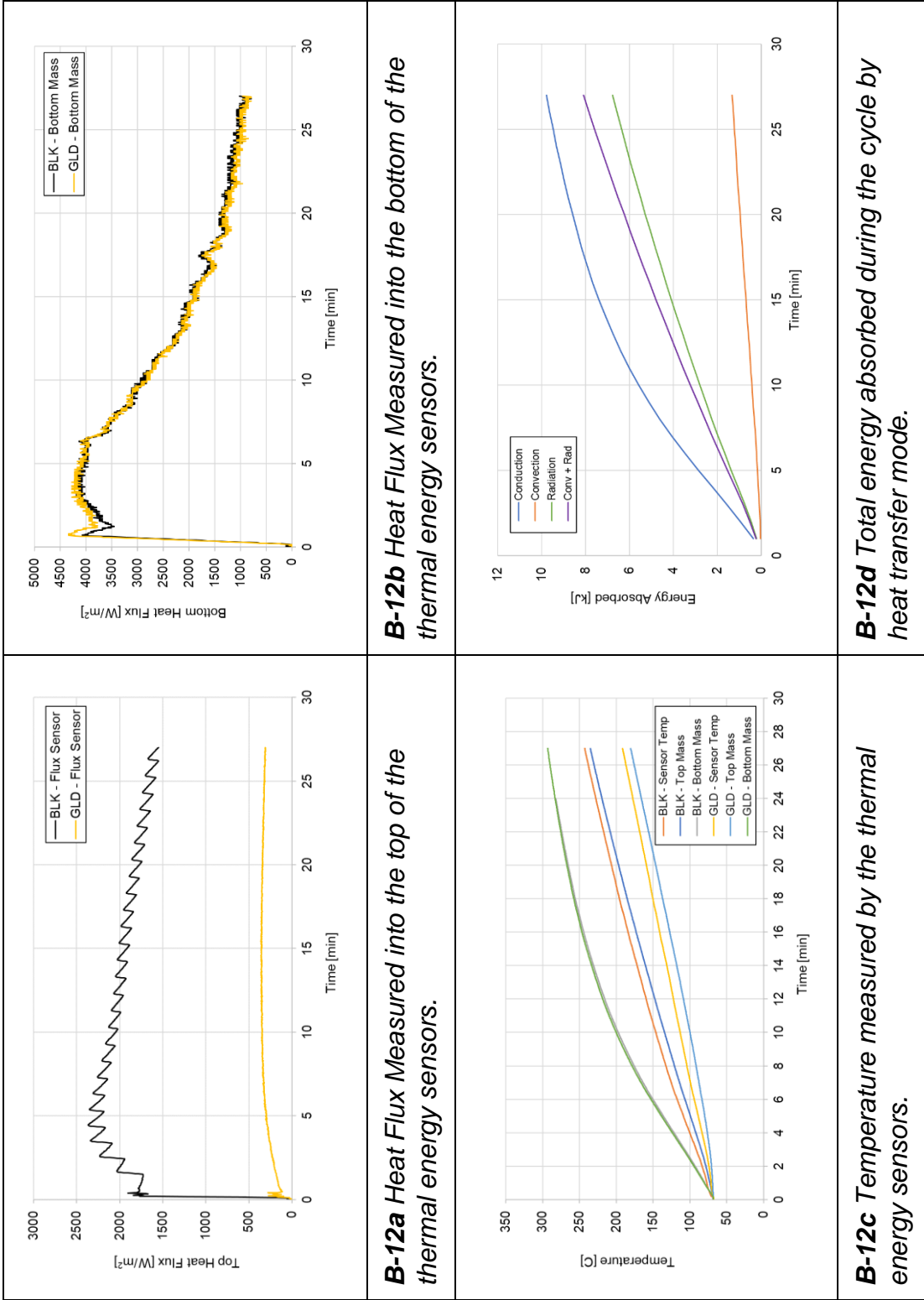


Figure B-12 Test 12, Traditional Bake, 350°F Setpoint, 27 minutes, middle rack.

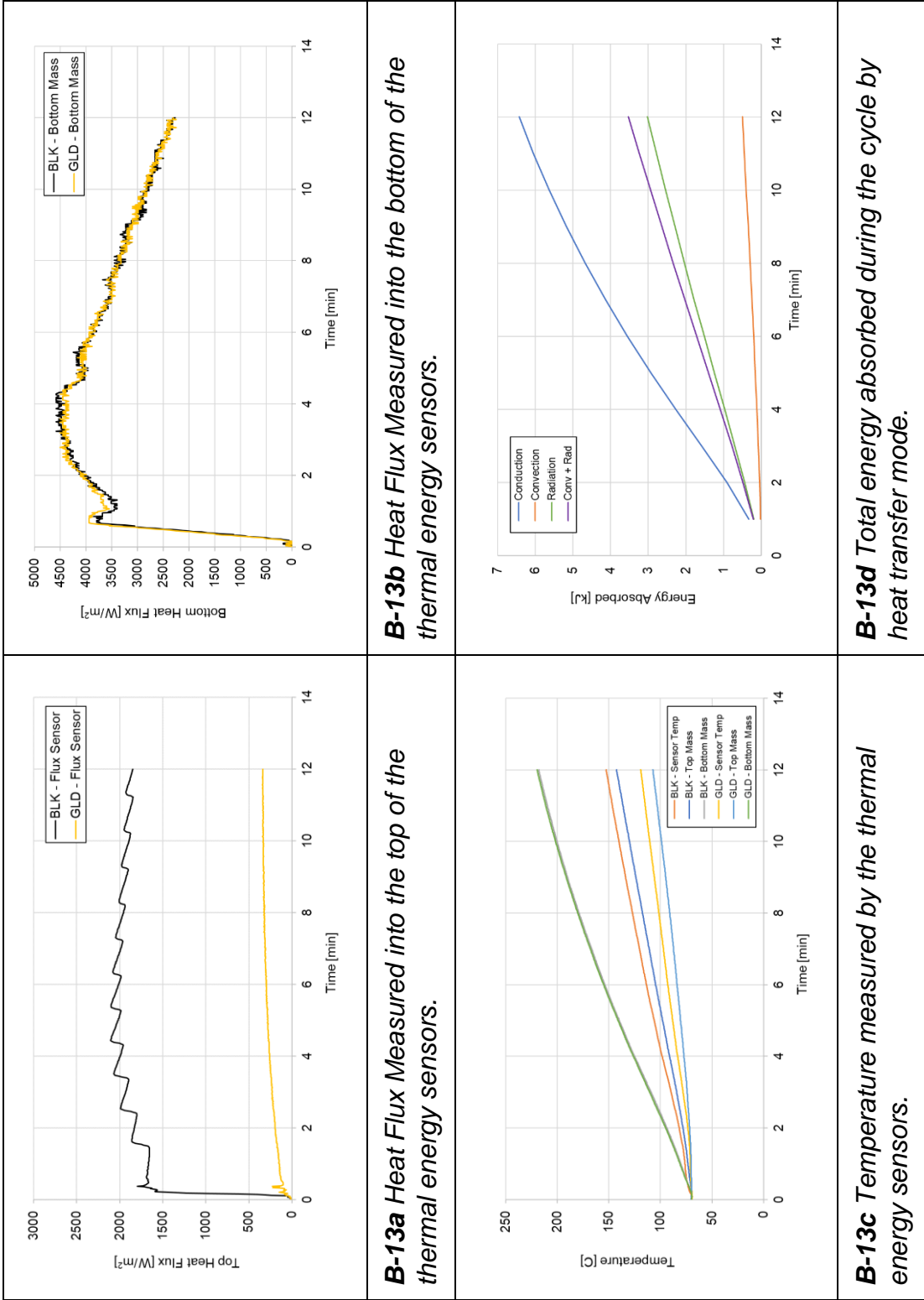


Figure B-13 Test 13, Traditional Bake, 350°F Setpoint, 12 minutes, bottom rack.

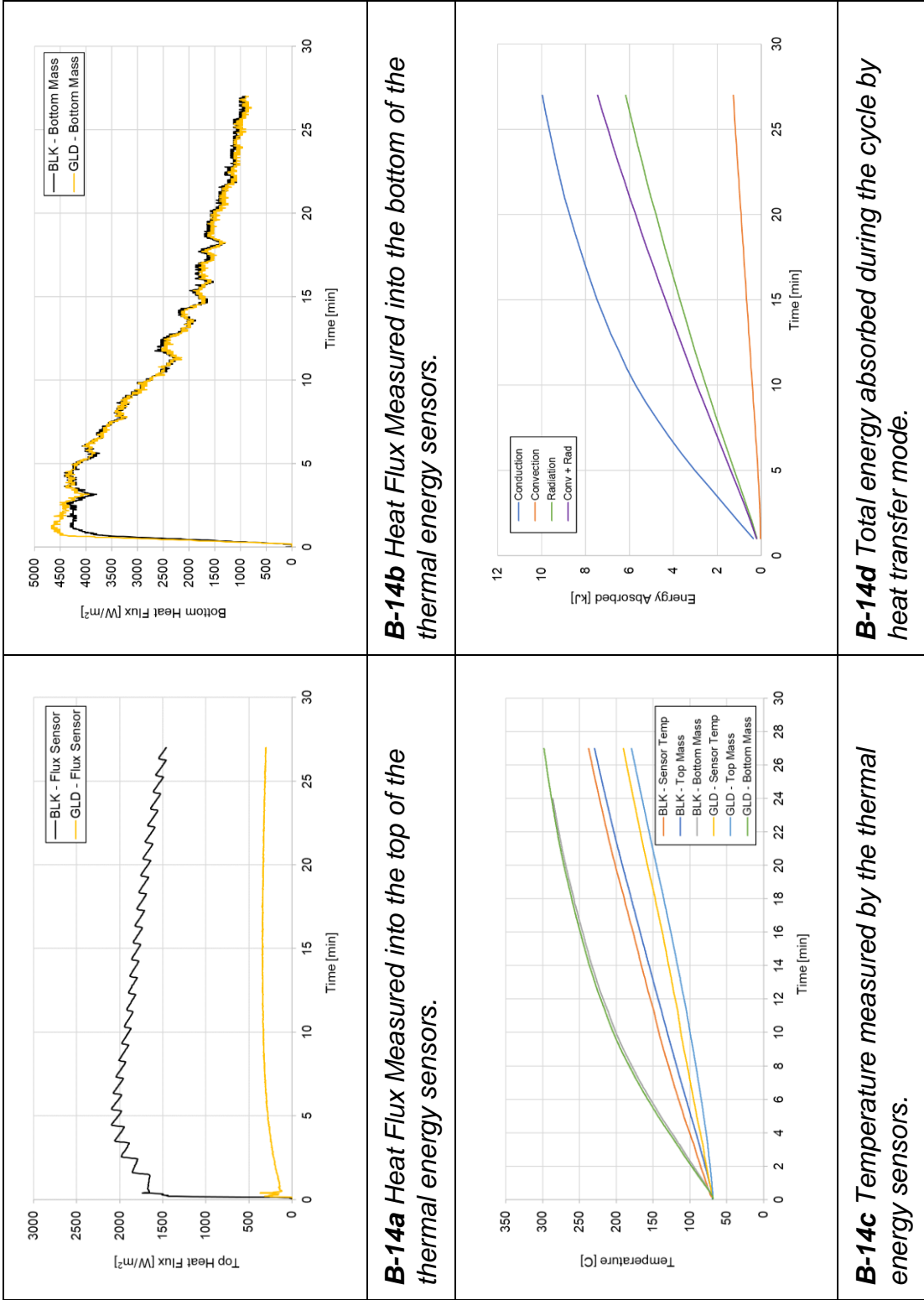


Figure B-14 Test 14, Traditional Bake, 350°F Setpoint, 27 minutes, bottom rack.

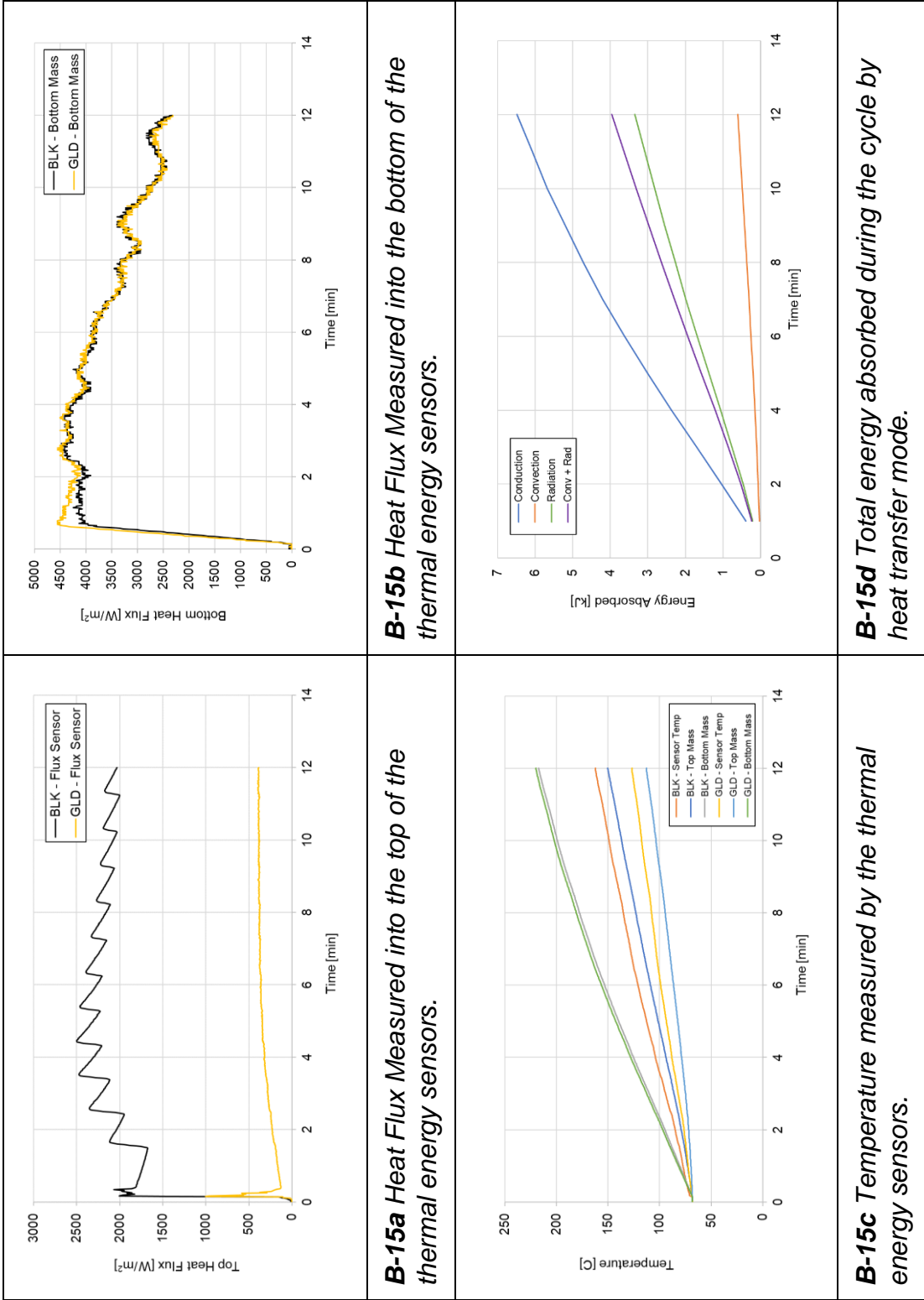


Figure B-15 Test 15, Traditional Bake, 350°F Setpoint, 12 minutes, top rack.

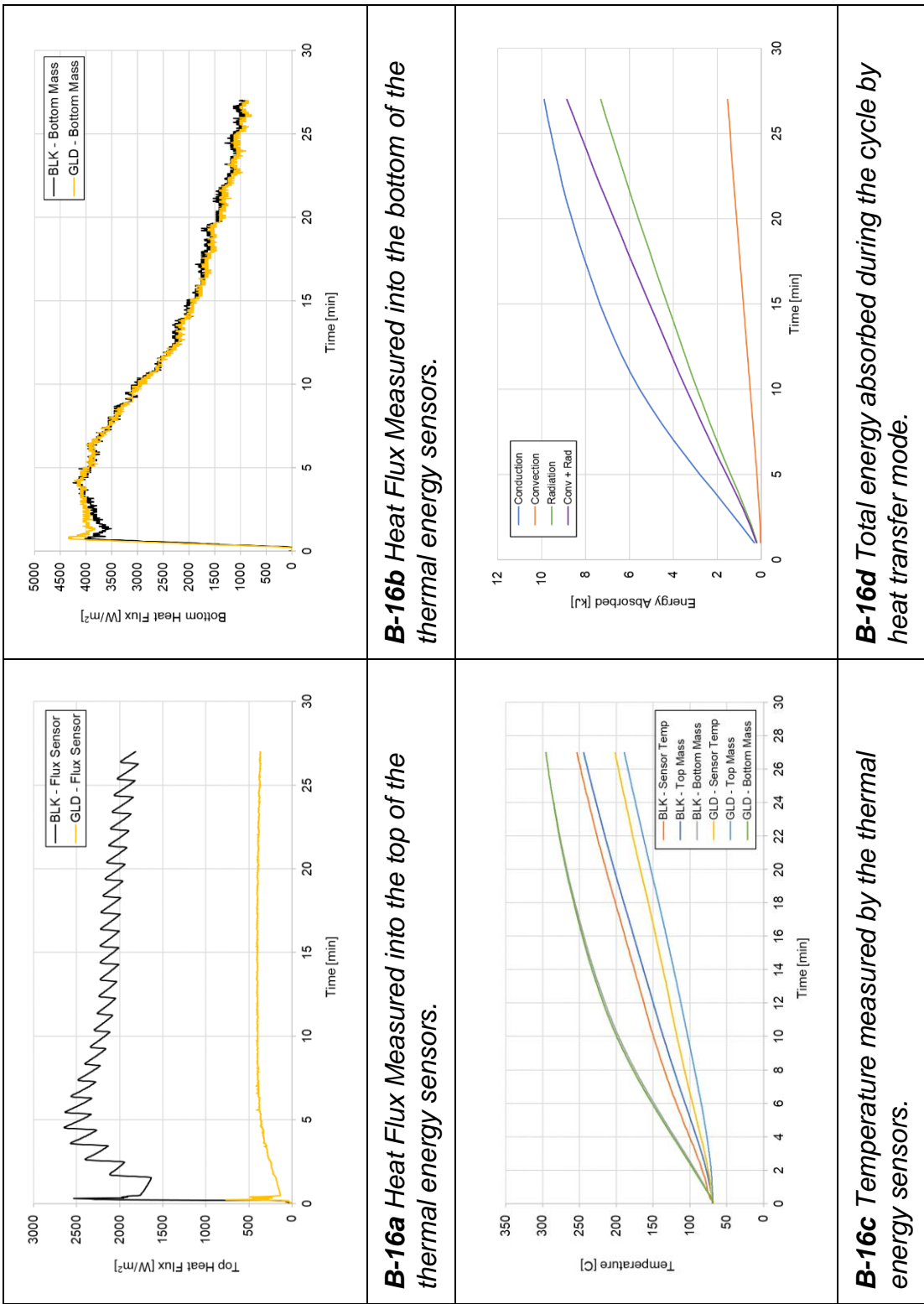


Figure B-16 Test 16, Traditional Bake, 350°F Setpoint, 27 minutes, top rack.

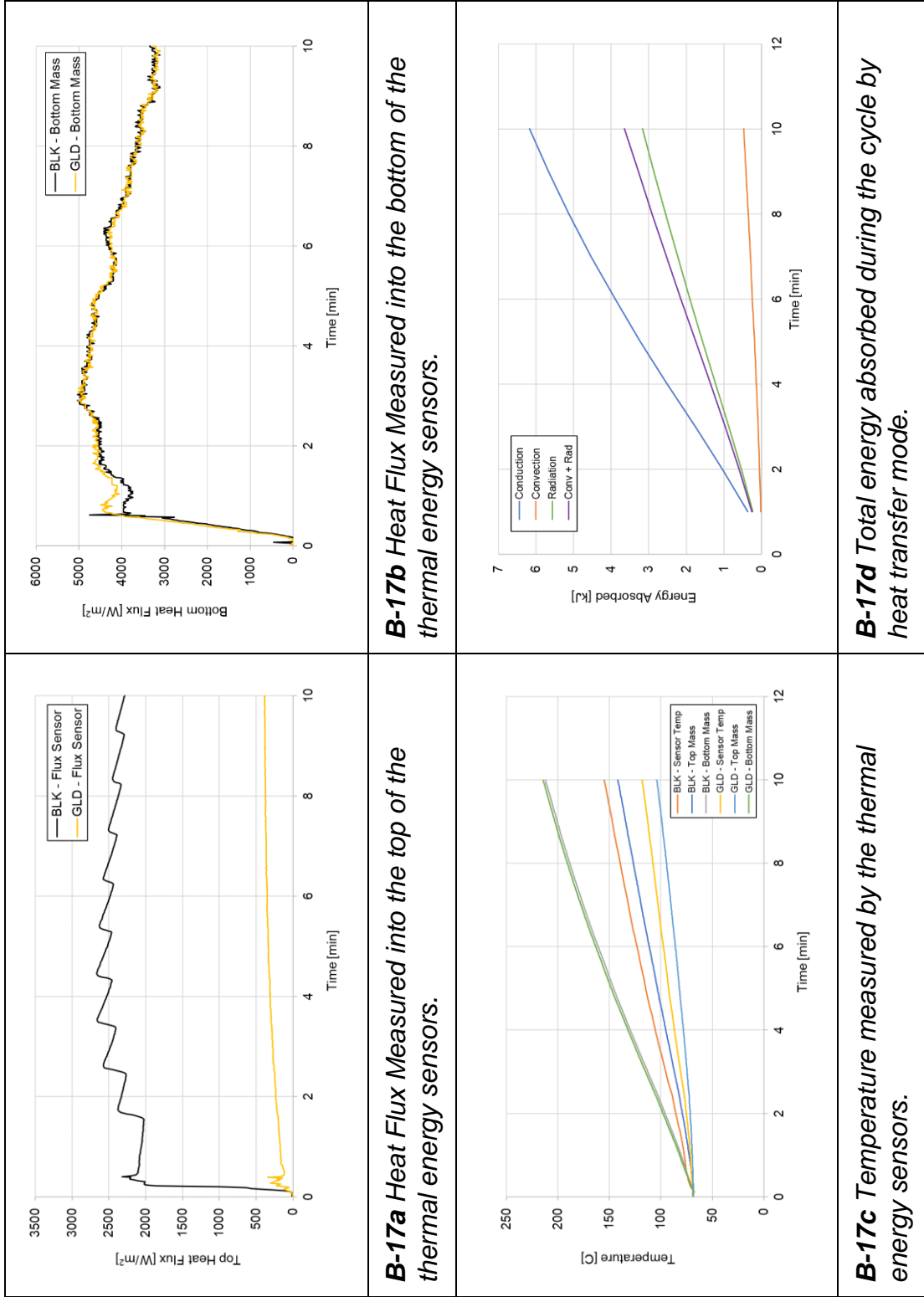


Figure B-17 Test 17, Traditional Bake, 375°F Setpoint, 10 minutes, middle rack.

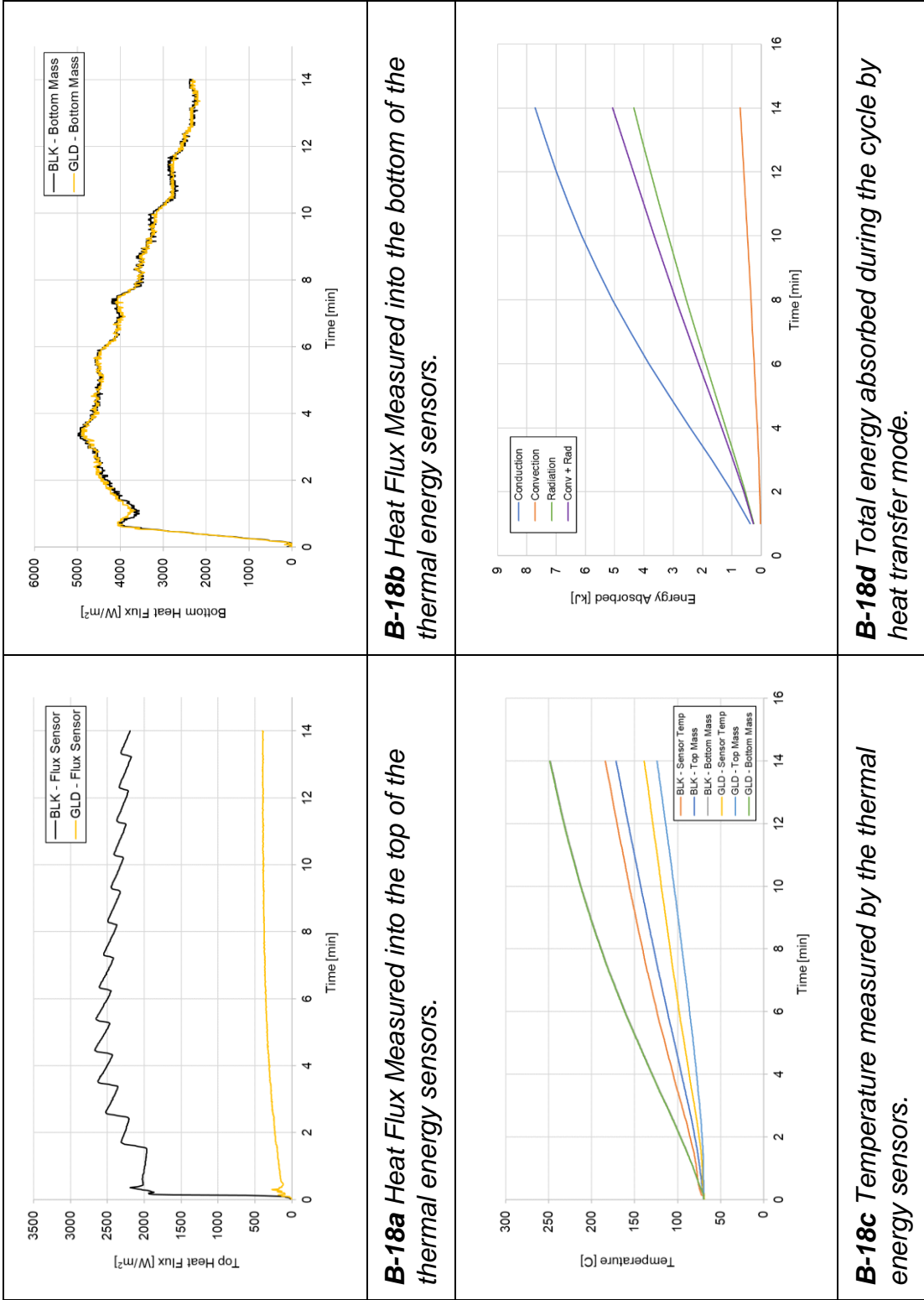


Figure B-18 Test 18, Traditional Bake, 375°F Setpoint, 14 minutes, middle rack.

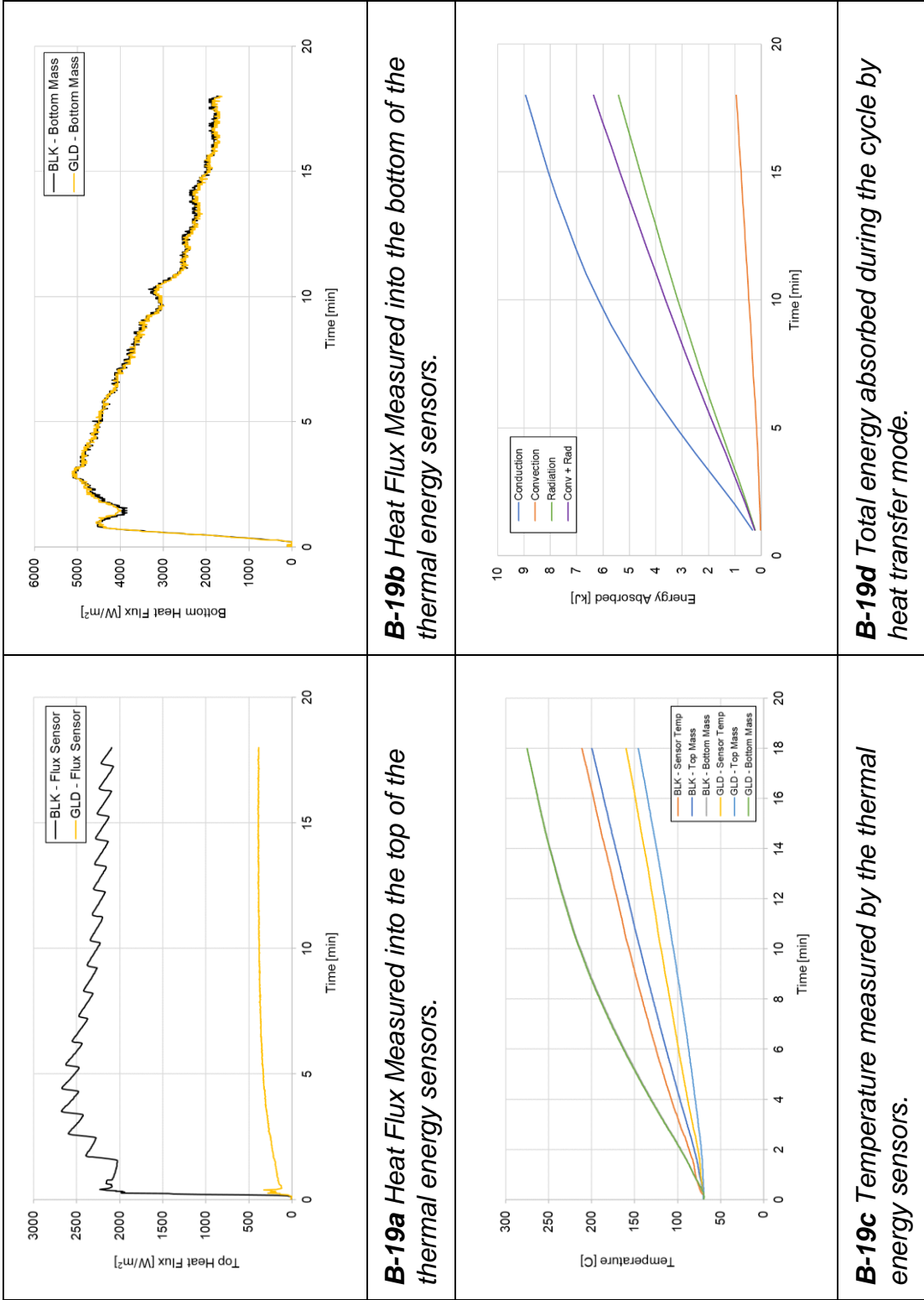


Figure B-19 Test 19, Traditional Bake, 375°F Setpoint, 18 minutes, middle rack.

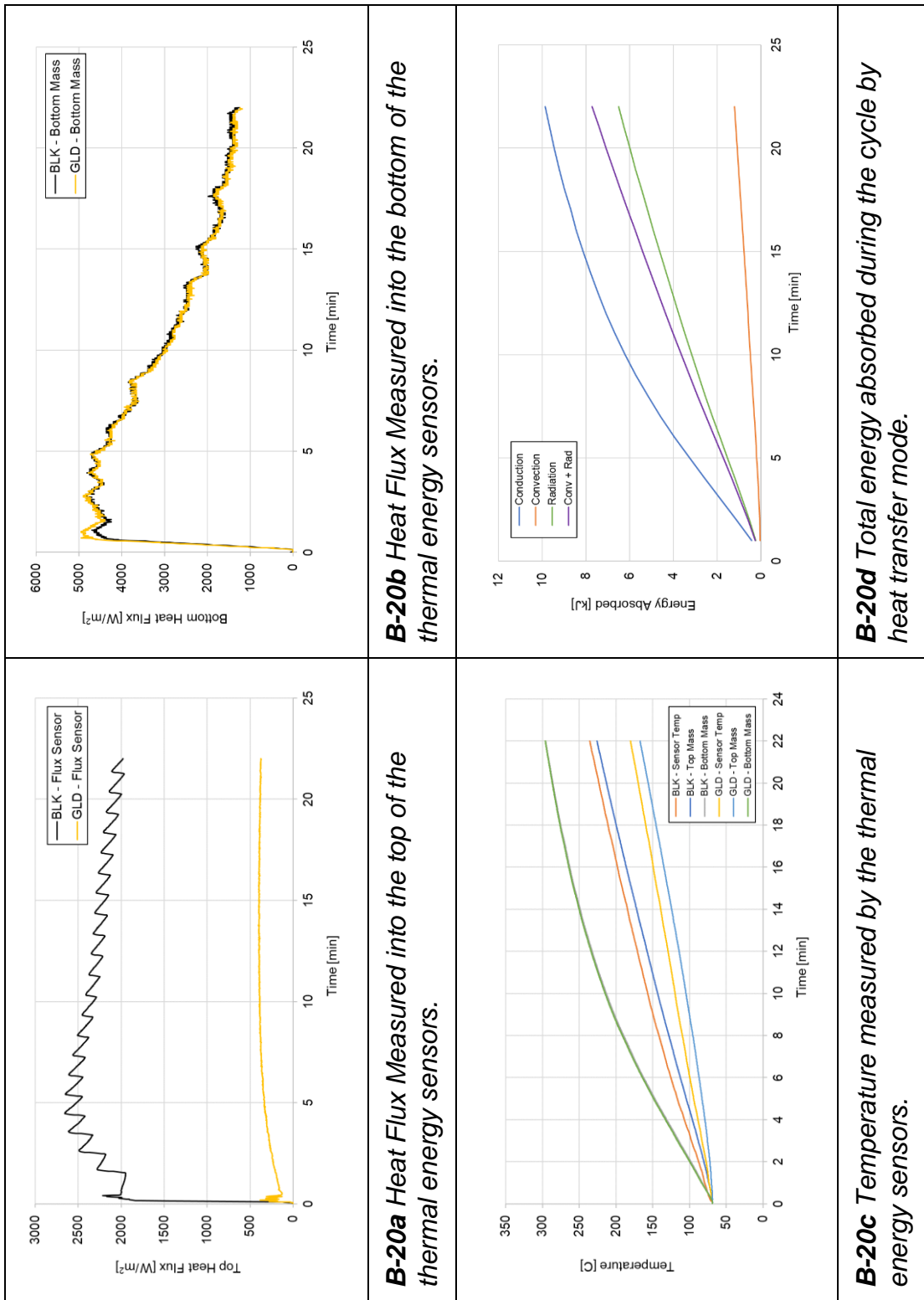


Figure B-20 Test 20, Traditional Bake, 375°F Setpoint, 22 minutes, middle rack.

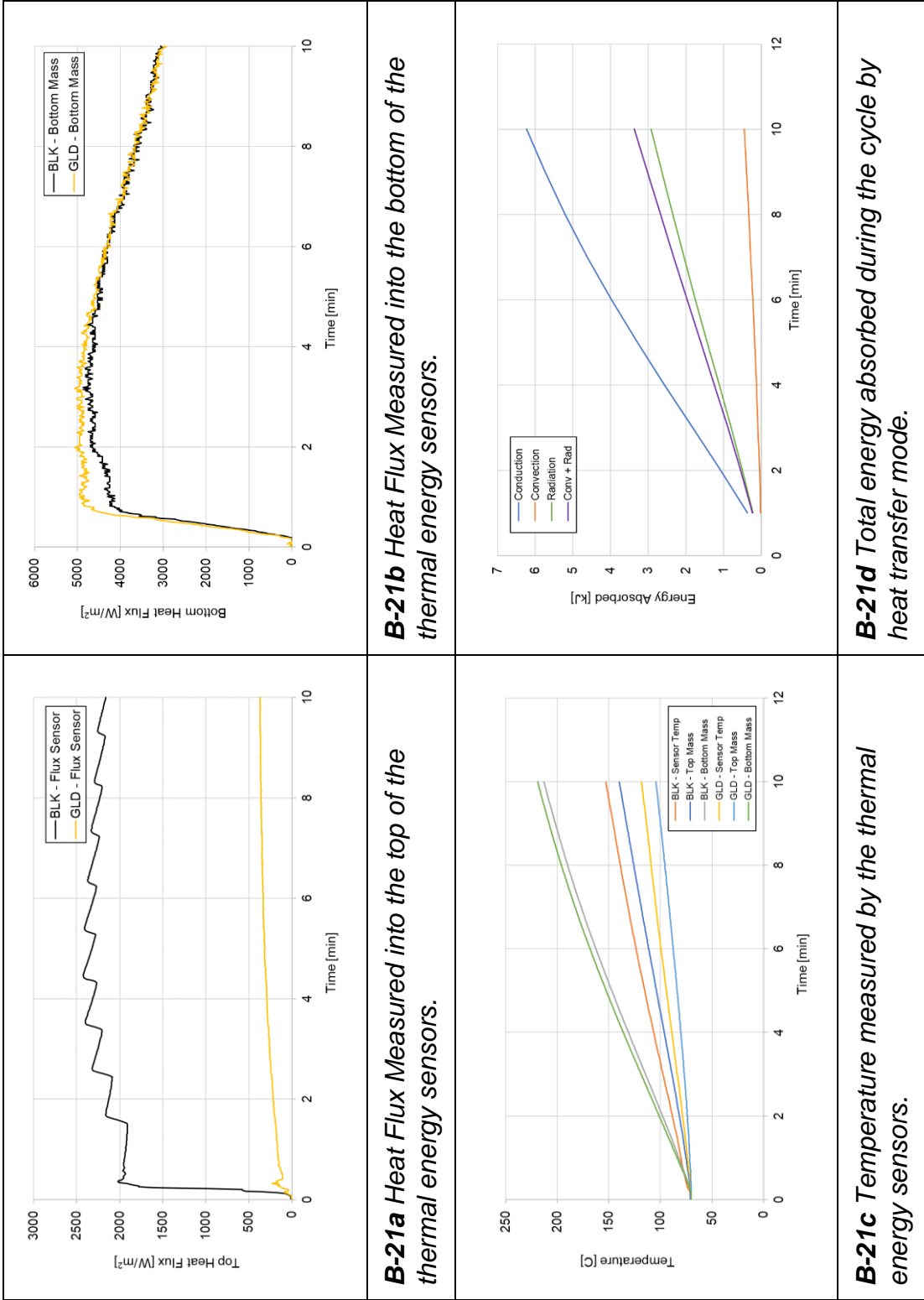


Figure B-21 Test 21, Traditional Bake, 375°F Setpoint, 10 minutes, bottom rack.

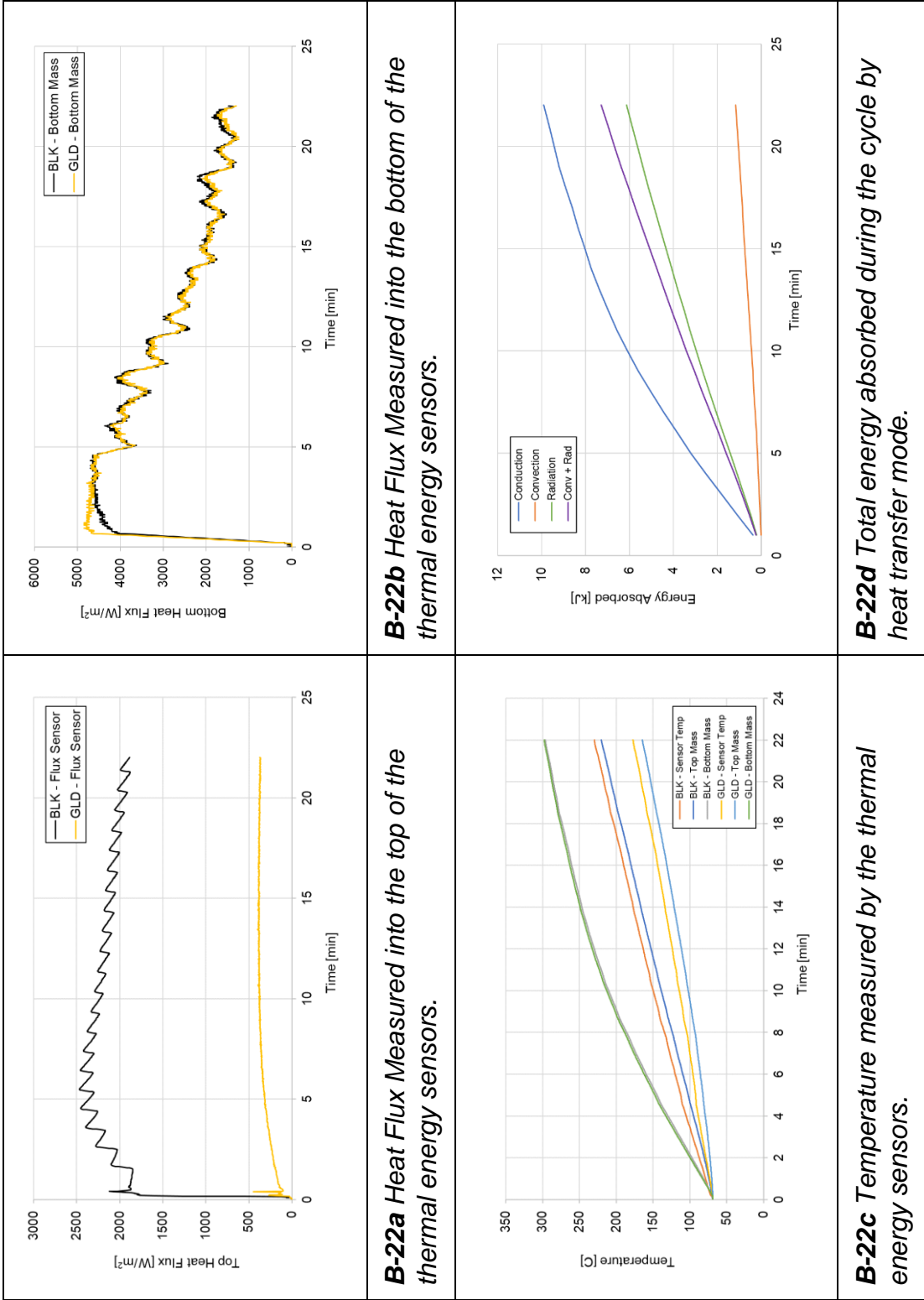


Figure B-22 Test 22, Traditional Bake, 375°F Setpoint, 22 minutes, bottom rack.

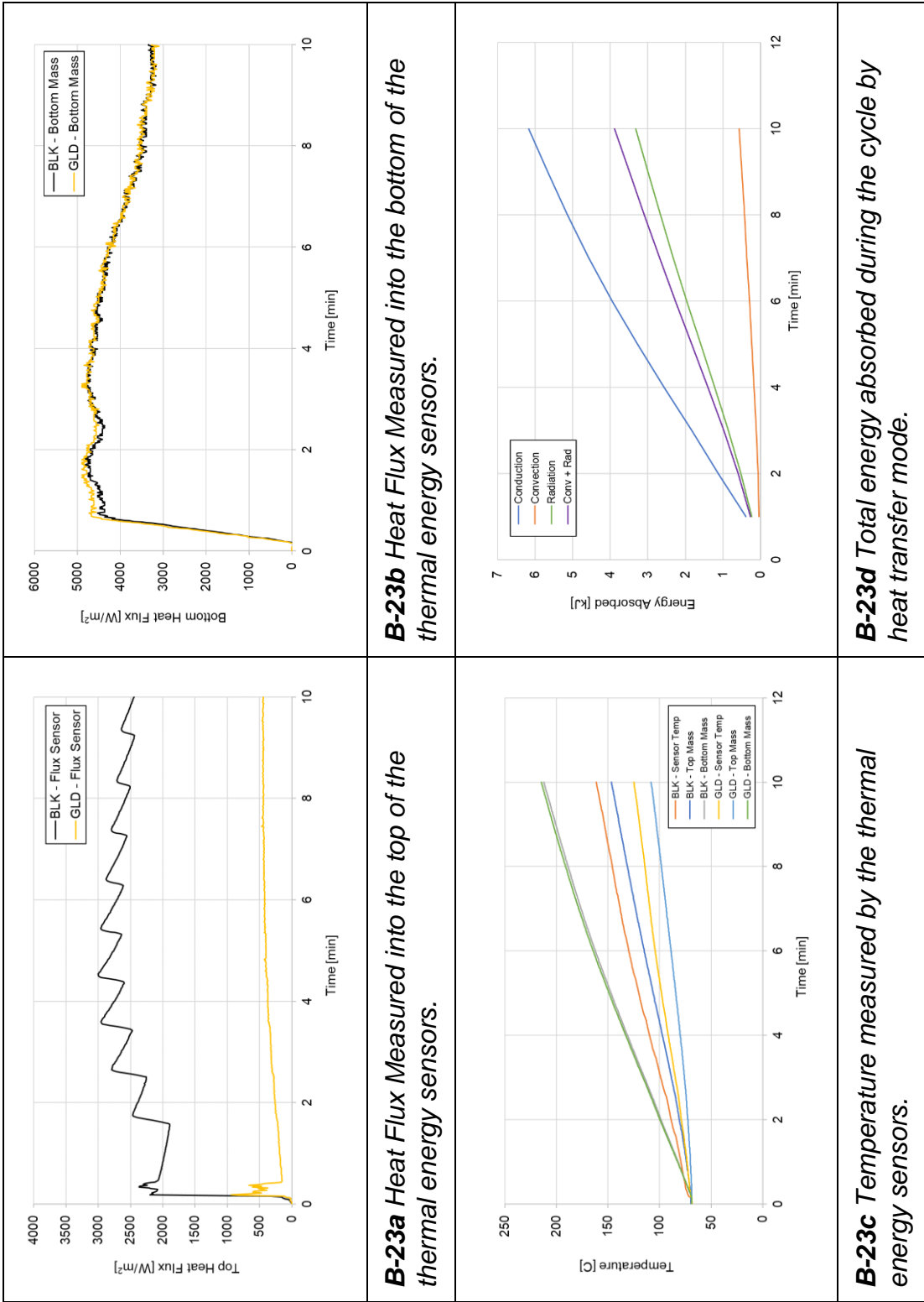


Figure B-23 Test 23, Traditional Bake, 375°F Setpoint, 10 minutes, top rack.

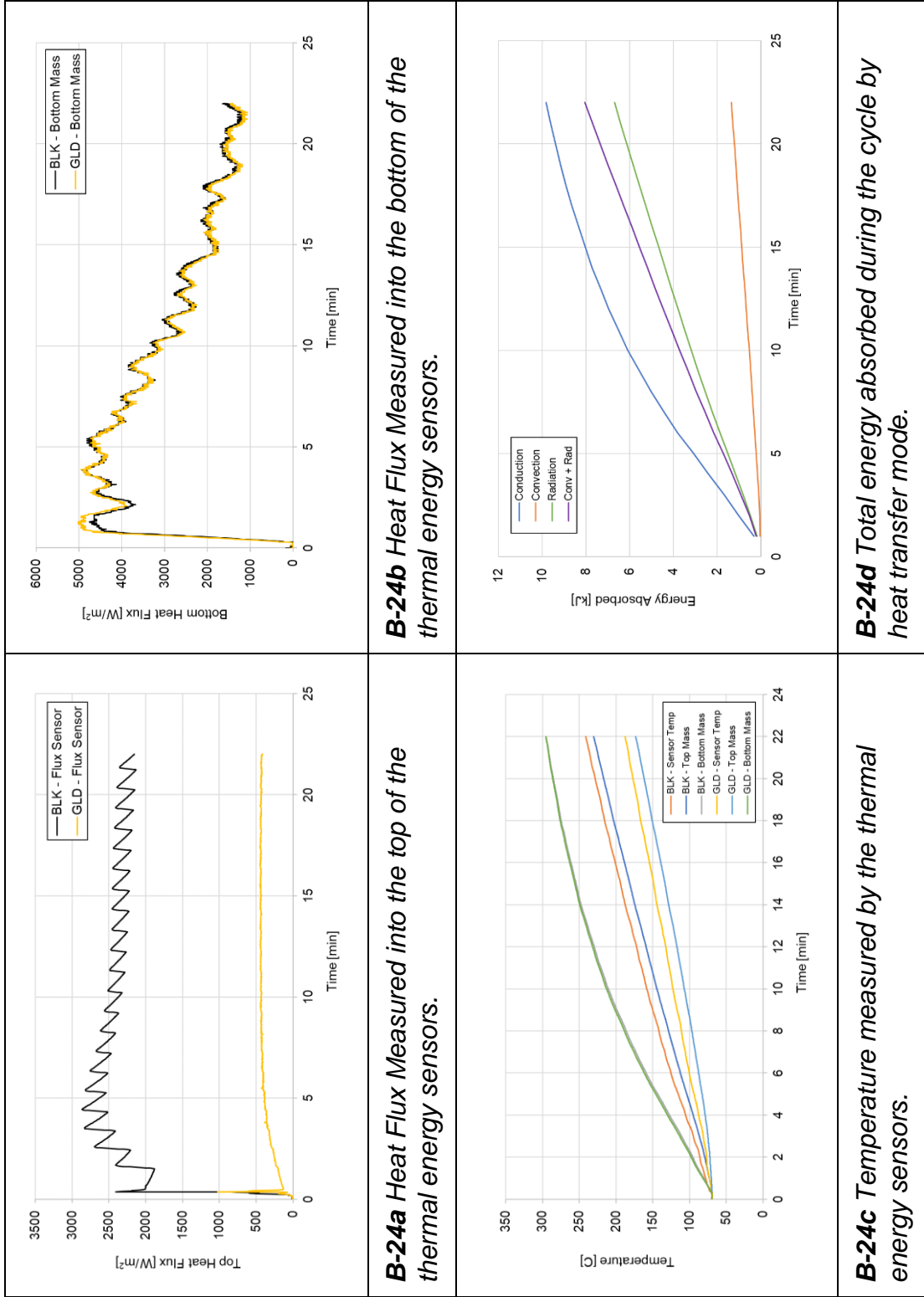


Figure B-24 Test 24, Traditional Bake, 375°F Setpoint, 22 minutes, top rack.

C Thermal Energy Sensor Repeatability

Table C-1 Repeatability data based on four runs (325°F, mid rack) using coefficient of variation. Colors show comparison of relative values, green is smaller and red is larger.

Cycle Time	Black Sensor (Left)		Gold Sensor (Right)	
	Top Mass	Bottom Mass	Top Mass	Bottom Mass
[min]	[%]	[%]	[%]	[%]
1	2.94	3.99	4.93	3.23
2	1.60	6.94	2.18	6.81
3	1.68	6.04	1.39	6.02
4	1.75	4.39	1.13	4.56
5	1.78	2.66	1.01	3.08
6	1.80	2.05	0.95	2.37
7	1.80	1.38	0.94	1.74
8	1.78	1.14	0.95	1.35
9	1.75	1.04	0.91	1.17
10	1.71	0.89	0.88	1.04
11	1.66	0.79	0.85	0.96
12	1.62	0.66	0.82	0.86
13	1.57	0.49	0.77	0.67
14	1.53	0.56	0.73	0.38
15	1.50	0.82	0.69	0.36

Table C-2 Repeatability data based on four runs (350°F, mid rack) using coefficient of variation. Colors show comparison of relative values, green is smaller and red is larger.

Cycle Time	Black Sensor (Left)		Gold Sensor (Right)	
	Top Mass	Bottom Mass	Top Mass	Bottom Mass
[min]	[%]	[%]	[%]	[%]
1	4.14	4.87	2.25	6.28
2	2.52	1.29	2.06	2.17
3	2.06	1.29	1.66	0.93
4	1.74	1.88	1.44	0.69
5	1.53	1.38	1.34	0.37
6	1.47	1.46	1.31	0.74
7	1.49	1.15	1.34	0.80
8	1.56	0.83	1.38	0.59
9	1.63	0.74	1.40	0.80
10	1.69	0.70	1.43	0.63
11	1.75	0.52	1.43	0.73
12	1.79	0.59	1.42	0.84

Table C-3 Repeatability data based on four runs (375°F, mid rack) using coefficient of variation. Colors show comparison of relative values, green is smaller and red is larger.

Cycle Time	Black Sensor (Left)		Gold Sensor (Right)	
	Top Mass	Bottom Mass	Top Mass	Bottom Mass
[min]	[%]	[%]	[%]	[%]
1	2.85	7.12	8.95	9.55
2	0.60	4.84	3.85	6.26
3	0.78	3.23	2.17	3.90
4	0.93	1.75	1.37	2.31
5	0.84	1.55	0.99	1.98
6	0.66	1.06	0.82	1.32
7	0.45	0.90	0.74	1.15
8	0.28	0.61	0.74	0.83
9	0.23	0.71	0.77	0.88
10	0.28	0.55	0.78	0.72

D Uncertainty Analysis

Table D-1 *Uncertainty values for thermal energy sensor measurements based on worst case conditions (longest test time, etc.).*

Avg Mass	87.9 g
Mass Uncertainty	0.1 g
Temperature Delta	100 K
Temperature Uncertainty	1.5 K
End of Cycle Bottom Sensor Energy Uncertainty	167 J
Hukseflux Sensor Uncertainty	5.7E-07 $\text{V}/(\text{W}/\text{m}^2)$
Average Power Uncertainty	0.215 W
End of Cycle Top Sensor Energy Uncertainty	387 J

E Cake Performance Repeatability

Table E-1 Cake browning repeatability data comparing the two cakes from each test run.

Test Number	Temp Setpoint	Cook Time	Rack Position	Bottom Browning		Top Browning		Bottom Browning Difference	Top Browning Difference		
				Cake 1	Cake 2	Cake 1	Cake 2				
[-]	[F]	[min]	[-]	[L*]	[L*]	[L*]	[L*]	[ΔL*]	[ΔL*]		
1	325	15	Mid	60.63	57.98	66.65	66.40	2.65	0.25		
2	325	20	Mid	73.68	69.41	74.44	73.87	4.27	0.57		
3	325	25	Mid	57.01	53.21	66.28	65.80	3.80	0.48		
4	325	30	Mid	79.96	78.84	81.58	81.41	1.12	0.17		
5	325	15	Bot	56.75	55.15	61.65	60.27	1.60	1.38		
6	325	30	Bot	81.45	80.34	79.08	78.80	1.11	0.28		
7	325	15	Top	70.84	68.30	75.62	74.08	2.54	1.54		
8	325	30	Top	80.33	79.85	81.08	80.38	0.48	0.70		
9	350	12	Mid	82.77	80.77	79.20	78.94	2.00	0.26		
10	350	17	Mid	80.51	78.57	79.66	79.46	1.94	0.20		
11	350	22	Mid	81.78	79.98	78.74	77.97	1.80	0.77		
12	350	27	Mid	63.76	60.55	68.42	67.94	3.21	0.48		
13	350	12	Bot	58.69	56.40	63.84	63.67	2.29	0.17		
14	350	27	Bot	50.37	47.88	59.86	58.02	2.49	1.84		
15	350	12	Top	52.77	49.81	61.63	59.87	2.96	1.76		
16	350	27	Top	51.03	47.34	60.85	58.95	3.69	1.90		
17	375	10	Mid	52.55	50.60	59.50	57.56	1.95	1.94		
18	375	14	Mid	69.18	67.24	74.67	73.93	1.94	0.74		
19	375	18	Mid	47.22	47.04	55.30	54.23	0.18	1.07		
20	375	22	Mid	51.18	46.85	59.28	57.45	4.33	1.83		
21	375	10	Bot	80.26	77.55	77.69	77.12	2.71	0.57		
22	375	22	Bot	48.60	48.01	55.55	54.11	0.59	1.44		
23	375	10	Top	79.68	77.73	78.59	78.05	1.95	0.54		
24	375	22	Top	78.69	75.62	81.77	81.51	3.07	0.26		
Average								2.28	(3.5%)	0.88	(1.3%)
Minimum								0.18	(0.3%)	0.17	(0.2%)
Maximum								4.33	(6.7%)	1.94	(2.8%)

Table E-2 Cake porosity repeatability data comparing the two cakes from each test run.

Test Number	Temp Setpoint	Cook Time	Rack Position	Porosity		
				Cake 1	Cake 2	Difference
[-]	[F]	[min]	[-]	[%]	[%]	[%]
1	325	15	Mid	14.3	18.2	3.82
2	325	20	Mid	17.0	18.8	1.85
3	325	25	Mid	21.8	27.0	5.23
4	325	30	Mid	25.0	20.7	4.33
5	325	15	Bot	19.1	15.9	3.26
6	325	30	Bot	21.0	21.5	0.43
7	325	15	Top	17.1	20.1	2.95
8	325	30	Top	21.7	20.2	1.55
9	350	12	Mid	19.5	11.9	7.61
10	350	17	Mid	16.5	23.7	7.23
11	350	22	Mid	15.4	17.2	1.75
12	350	27	Mid	14.4	22.4	7.96
13	350	12	Bot	15.9	12.6	3.32
14	350	27	Bot	22.5	13.8	8.64
15	350	12	Top	17.3	18.9	1.65
16	350	27	Top	26.1	25.8	0.28
17	375	10	Mid	22.5	22.1	0.35
18	375	14	Mid	22.3	24.0	1.70
19	375	18	Mid	24.2	25.0	0.86
20	375	22	Mid	12.6	18.4	5.75
21	375	10	Bot	24.4	2.2	22.21
22	375	22	Bot	24.4	17.4	7.06
23	375	10	Top	15.5	18.0	2.51
24	375	22	Top	26.0	15.2	10.78
				Average	4.7	(24%)
				Minimum	0.3	(1%)
				Maximum	22.2	(115%)

Table E-3 Cake rise height repeatability data comparing the two cakes from each test run.

Test Number	Temp Setpoint	Cook Time	Rack Position	Side Rise		Center Rise		Side Rise Difference	Center Rise Difference
				Cake 1	Cake 2	Cake 1	Cake 2		
[-]	[F]	[min]	[-]	[in]	[in]	[in]	[in]	[in]	[in]
1	325	15	Mid	0.938	0.927	1.200	1.163	0.011	0.037
2	325	20	Mid	1.009	0.977	1.250	1.290	0.032	0.040
3	325	25	Mid	0.894	0.883	1.219	1.235	0.012	0.017
4	325	30	Mid	1.019	1.006	1.263	1.282	0.013	0.020
5	325	15	Bot	0.946	0.934	1.220	1.212	0.013	0.008
6	325	30	Bot	0.996	0.950	1.282	1.304	0.046	0.022
7	325	15	Top	0.927	0.894	1.209	1.207	0.033	0.002
8	325	30	Top	0.992	0.995	1.297	1.303	0.003	0.006
9	350	12	Mid	0.952	0.952	1.293	1.325	0.000	0.032
10	350	17	Mid	1.030	1.007	1.326	1.355	0.023	0.030
11	350	22	Mid	0.972	0.944	1.249	1.285	0.028	0.037
12	350	27	Mid	0.992	0.957	1.268	1.255	0.035	0.013
13	350	12	Bot	0.950	0.953	1.224	1.270	0.003	0.046
14	350	27	Bot	0.909	0.860	1.211	1.229	0.049	0.017
15	350	12	Top	0.939	0.897	1.185	1.169	0.042	0.016
16	350	27	Top	0.906	0.856	1.190	1.177	0.050	0.013
17	375	10	Mid	0.917	0.903	1.218	1.204	0.014	0.014
18	375	14	Mid	0.924	0.895	1.264	1.272	0.029	0.008
19	375	18	Mid	0.879	0.878	1.192	1.227	0.001	0.035
20	375	22	Mid	0.869	0.853	1.261	1.197	0.016	0.064
21	375	10	Bot	0.985	0.962	1.362	1.343	0.023	0.019
22	375	22	Bot	0.881	0.902	1.188	1.228	0.021	0.040
23	375	10	Top	1.067	0.968	1.334	1.355	0.100	0.021
24	375	22	Top	1.004	1.033	1.338	1.352	0.030	0.015
Average								0.026 (3%)	0.024 (2%)
Minimum								0.000 (0%)	0.002 (0%)
Maximum								0.100 (11%)	0.064 (5%)

Table E-4 Cake mass loss repeatability data comparing the two cakes from each test run.

Test Number	Temp Setpoint	Cook Time	Rack Position	Mass Loss		
				Cake 1	Cake 2	Difference
[-]	[F]	[min]	[-]	[g]	[g]	[g]
1	325	15	Mid	3.5	3.8	0.3
2	325	20	Mid	5.6	6.2	0.6
3	325	25	Mid	7.7	8	0.3
4	325	30	Mid	9.7	10.2	0.5
5	325	15	Bot	3.3	3.8	0.5
6	325	30	Bot	11.4	12.4	1.0
7	325	15	Top	3.8	4.1	0.3
8	325	30	Top	10.8	11.1	0.3
9	350	12	Mid	3.1	3.5	0.4
10	350	17	Mid	5.6	5.7	0.1
11	350	22	Mid	7.8	8.2	0.4
12	350	27	Mid	10.7	10.8	0.1
13	350	12	Bot	3.3	3.1	0.2
14	350	27	Bot	10.3	10.7	0.4
15	350	12	Top	3.5	3.6	0.1
16	350	27	Top	11.2	11.7	0.5
17	375	10	Mid	2.8	3	0.2
18	375	14	Mid	5.3	5.4	0.1
19	375	18	Mid	7.4	8.1	0.7
20	375	22	Mid	9.4	10.1	0.7
21	375	10	Bot	3.1	3.3	0.2
22	375	22	Bot	9.5	9.6	0.1
23	375	10	Top	3.3	3.6	0.3
24	375	22	Top	10.3	10.5	0.2
				Average	0.35	(5%)
				Minimum	0.10	(1%)
				Maximum	1.00	(14%)

F Correlations

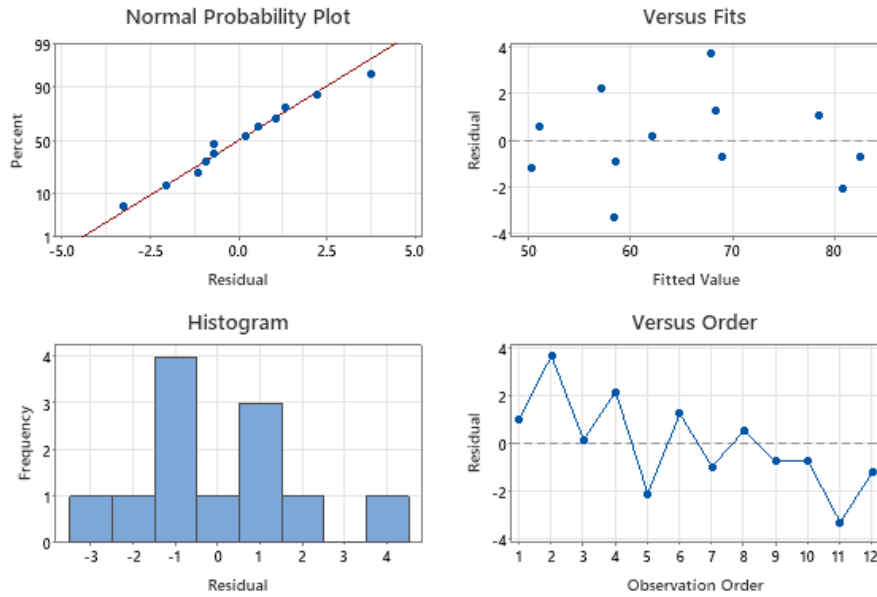


Figure F-1 Residual plots for correlation between bottom browning and conduction energy absorbed.

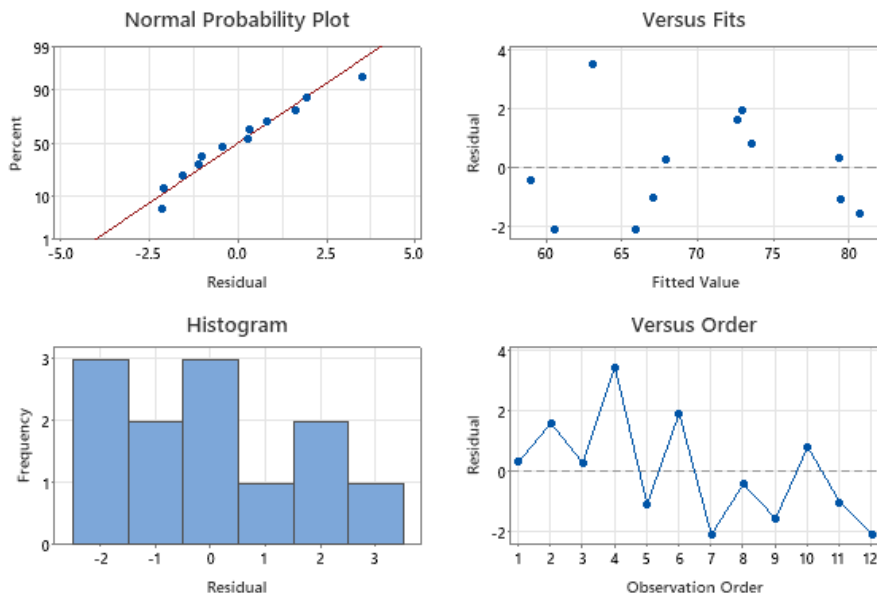


Figure F-2 Residual plots for correlation between top browning and radiation energy absorbed.

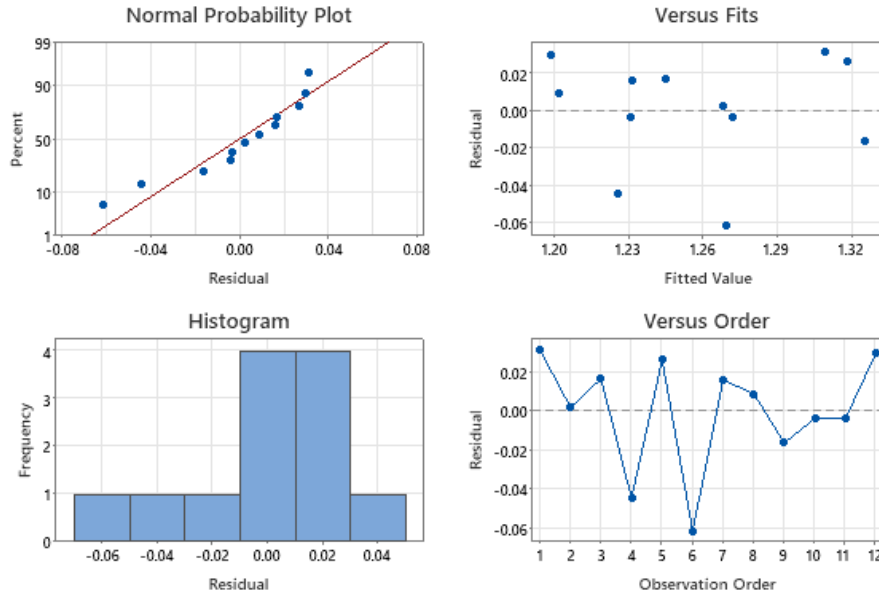


Figure F-3 Residual plots for attempted correlation between center rise and conduction energy.

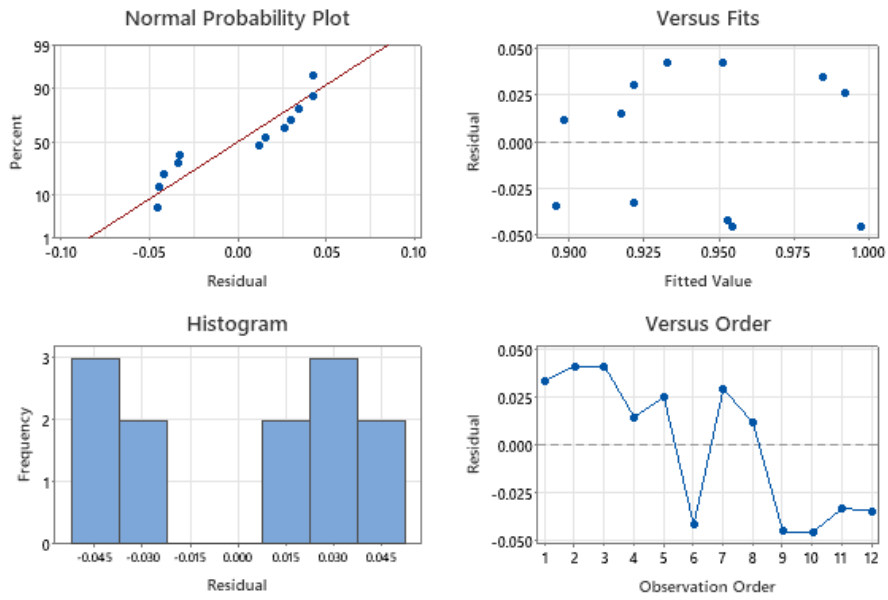


Figure F-4 Residual plots for attempted correlation between side rise and conduction energy.

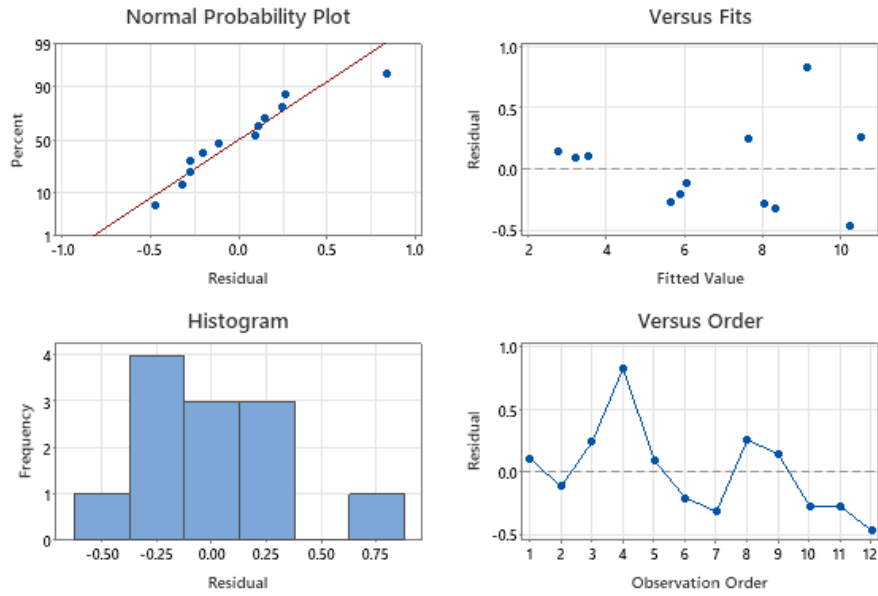


Figure F-5 Residual plots for the linear correlation between mass loss and total energy absorbed.

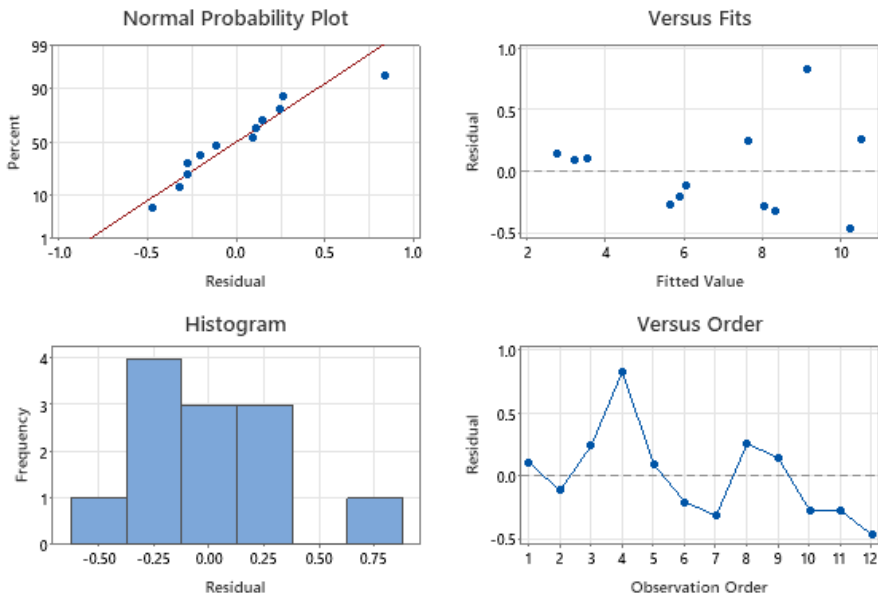


Figure F-6 Residual plots for polynomial correlation between mass loss and total energy absorbed.

CURRICULUM VITAE

NAME: Sean Simpson

ADDRESS: GE Appliances
4000 Buechel Bank Road
Louisville, KY 40225

DOB: Charlottesville, Virginia – October 17, 1996

EDUCATION
& TRAINING: B.S., Mechanical Engineering
Virginia Polytechnic and State University
2015-20

M.S., Mechanical Engineering
University of Louisville
2020-23

AWARDS:

PROFESSIONAL SOCIETIES:

PUBLICATIONS:

NATIONAL MEETING PRESENTATIONS:

REFERED JOURNALS:

BOOKS AND SYMPOSIA:

INVITED PRESENTATIONS: